SIMULATION OF PROGRESSIVE SHEAR FAILURE IN RAILWAY FOUNDATION

Xu Dong Li

A thesis submitted to the examination committee in Partial Fulfillment of the requirements for the degree of

DOCTOR OF PHILOSOPHY IN CIVIL ENGINEERING

A joint program between Carleton University and University of Ottawa, which is administered by the Ottawa-Carleton Institute for Civil Engineering

Department of Civil Engineering
Faculty of Engineering
University of Ottawa
Ottawa, Ontario, Canada

ABSTRACT

Railways are one of the largest transportation networks in the world that play an important role in the mass transportation of both the passengers and freight. The speed of trains and as well as the axial load carrying capacity have been increasing significantly during the past few decades to keep in pace with the population and economy growth and to compete with other modes of transportation such as the road, air and water transportation system. Billions of dollars are spent annually for maintenance of rail tracks in the world. The efficient and optimum use of these funds is a challenging task that demands innovative and cutting edge technologies in railway engineering.

The railway subgrade is an important part of railway foundation and should be capable of providing a suitable base supporting the ballast and subballast to accommodate the stresses due to traffic loads without failure or excessive deformation. The progressive shear failure is a well-known and age old challenging problem for railways over the world for centuries. The subgrade of railway track which typically constitutes of fine-grained material tends to fail through the accumulation of soil movements up- and sideward developing a path for the least resistance along which progressive shear failure occurs under repeated train-induced loads and due to the effects of climate factors. To-date, limited number of studies have addressed failure mechanism associated with the progressive shear failure, especially using the mechanics of unsaturated soils.

In this thesis, a novel and first of its kind, Visual Basic program developed in AutoCAD environment based on Mohr-Coulomb failure criteria and unsaturated soil mechanics theory. This program is capable of taking account of the influence of matric suction and simulate progressive shear failure in the subgrade under moving train. Simulation results suggest several parameters that include stress distribution, matric suction, cohesion, coefficient of lateral earth pressure at rest, and coefficient of residual friction as well as the angle of internal friction have a significant effect on the progressive shear failure and the shape of failure planes in the subgrade. The progressive shear failure in subgrade can be reduced by increasing matric suction, cohesion, coefficient of lateral earth pressure at rest, and coefficient of residual friction as well as the angle of internal friction, and optimizing combination of these parameters.

The simulation results suggest the progressive shear failure can be well simulated with the Mohr-Coulomb failure criteria. Several suggestions are made for railway subgrade construction and maintenance based on the results of this study.

ACKNOWLEDGMENTS

Studies presented in this thesis were conducted at the Department of Civil Engineering, University of Ottawa under the supervision of Prof. Sai K. Vanapalli. I am so proud to be Dr. Vanapalli's student and benefit my research from his encouragement, enlightened supervision and insightful suggestions. I sincerely thank Dr. Vanapalli's continuous supports and supervision on my way towards exploring the mysteries of unsaturated soils and broadening my horizon and vision.

The financial supports of Admission Scholarship received from the University of Ottawa are gratefully acknowledged.

My appreciations extend to my colleagues at the University of Ottawa for their friendship, company and support. They are: Mengxi Tan, Shunchao Qi, Mohammed Al-Khazaali, Yunlong Liu, Hongyu Tu, Penghai Yin, Zhong Han and Weilie Zou.

I would like to express my sincere thanks to my wife and three sons for their love and supports that provided me the energy and encouragement to complete this PhD thesis.

CONTENTS

ABSTRACT ii
ACKNOWLEDGMENTS iv
CONTENTS v
LIST OF FIGURES ix
LIST OF TABLES xi
Chapter 1 Introduction 1
1.1 Introduction 1
1.2 Objective 2
1.3 Layout of the Thesis 3
Chapter 2 Rail Transport and Railway 4
2.1 Rail Transport 4
2.2 Railway Track Structure 5
2.3 Railway Track Superstructure 6
2.3.1 The Rail 6
2.3.2 The Tie 7
2.3.3 The Fasteners 8
2.4 Railway Track Substructure 9
2.4.1 Ballast 9
2.4.2 Subballast 11
2.4.3 Subgrade (trackbed, formation) 12
2.5 Rail Load and Distribution 13
2.5.1 Track Forces 14
2.5.2 Load Transmission in Track Foundation 18
2.6 Progressive Shear failure 23
Chapter 3 Literature Review 26

3.1 The Basics of Soil Mechanics 26
3.1.1 Soil Mechanics 26
3.1.2 Formation of Soils 26
3.1.3 Basic Characteristics of Soils 27
3.1.4 The soil shear strength 27
3.2 Unsaturated Soil Mechanics 29
3.2.1 Introduction 29
3.2.2 Various Phases in Unsaturated Soils 30
3.2.3 Soil Water Characteristic Curve 32
3.2.4 Shear Strength 33
3.3 The nature of compacted subgrade 36
3.4 The Coefficient of Earth Pressure at Rest 40
3.4.1 Definition of Coefficient of Earth Pressure at Rest (K_0) 40
3.4.2 The previous study 40
3.4.3 The factors influencing the value of coefficient of earth pressure at rest 42
3.5 The Residual Shear Strength 49
3.5.1 Drained residual strength of cohesive soils 49
3.5.2 Correlation for residual strength 51
3.5.3 Residual Shear Strength Mobilized in First-Time Slope Failures 51
3.5.4 Residual shear strength of unsaturated soils via suction-controlled ring shear testing 53
3.5.5 Residual shear strength of fine-grained soils 54
3.5.6 Drained residual shear strength at effective normal stresses relevant to soil slope stability analyses 55
3.5.7 Influence of displacement rate on residual shear strength of clays 56
3.5.8 Effect of shear rate on the residual shear strength of pre-sheared clays 57

Chapter 4 Simulation of Progressive Shear Failure in Subgrade 58
4.1 Assumptions of progressive shear failure in Subgrade 58
4.2 Shear Failure Criterion and Stresses in Subgrade 62
4.3 Program of the Simulation 65
Chapter 5 Simulation results of Progressive shear failure in subgrade 67
5.1 Input Data and Subgrade Parameters 67
5.1.1 The Density and Thickness of Ballast 67
5.1.2 The density of subgrade soil 67
5.1.3 The effective cohesion of subgrade soil and matric suction, c 68
5.1.4 The effective angle of friction of subgrade soil 69
5.1.5 The coefficient of earth pressure at rest 71
5.1.6 The coefficient of friction on failure plane K_r 74
5.1.7 The Stress Distribution in Railway Subgrade 79
5.2 Result of Simulation for Point Load 81
5.2.1 Effect of Angle of Friction 84
5.2.2 Effect of Subgrade Effective Cohesion 85
5.2.3 Effect of Coefficient of Earth Pressure at Rest 86
5.2.4 Effect of Coefficient of Friction on Failure Plane 87
5.3 Result of Simulation for normal spreading load 88
5.3.1 Effect of Stress Distribution to Progressive Shear Failure 90
5.3.2 Effect of Matric Suction 90
5.3.3 Effect of frication angle, cohesion and coefficient of earth pressure at rest 91
5.4 Sensitivity of element size 93
Chapter 6 Conclusions and Suggestions for the Future Research 95
6.1 Conclusions 95
6.2 Recommendations for Subgrade Design and Maintenance 96

6.2.1 Reduce the uneven stress distribution in railway subgrade 96
6.2.2 Use geotextile 96
6.2.3 Use high-qualified materials for subgrade 96
6.2.4 Use various methods 96
6.3 Suggestion for the Future Research 97
BIBLIOGRAPHY 98
APPENDIX 109
1. Code of the Program 110
2. Input File 119
3. Result of Simulation for Point Load 123
4. Result of Simulation for Normal Spreading Load 157

LIST OF FIGURES

Figure 2-1 Elements of railway infrastructure (from Li et al., 2016) 5
Figure 2-2: A typical railway track structure 5
Figure 2-3 Rail (https://www.bemorail.com/portfolio-item/vignola-rail) 7
Figure 2-4 Railway Ties and fastening systems (https://www.bemorail.com/portfolio-item/sleepers) 8
Figure 2-5 Ballast (https://www.123rf.com/photo_93877176&75780006) 9
Figure 2-6 Quasi-static vehicle forces on a curve track (from Indraratna et al., 2011) 16
Figure 2-7 Stresses in track foundation (Li et al. 2016) 19
Figure 2-8 Load transmission from rail downward along (a) and across (b) concrete and wood tie in tracks (Li et al. 2016) 22
Figure 2-9 Subgrade progressive shear failure (Burrow et al., 2011) 24
Figure 3-1 Mohr Coulomb shear failure criterion with Mohr circle of stress 28
Figure 3-2 Soil–water characteristic curve and its various zones (modified after Vanapalli et al. 1999) 31
Figure 3-3 Bounding and scanning curves that comprisethe drying and wetting behavior of an unsaturated soil (Fredlund et al., 2012) 33
Figure 3-4 Extended Mohr-Coulomb failure surface written as a function of the stress state using Fredlund et al. 1978 equation 34
Figure 3-5 Curvature to the shear strength envelope with respect to matric suction (modified after Vanapalli et al. 1996) 35
Figure 3-6 SWCC Curve and its relationship with shear strength (modified after Vanapalli et al., 1996) 38
Figure 3-7 K_0, Relationship of radial versus axial stress for Reid-Bedford sand (Al-Hussaini, 1981) 44
Figure 3-8 Variation of vertical and horizontal stresses during loading and unloading (Sivakumar et al. 2002) 45
Figure 4-1 Subgrade squeeze at end of tie (Li et al., 2016): (a) track cross section with a subgrade squeeze and (b) subgrade squeeze and lime injection hole 59

Figure 4-2 Failure elements and plane in Subgrade..... 61
Figure 4-3 Failure element and its stresses: a. Stress status and failure plane in an element. b. New stresses status as the unbalanced shear stress from previous element is transferred in. c. Calculating new major principle stress according to initial principle stresses and unballanced shear stress from previous element..... 62
Figure 5-1 Subgrade stress distribution below geocell-reinforced embankment overlying very soft foundation (2 MPa) (Leshchinsky, 2012). 80
Figure 5-2 Subgrade stress distribution below geocell-reinforced embankment overlying soft foundation (20 MPa) (Leshchinsky, 2012). 81
Figure 5-3 Failure planes of simulation for point load 83
Figure 5-4 Effect of Angle of Friction to progressive shear failure 84
Figure 5-5 Effect of Subgrade Effective Cohesion to progressive shear failure 85
Figure 5-6 Effect of Coefficient of Earth Pressure at Rest to progressive shear failure..... 86
Figure 5-7 Effect of Coefficient of residual Friction on Failure Plane..... 87
Figure 5-8 Failure planes under normal spreading load 90
Figure 5-9 Effect of Matric Suction to Progressive Shear Failure..... 91
Figure 5-10 The relationship of frication angle ϕ', cohesion c' and coefficient of earth pressure at rest K_0 at critical condition of shear failure 93
Figure 5-11 Sensitivity of element size 94

LIST OF TABLES

Table 2-1 Ballast Grade 10
Table 5-1 Density Ranges for Different Soil Types (kg/m^3) 68
Table 5-2 The Cohesive strength (c) or (c prime) 69
Table 5-3 Angle of internal friction (ϕ) or (ϕ prime) 69
Table 5-4 Typical values of soil friction angle 70
Table 5-5 Values of K_0 for the sand tested by (Al-Hussaini, 1981) 71
Table 5-6 Experimental Values of Coefficient K_0 72
Table 5-7 Index Properties, Mineralogical Composition, and residual friction angle of Natural Samples (Tiwari & Marui, 2005) 74
Table 5-8 Reactivated landslides and reported soil residual shear strength correlations (Eid et al., 2016) 77
Table 5-9 Model material properties (Leshchinsky & Ling, 2013) 80
Table 5-10 Some typical results of simulation under point load 82
Table 5-11 Some typical results of the simulation under normal spreading load 89
Table 5-12 The relationship of frication angle ϕ', cohesion c' and coefficient of earth pressure at rest K_0 at critical condition of shear failure 92

CHAPTER 1
INTRODUCTION

1.1 Introduction

Rail transport is one of the most commonly used, cost effective and the largest transportation modes in various countries of the world. For the past two centuries, railways served people all over the world by transporting passengers, freight and bulk commodities among major cities, ports, mines and sources of agricultural goods, as well as commuters to contribute to the economic development.

There are 1.1 million kilometers of railway lines in the world, 7 million personnel working in the railway industry, 3.9 trillion passenger-kilometers, and 10.6 trillion ton-kilometers of freight are transported by railway per year, according to data from International Union of Railways (UIC) (Railisa, 2018).

To keep pace with the growth in population and economies and to compete with other modes of transportation such as road, air and water transport with respect to speed and carrying capacity, axial loads must increase and maintenance costs must reduce in order to improve efficiency. Countries such as Canada, China, USA, India and Australia are playing a leading role in the development of heavy haul railway operations that include 3–4 km long trains with axle loads exceeding 35 tons to optimize the efficiency of supply chains in the mining and agricultural sectors (Indraratna, 2016). On one front, this implies continuous needs for upgrading the railway tracks; and, on the other hand, there are challenges for adopting innovative technology to minimize construction and maintenance costs.

Billions of dollars are spent annually for the construction and maintenance of railway tracks in many countries. Euro Rail Consult (Jovanovic, 2016) studied the maintenance costs of railway infrastructure and concluded average 50€ costed per meter of railway per year on conventional lines in Western Europe. This translates to approximately $ 50 billion dollars annually for

maintenance costs worldwide. The efficient and optimum use of these funds is a challenging task which demands innovative and edge-cutting technologies in railway engineering (Indraratna et al., 2011).

1.2 Objective

The progressive shear failure is a well-known and age old problem for railways all over the world for centuries. The subgrade of railway track that is typically made of fine-grained materials tends to fail through the cumulative accumulation of plastic strain and reduction of the shear strength associated with repeated train-induced loads and due to the effects of climate factors (Li et al., 2016). Because of repeated cycles of overstressing, surface soil moves up- and sideward developing a path for the least resistance along which progressive shear failure occurs.

The progressive shear failure is one of the most common causes for railway subgrade failure (Hendry et al. 2013; Li, 2018; Miller et al. 2000). Several research studies (Boler et al. 2018; Dareeju, 2017; Dey et al. 2010; Loh, 2011; Sánchez et al. 2014) addressed the progressive shear failure in railway subgrade focusing on studying subgrade deformation and stress in ballast and subgrade. The focus of some these studies were directed to propose design solutions to alleviate the occurrence of progressive shear failure. In addition, some of the studies suggested methods for subgrade repair to reduce the progressive shear failure in the existing railway.

To-date, very few studies (Li & Selig, 1995) have focused in detail and addressed the process and mechanism of progressive shear failure in railway subgrade. In this thesis, a first of its kind and novel Visual Basic computer program is developed in AutoCAD environment to simulate the process of progressive shear failure. This program is capable to suggest the failure planes based on Mohr-Coulomb failure criteria extending unsaturated soil mechanics. This program facilitates to take into account of the influence of matric suction. In this thesis, 2800 simulations have been conducted to understand mechanics of progressive shear failure and locate failure plane in the subgrade. In this study, the influence of stress distribution under bottom of ballast and other parameters which include matric suction, cohesion, coefficient of lateral earth pressure at rest, and coefficient of residual friction as well as the angle of internal friction are considered to analyze the progressive shear failure conditions. Based on the study results, improved design

and mitigation methods are suggested that can contribute to prevent or drastically reduce progressive shear failure development and repair failed track foundation.

1.3 Layout of the Thesis

This thesis is organized as a "Monograph Thesis". This thesis is summarized six chapters. The main contents of each of these six chapters are briefly described below:

1) Chapter One, entitled "Introduction", presents the introduction, objective, novelty and layout of the thesis.
2) Chapter Two, entitled "Rail Transport and Railway" provides a succinct background of rail transport and railway track structure, and load transmission in track foundation, as well as progressive shear failure in railway subgrade.
3) Chapter Three, entitled "Literature Review" consists of a comprehensive state-of-the-art review on soil mechanics and unsaturated soil mechanics as well as soil properties related to its strength.
4) Chapter Four, entitled "Simulation of Progressive Shear Failure in Subgrade", explain the mechanics of simulating progressive shear failure and its principle equations as well as program.
5) Chapter Five, entitled "Simulation Result of Progressive Shear Failure in Subgrade", consists of detail of the input data selections and discussing the simulation results.
6) Chapter Six, entitled "Conclusion and Suggestions for the Future Research", presents conclusion, recommendation for railway subgrade design and construction, and suggestions for the future research.

In addition, Bibliography summarizes references cited in this thesis and Appendix, containing the code of program, one input data file and two output data tables.

CHAPTER 2
RAIL TRANSPORT AND RAILWAY

This Chapter presents basic knowledge of railway track structures and its foundation, as well as the stress distribution in railway foundations and the mechanism associated with the progressive shear failure.

2.1 Rail Transport

Rail transport is also known as train transport (Wikipedia, 2020). It is a means of transport, on which vehicles run on tracks (rails or railroads). It is one of the most important, safe, commonly used and cost effective modes of commuting and goods carriage over long, as well as, short distances. Since this system runs on metal (usually steel) rails and wheels, it has an inherent benefit of lesser frictional resistance which helps attach more load in terms of wagons or carriages. This system is widely known as a train. Usually, trains are powered by an engine locomotive running on electricity or on diesel. Complex signaling systems are utilized if there are multiple route networks. Rail transport is also one of the fastest modes of land transport.

Trains are safe, fast, cost effective and the least affected by usual weather turbulences like rain or fog, compared to other transport mechanisms. Rail transport is better organized than any other modes of transport. It has fixed routes and schedules. Its services are more certain, uniform and regular compared to other modes of transport.

Rail transport however has some constraints and limitations. One of the biggest constraints of rail transport is heavy cost. The cost of building and maintaining a railway and trains as well as its facilities is magnified when a whole rail network is to be built. Also, rail transport cannot provide door-to-door service as it is tied to a particular track. Intermediate loading or unloading involves greater cost, more wear and tear and wastage of time.

The railway system consists railway infrastructure (Figure 2-1) (Li et al., 2016) and Rolling stock.

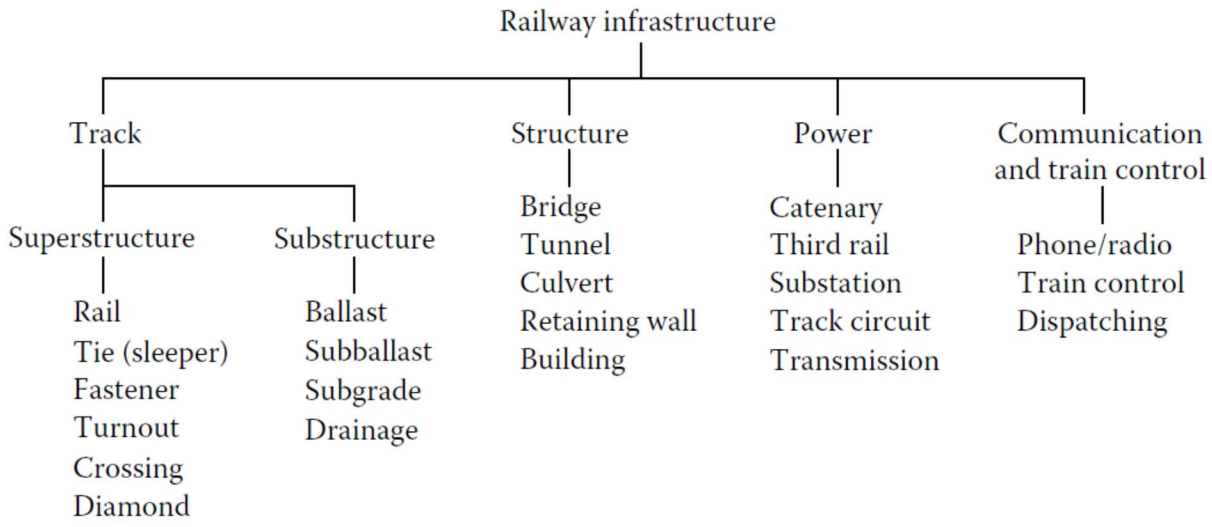

Figure 2-1 Elements of railway infrastructure (from Li et al., 2016)

2.2 Railway Track Structure

Track is the most fundamental component of the railway infrastructure, is divided into superstructure and substructure (Figure 2-2). Track supports the rolling stock by distributing wheel loads from the track superstructure to the track substructure. The substructure consists of ballast, subl systems, and concret .

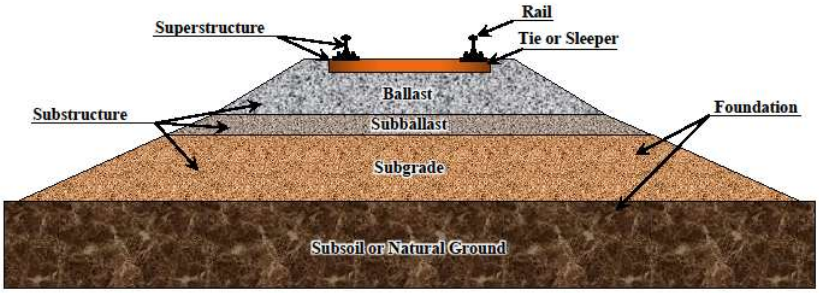

Figure 2-2: A typical railway track structure

The structure of railway track has evolved since its first development more than 150 years ago. The evolution to a strong and durable track structure is the result of overcoming ever-increasing

challenges associated with moving more, faster, or heavier trains. Safety and cost have always been the primary concerns. The quest for safe and cost effective railway transportation have driven improvements in materials and processes that have provided a track structure with increased reliability and durability (Indraratna et al., 2011; Li et al., 2016).

Modern-day track superstructure and substructure components have changed greatly from the materials used historically. The superstructure of the track has benefitted from many years of research, development, and testing that have resulted in a good understanding of materials, inspection, and maintenance options. Rail steel has become durable, and rail inspection technologies as well as preventive maintenance strategies have advanced significantly. Tie (sleeper) materials have improved both in their strength and durability. Some of these improvements in hardwood tie treatment and use of other materials such as concrete, composite, and steel. The fastening system has evolved from cut spike and tie plate to elastic systems that improve rail restraint from movement relative to the ties.

Railway ballast gradually evolved from the early practice of simply using locally available gravel to the use of coarse and open-graded hard crushed rock. Appreciation for ballast and other components of the track substructure has grown extensively since railway industry started more than 200 years ago.

2.3 Railway Track Superstructure

The track superstructure includes the main load-supporting elements of the track that react and transfer train load to the track substructure. The superstructure includes the rail, tie (sleeper), and fastening system that work together to support train loading by reducing the large stresses at the wheel–rail interface to levels that are tolerable for the substructure layers.

The superstructure is required to resist both vertical and lateral loads with only limited elastic and permanent deformation.

2.3.1 The Rail

The rail is the most visible element of the track structure that directly supports passing wheels. The rail (Figure 2-3) has changed substantially over the years, from smaller rail cross sections that were installed as individual rail lengths to larger rail cross sections welded into continuous

strings common in track today. The most recent rails are 39 ft long. The use of high-strength steels and head hardening have resulted in superior rail performance, while the head of the rail has been made larger by proportion to the remainder of the rail section to provide a larger area for wear. Improvements in rail welds can significantly improve track substructure performance if the weld can provide increased yield strength, particularly in the heat-affected zone. Weld rail result in reduced plastic deformation of the rail, less variations in rail profiles, and lower dynamic loading and track deterioration (Li et al., 2016).

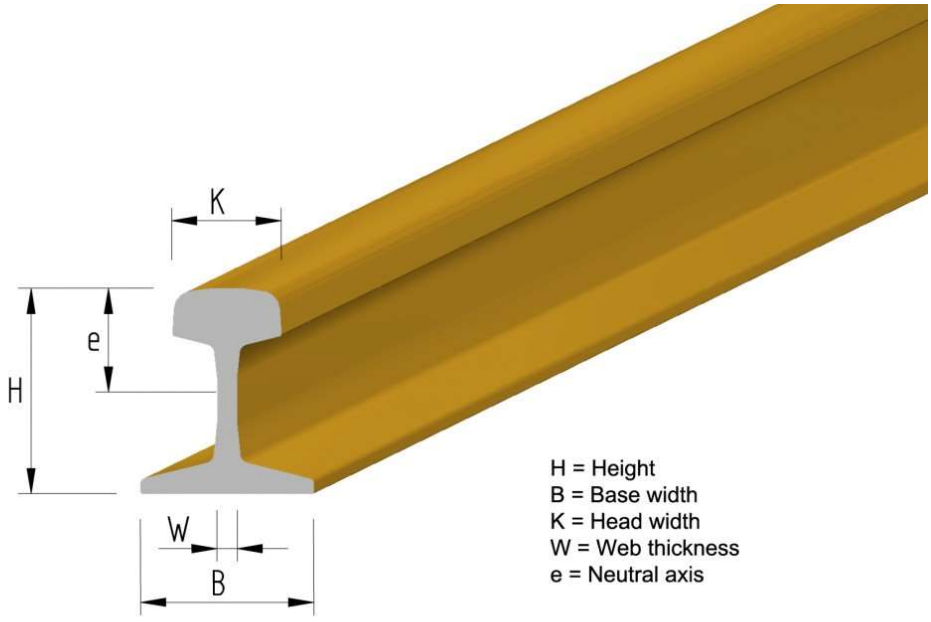

Figure 2-3 Rail (https://www.bemorail.com/portfolio-item/vignola-rail)

Improved rail can enhance track performance and life in well-supported track sections, but heavier and stronger rail do not solve track support problems. Some have assumed that heavier rail can accommodate, or bridge over, track support problem as stronger and stiffer rail will distribute the load over a larger area. However, the effect is minimal, because once the track support has deteriorated, the only choice is to improve the track support.

2.3.2 The Tie

Cross-ties (sleepers)(Figure 2-4) are typically wood or concrete elements. Although composite/plastic and steel ties have been developed for specific applications or to obtain desired properties, these types of ties have not yet been widely adopted. Wood ties tend to be most

common in the United States and Canada not only because of lower cost but also because of the superior resilience of wood towards dynamic track interaction. Both concrete and wood ties are affected by abrasion from the ballast and wear at the rail–tie contact area. Wood ties are more sensitive to drainage problems mainly due to their susceptibility to rot and decay (Li et al., 2016).

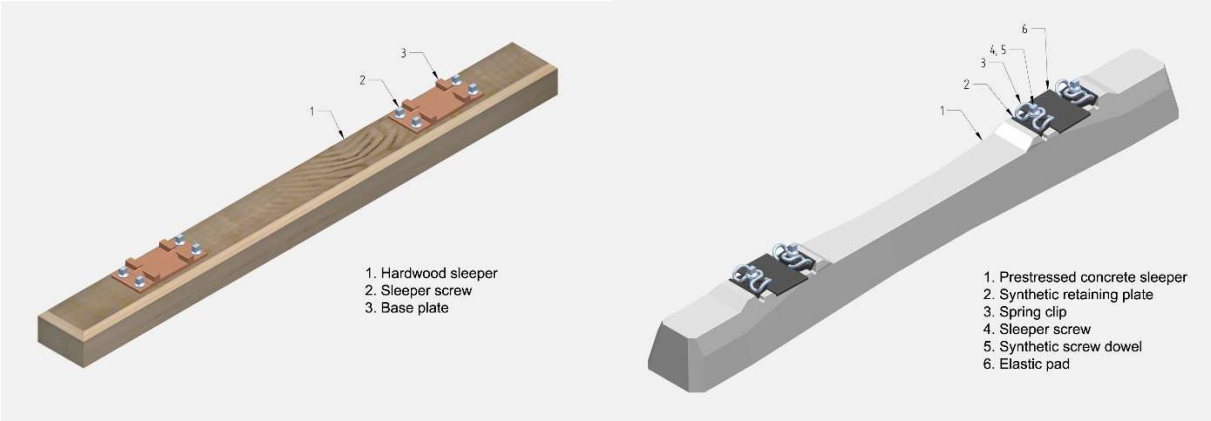

Figure 2-4 Railway Ties and fastening systems (https://www.bemorail.com/portfolio-item/sleepers)

2.3.3 The Fasteners

Fastening systems (Figure 2-4) retain the rail in place by restraining lateral, longitudinal, and vertical relative movement between the rail and tie. The rail fastening system, including the rail seat pad (if any), affects track behavior, and pad stiffness influences dynamic load attenuation and vibration transmission, both of which influence track superstructure performance. The plate and cut spike fastener is still the most common fastening system on wood ties, which must be coupled with appropriate rail anchoring to restrain rail longitudinal movement (Li et al., 2016).

Elastic fasteners form the rail–tie fastening system that provide resilient lateral, longitudinal, and vertical rail restraint. The resilience of this fastening system develops with deformation similar to spring stiffness, although not all fasteners provide a linear stiffness variation with deflection. Elastic fasteners are widely used with concrete ties; they are sometimes used on wood tie track. In concrete tie installations, the rail seat pad is an important consideration to control dynamic loads and rail seat abrasion, while ensuring adequate longevity of the pad. In addition, concrete tie track requires insulators to provide electrical insulation of track signals and a degree of

resilience to the lateral rail–tie interaction. Elastic fasteners and fastening systems have many common elements whether applied to concrete ties or as direct fixation fasteners on slab track.

Under-tie pads have been used successfully on the bottom face of concrete ties. One problem with concrete ties has been the deterioration in the tie–ballast contact zone. The under-tie pad has improved tie–ballast contact, reduced abrasion, as well as added resilience to the stiff concrete tie, all of which contribute to improve ballast life in concrete tie track.

Special trackwork is also part of the track superstructure and includes turnouts, crossing diamonds, insulated joints, and along with grade-crossings and other locations of unique track construction are locations that often experience more rapid degradation. Each of these track features can generate large dynamic loads that are transferred to the substructure.

2.4 Railway Track Substructure

Track substructure consists of the foundation layers that support the track superstructure and the drainage arrangements. The foundation layer consists of ballast, subballast, and subgrade. In the case of slab track, the track structure is ballast-less, and the track substructure includes subbase and subgrade.

2.4.1 Ballast

Ballast is the granular material placed as the top substructure layer and is the layer that is in direct contact with the ties (sleepers). Ballast is generally large, angular, and uniformly graded (similar size) granular particles (Figure 2-5) derived from crushed hard rock material such as granite and basalt (Li et al., 2016).

Figure 2-5 Ballast (https://www.123rf.com/photo_93877176&75780006)

Ballast has many functions that are requirements for good, well- supported track. The most important are summarized below:

- Supports the rail–fastener–tie track panel by providing adequate vertical, lateral, and longitudinal resistance.
- Transmits and reduces wheel/rail forces.
- Facilitates surfacing and lining operations.
- Provides drainage.
- Provides resilience and damping of dynamic wheel/rail forces.

Ballasted track is not sealed like highway pavement but is designed as an open structure to provide rapid drainage and facilitate maintenance. Ballast-related track maintenance methods include surfacing and lining, stoneblowing, track renewal and superstructure replacement, ballast undercutting to restore drainage and resilience, fouled ballast removal including crib excavation with backhoe or vacuum, and ballast compaction often with a dynamic track stabilizer. Maintenance is required when one of the following problems occurs: excessive vertical or lateral track deformation, excessive ballast degradation (ballast fouling), or drainage is no longer effective (Li et al., 2016).

Table 2-1 Ballast Grade

Sieve size (mm)	Ballast Grade	
	Standard	Fine
	Nominal size (mm)	
	60 (graded ballast)	50 (graded aggregate)
	% passing by mass	
63.0	100	–
53.0	85 – 100	100
37.5	50 – 70	70 – 100
26.5	20 – 35	–
19.0	10 – 20	40 – 60
13.2	2 – 10	–
9.50	0 – 5	20 – 30

4.75	0 – 2	10 – 20
2.36	–	5 - 10

To fulfill the ballast functions, there must be adequate ballast layer thickness and proper particle size and gradation. The ballast layer must have a proper gradation to provide a large void space that facilitates both drainage and storage of fouling material. Materials that are smaller in size accumulate in the void spaces within the ballast layer are called fouling material. Fouling material can originate from abraded or broken ballast, material that spills or blows into the track, or material that flows onto the track from water drainage or flooding.

According to ballast specification of RailCorp (ESC 240 BALLAST Version 2.4, 2013), the particle size distribution (grading) of ballast aggregates shall conform to the requirements set out in following Table 2-1.

The thickness of the ballast layer should be specified based on the structural capacity of the track to ensure that it can withstand and distribute the applied train loading at a stress level that will not deform the subgrade over the expected life of the track (Indraratna et al., 2011; Li et al., 2016).

Ballast compaction is essential to provide lateral track resistance. Although ballasted track is normally stable with a considerable lateral strength reserve to resist imposed stresses, when ballast is newly placed or if it has been disturbed by maintenance (tamping or tie replacement), lateral resistance of the track may only be half of its value compared to when it is compacted. Resumed traffic following the maintenance will lead to gradual ballast recompaction and eventual restoration of its lateral strength and track buckling resistance.

2.4.2 Subballast

The subballast, or the blanket (another term often used), is the granular layer between the ballast and the subgrade (Figure 2-2). This granular layer often consists of broadly graded gravel and sand. The subballast complements the ballast by further distributing the applied loads and reducing the stresses on the subgrade, and it provides protection from frost action. However, the subballast has some important functions that cannot be fulfilled by ballast:

- Prevents penetration and mixing of subgrade and ballast.
- Prevents subgrade attrition by ballast, when the top subgrade is composed of clay stone or shale that may be abraded by large ballast stones.

The subballast has a critical role in drainage and has competing requirements to both drain readily and direct water away from the subgrade (Indraratna et al., 2011; Li et al., 2016).

When the groundwater is shallow, the subballast should be capable of providing drainage of water that might be flowing upward from the subgrade. Design of the subballast layer also requires the analyses of layer thickness and gradation. Drainage requirements often conflict with separation and filtration criteria that must also be satisfied to prevent soil migration and piping.

Subballast saturation is a common problem that is often ignored. This results from inadequate drainage of the subballast layer from conditions such as the formation of subgrade settlement depressions that trap water or subballast gradation that makes the subballast inadequately permeable. Under repeated wheel/rail forces, significant deformation and even rapid failure can occur in the subballast layer when drainage is impeded. Not only does the accumulated water soften fine-grained subgrade, it also greatly reduces the stiffness of the subballast along with the ability of the subballast layer to distribute applied loads (Li et al., 2016).

2.4.3 Subgrade (trackbed, formation)

Subgrade may consist of either soil or rock and is the platform on which the track structure from the subballast up is built, as shown in Figure 2-2. It can be part of an embankment that is built with fill materials or can be natural ground in cut sections of track where subgrade may consist of the natural soil or placed soil layer(s) (Li et al., 2016).

Trackbed, roadbed, track foundation, and formation are other terms used to describe track substructure. Trackbed is used mainly to refer to the tie/sleeper support layers inclusive of the entire track substructure below the bottom of tie, and this will be the manner in which the term trackbed (roadbed, track foundation) will be used as subgrade in this thesis. Formation is another common term used to refer to the subgrade but includes any placed fill such as the subballast (blanket) layer directly under the ballast.

The primary function of the subgrade is to act as the track foundation by providing uniform and adequate support. In other words, subgrade should be capable of providing a suitable working

base for the construction of ballast and subballast (or the subbase in the case of slab track), supporting the track structure, and accommodating the stresses due to traffic loads without failure or excessive deformation.

The influence of wheel loads can extend several meters below the bottom of the ties in spite of wheel loads reduce significantly in the subgrade through the load distribution provided by the superstructure, ballast, and subballast. As such, the subgrade over this depth should be strong to resist failure and excessive deformation due to wheel loads as well as the weight of track and substructure. In addition, a stable platform must be maintained over time and should not be excessively affected by environmental conditions (e.g., wet/dry and freeze/thaw cycles). Subgrade should also be designed so that surface water and ground water drain away from the track. A poorly designed and constructed subgrade can cause many track performance problems, so it is imperative that design and construction of subgrade be done according to the best practices available.

Under repeated wheel loads, an overstressed subgrade can experience "cumulative plastic deformation" (ballast pocket) or "progressive shear failure" (subgrade squeezing, shown in Figure 2-9). These are the two most common failure modes for subgrade composed of fine-grained cohesive soils. These problems can lead to deterioration of track-geometry conditions, which in turn will increase dynamic wheel loads and accelerate deterioration.

Although soft subgrade failures are more common, problems on hard subgrade also exist. While track stability is not typically a problem on hard subgrade, abrasion of hard subgrade by coarse ballast particles in the presence of water can cause the abraded subgrade fines to infiltrate and foul the ballast, reducing its permeability, which affects track life, performance, and maintenance requirements.

2.5 Rail Load and Distribution

A railway track structure not only provides a stable, safe and efficient guided platform for the train wheels to run at various speeds with different axle loadings, but also transfer different types of loading imposed on a track system down to ground.

2.5.1 Track Forces

The loads from standing or running trains (wheel-rail-tie interactions) are a complex combination of 'moving' static loads and dynamic forces. The requirements for the bearing strength and overall quality of the track depend largely on the vertical load per axle, tonnage borne as the sum of the axle loads and the running speed. The static axle load level, to which the dynamic increment is added as a function of speed, determines the required load carrying capacity of the track. The accumulated tonnage determines the deterioration of the track quality and provides an indication of when maintenance and renewal are necessary. The dynamic load component, which depends on speed and horizontal and vertical track geometry, also plays an essential role.

2.5.1.1 Vertical forces

The total vertical wheel load on a rail may be classified into two groups: quasi-static load and dynamic load (Indraratna et al., 2011). The quasi-static load is composed of three components, as given below:

$$Q_{total} = Q_{quasi-static} + Q_{dyamic} \quad (2.1)$$

$$Q_{quasi-static} = Q_{static} + Q_{centrifugal} + Q_{wind} \quad (2.2)$$

where, Q_{static} = static wheel load,

$Q_{centrifugal}$ = increase in wheel load on the outer rail in curves due to non-compensated centrifugal force,

Q_{wind} = increase in wheel load due to wind,

$Q_{dynamic}$ = dynamic wheel load component resulting from sprung mass, unsprung mass, corrugations, welds, wheel flats etc.

The static load on each wheel is equal to half of static axle load, thus:

$$Q_{static} = \frac{G}{2} \quad (2.3)$$

where, G = weight of vehicle per axle.

Considering the limit equilibrium of forces acting on a vehicle, as shown in Figure 2-6 Quasi-static vehicle forces on a curve track, the following expressions are proposed (Indraratna et al., 2011) for the centrifugal and wind forces:

$$Q_{centrifugal} + Q_{wind} = G\ \frac{p_c h_d}{s^2} + H_w \frac{p_w}{s} \quad (2.4)$$

$$h_d = \frac{sV^2}{gR} - h \quad (2.5)$$

where, H_w = cross wind force,

s = track width,

V = speed,

g = acceleration due to gravity,

R = radius of curved track,

H = cant (or superelevation),

p_c = distance between center of rails and center of gravity of vehicle, and

p_w = vertical distance of resultant wind force from center of rails.

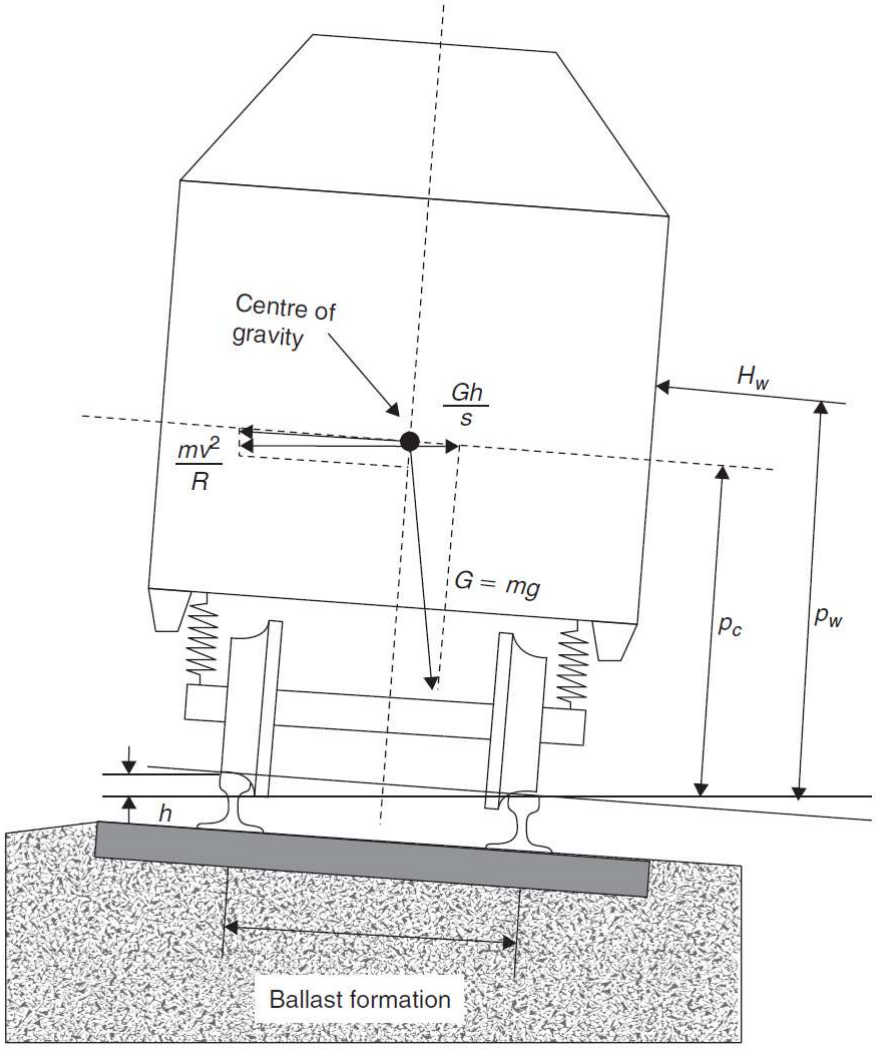

Figure 2-6 Quasi-static vehicle forces on a curve track (from Indraratna et al., 2011)

The maximum wheel load usually occurs at the outer rail (h_d >0), thus Equation 2.6 can be obtained combining Equations 2.3 and 2.4, as given below:

$$Q_{emax} \approx \frac{G}{2} + G\,\frac{p_c h_d}{s^2} + H_w \frac{p_w}{s} \qquad 2.6$$

The most uncertain part of the wheel load is the dynamic component, $Q_{dynamic}$. In order to obtain an approximate rough estimate of $Q_{dynamic}$, the static wheel load may be multiplied by a dynamic amplification factor (otherwise known as the impact factor), in lieu of conducting a purely cyclic load analysis. The major factors affecting the magnitude of dynamic load component are:

- Speed of train,
- Static wheel load and wheel diameter,
- Vehicle unsprung mass and vehicle condition,
- Track condition (including track joints, track geometry and track modulus), and
- Track construction aspects and properties of ballast and subballast.

A range of empirical formulae has been used by different railway organizations for determining the design vertical wheel load. It is usually expressed empirically as a function of the static wheel load.

American Railway Engineering Association (AREA) recommended the following simple expression for the computation of design wheel load for the purpose of track design (Indraratna et al., 2011):

$$P_d = \emptyset P_s \qquad 2.7$$

where, P_d = design wheel load (kN) incorporating dynamic effects,

P_s = static wheel load (kN), and

Φ = dimensionless impact factor (>1.0) and is given by Equation 2.8.

$$\emptyset = \left(1 + \frac{0.0052V}{D_w}\right) \qquad 2.8$$

where, D_w = diameter of the wheel (m), and

V = velocity of the train (km/h).

2.5.1.2 Lateral forces

Lateral loads in tracks are far more complex than vertical loads. There are two principal sources of lateral loads: (a) lateral wheel force, and (b) buckling reaction force. Lateral wheel forces are initiated by the lateral force component of friction between the wheel and rail, plus the lateral force applied by the wheel flange on the rail. Buckling reaction forces in the lateral direction are developed due to the high compressive stresses caused by high rail temperatures.

Similar to vertical force (Equation 2.1), lateral force exerted by the wheel on outer rail is also equal to the sum of the quasi-static and dynamic loads, thus,

$$Y_{total} = Y_{quasi-static} + Y_{dyamic} \quad 2.9$$

$$Y_{quasi-static} = Y_{flange} + Y_{centrifugal} + Y_{wind} \quad 2.10$$

where, Y_{flange} = lateral force in curve caused by flanging against the outer rail,

$Y_{centrifugal}$ = lateral force due to non-compensated centrifugal force,

Y_{wind} = increase in lateral force due to cross wind,

$Y_{dynamic}$ = dynamic lateral force component.

Now, if an assumption is made that the centrifugal and wind lateral forces act entirely on the outer rail, then the lateral equilibrium equation obtained from Figure 2-6 will be as follows:

$$Y_{emax} \approx G \frac{h_d}{s} + H_w \quad 2.11$$

Similarly, as in vertical force estimation, to account for dynamic component of lateral force, the static component of the force can be multiplied by the dynamic amplification factor (DAF), thus,

$$H = DAF\left(G \frac{h_d}{s} + H_w\right) \quad 2.12$$

The Office of Research and Experiments (ORE) in Netherlands (Indraratna et al., 2011), also found that the lateral track force is dependent only on the radius of curvature, and the following empirical expression was proposed:

$$H = 35 + \frac{7400}{R} \quad 2.13$$

where, H = lateral force at curved track (kN), and

R = radius of curve (m).

2.5.1.3 Longitudinal forces

The longitudinal force imposed on the rail head can be due to any change in length of the released rail occurring as a result of a significant change in temperature. This is insignificant in fixed rails because the resistance is produced by friction forces between rails and ties and between ties and ballast. Other phenomenon causing longitudinal forces include, track creep, accelerating and braking of the vehicle, and shrinkage stresses caused by rail welding.

2.5.1.4 Impact forces

Rail track structures are often subjected to the impact loads due to abnormalities in either a wheel or a rail. The magnitude of these impact loads is high within the short impulse duration (frequency range upto 2000 Hz) and usually depends on the nature of wheel or rail irregularities, as well as on the dynamic response of the track.

Impact loads are caused by wheel or rail abnormalities such as wheel-flat, wheelshells, dipped rails, turnouts, crossings, insulated joints, expansion gap between two rail segments, imperfect rail welds and rail corrugations etc.

2.5.2 Load Transmission in Track Foundation

Whether it is static, cyclic, or dynamic, loading is transmitted to the track and subgrade, resulting in stresses and strains in the track foundation. This transference of load, stress, and strain to the track foundation depends to a great degree on the strength and stiffness properties of track substructure. With adequate strength and stiffness of track foundation materials, stresses and strains due to various types of loadings should not cause track and subgrade failure or excessive deformation.

2.5.2.1 Stresses and strains in track foundation

Figure 2-7 illustrates the stress state of three different elements in the track foundation under a moving wheel load. Only stresses in the vertical and longitudinal directions are shown. In general, the three-dimensional stress state for an element in the track foundation can be expressed as

$$\{\sigma_{ij}\} = \{\sigma_x, \sigma_y, \sigma_z, \sigma_{xy}, \sigma_{yz}, \sigma_{zx}\} \quad 2.14$$

where: σ_x, σ_y, σ_z are the normal stresses in the longitudinal, lateral, and vertical directions

σ_{xy}, σ_{yz}, σ_{zx} are the shear stresses in *xy*, *yz*, and *zx* planes.

Figure 2-7 shows the normal and shear stresses in the *zx* plane, as such $\sigma_{zx} = \tau$.

A normal stress is called a principal stress when the shear stress is equal to zero. As shown in Figure 2-7, for the element directly under the wheel load, both vertical and lateral normal stresses are principal stresses. The larger principal stress is referred to as the major principal stress and is denoted as σ_1. The smaller principal stress is referred to as the minor principal stress and is denoted as σ_3.

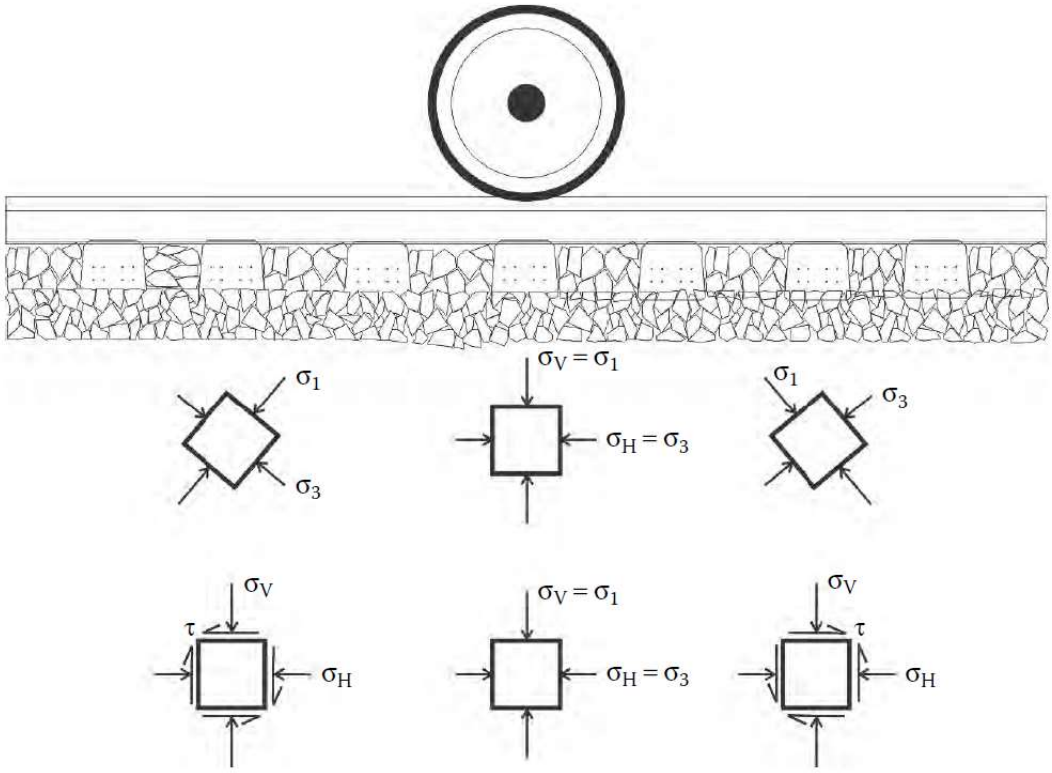

Figure 2-7 Stresses in track foundation (Li et al. 2016)

Bulk stress, as defined in Equation 2.15, is a stress parameter generally used for the granular layer (ballast and subballast) analysis, while deviator stress, as defined in Equation 2.16, is a stress parameter generally used for the analysis of subgrade consisting of cohesive soils.

$$\theta = \sigma_1 + \sigma_2 + \sigma_3 \qquad 2.15$$

$$\sigma_d = \sigma_1 - \sigma_3 \quad (2.16)$$

where: θ is the bulk stress

σ_d is the deviator stress

The ratio of horizontal to vertical stress is expressed by a factor called the coefficient of lateral stress or lateral stress ratio and is often denoted by the symbol K:

$$K = \frac{\sigma_H}{\sigma_V} \quad (2.17)$$

Where there is no lateral strain, this ratio is called the coefficient of lateral stress at rest or lateral stress ratio at rest and is often denoted using the symbol K_0. Typically, lateral stress ratio at rest is between 0.4 and 0.5, although it is possible that the horizontal stress exceeds the vertical stress, and in that case, this coefficient is greater than 1.0. This is especially true when residual stress in the ballast is high and resulting lateral stress ratio can be significantly higher than 1.0 (Li et al., 2016).

After stresses are determined, strains can be obtained by

$$\varepsilon_x = \frac{1}{E}\left[\sigma_x - \nu\left(\sigma_y + \sigma_z\right)\right] \quad (2.18)$$

$$\varepsilon_y = \frac{1}{E}\left[\sigma_y - \nu(\sigma_x + \sigma_z)\right] \quad (2.19)$$

$$\varepsilon_z = \frac{1}{E}\left[\sigma_z - \nu\left(\sigma_x + \sigma_y\right)\right] \quad (2.20)$$

$$\gamma_{xy} = \frac{\tau_{xy}}{G} \quad (2.21)$$

$$\gamma_{yz} = \frac{\tau_{yz}}{G} \quad (2.22)$$

$$\gamma_{zx} = \frac{\tau_{zx}}{G} \quad (2.23)$$

where: ε_x, ε_y, ε_z is the normal elastic strain in the longitudinal, lateral, and vertical directions

γ_{xy}, γ_{yz}, γ_{zx} is the elastic shear strain in xy, yz, and zx planes

E is the elastic modulus

v is the Poisson ratio

G is the shear modulus

The relationship between E, v, and G is defined by

$$G = \frac{E}{2(1+\nu)} \quad (2.24)$$

Under repeated wheel load applications, however, cumulative plastic strain may become a deformation parameter that is more critical than elastic strain. Elastic modulus, when defined in terms of resilient deformation and deviator stress, is referred to as resilient modulus. Resilient modulus and plastic deformation are two main parameters critical to the vertical strain, analysis and design of track foundation subjected to repeated wheel load applications.

2.5.2.2 Load transmission in track

Depending on the spectrum of frequency components, some of higher frequency force components will dissipate quickly when they are transmitted from the wheel–rail interface downward to the track substructure layer. Static or dynamic wheel loads of lower frequencies, however, are spread to the underling track substructure layers over larger area with increasing depth.

This spreading of load over larger area at greater depth, to a large degree, depends on the stiffness characteristic of each layer of the track structure, including the rail, ties, ballast, and subgrade.

GEOTRACK is a software for track structure analysis under vertical quasi-dynamic loads. It uses a three dimensional, multilayer elastic model for determining track and subgrade responses. However, the GEOTRACK software is not presently because is being reprogramed and updated.

Using GEOTRACK (old version), two examples are summarized from Li et al. 2016 to illustrate how a static wheel load is transmitted from the wheel–rail interface to the rail–tie interface, to the tie–ballast interface, and to various depths in the ballast and subgrade layers.

One example is for a typical concrete tie track, and the other is for a typical wood tie track, as shown in Figure 2-8. In these two examples, a single 40-kip (276 MPa) wheel load is applied on the rail directly above a tie, and this figure shows how this load is transmitted downward to different depths both along and across the track (Li et al., 2016).

Figure 2-8a show the results at various depths under the rail along the track longitudinally. The left sideplot of Figure 2-8b highlights the concrete tie track and the right side plot provides details of the wood tie track. As illustrated, for a 40-kip single wheel load on the concrete tie track, 12.4 kips (85 MPa, 31%) is transmitted to the rail–tie interface directly under the load, and 9 kips (62 mPa, 23%) is transmitted to the two adjacent concrete ties. The entire wheel load is

spread only to the fourth tie, because the rail–tie force is essentially zero on the fifth tie. On the other hand, for the wood tie track, 16.6 kips (114 MPa, 42%) is transmitted to the rail–tie interface directly under the 40-kip wheel load, which is spread over a shorter distance along the track, roughly to the third tie, as the plot on the top right shows.

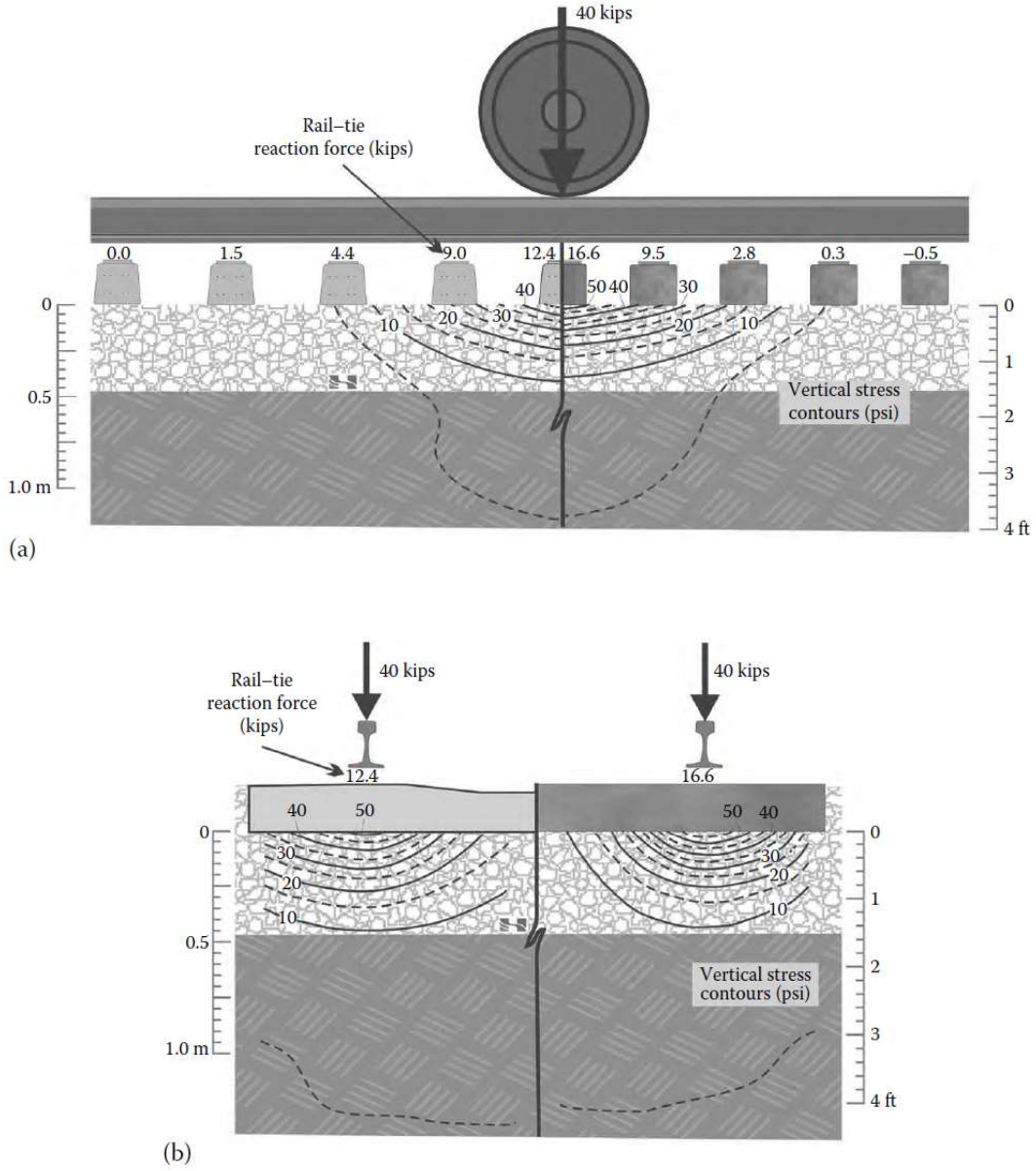

Figure 2-8 Load transmission from rail downward along
(a) and across (b) concrete and wood tie in tracks (Li et al. 2016)

At the ballast surface, maximum vertical stress is generated directly under the wheel load, although the wood tie track has higher maximum vertical stress than the concrete tie track,

because the former does not spread the load over a distance along the track as much as the latter does. The stress contours illustrate how vertical stress is distributed at various depths along the track. As shown, directly under the wheel load, stress is still somewhat significant 5 psi (e.g., 34 kPa) at a depth of approximately 4 ft (1.2 m) in the subgrade (from bottom of the tie), but this stress reduces quickly and becomes insignificant further away from the wheel load.

Figure 2-8 show how the 40-kip single wheel load is transmitted downward across half the track with respect to the center of the track, for both the concrete and wood tie tracks. Again, higher vertical stress over 50 psi (345 kPa) is generated directly under the rail for the wood tie track compared to the concrete tie track. Distribution of vertical stress across the track at various depths in the ballast and subgrade can be seen to be more uniform for the concrete track than for the wood tie track. It is also worth noting that toward the end of tie, the concrete tie generates higher vertical stress on the ballast surface than the wood tie does.

Note that the load transmission patterns, as shown in Figure 2-8, are based on an assumption of a typical concrete and wood tie track with a nominal ballast layer thickness of 18 in (457 mm). with modulus of 60,000 psi (414 MPa) and a subgrade modulus of 8,000 psi (55 MPa).

2.6 Progressive Shear failure

Conventional ballasted railway track (Figure 2-2) deteriorates progressively over time due to the combined effects of traffic and climate. Appropriate maintenance treatments are periodically applied to reduce the effects of this deterioration but an important and often neglected part of the track structure is the subgrade which, unlike the ballast, does not lend itself to be maintained easily (Burrow et al., 2011).

Subgrades of fine-grained material without adequate protection from repeated train induced loads and the effects of climate, may fail primarily by attrition from the ballast, progressive shear failure or excessive rate of settlement through the accumulation of plastic strain and massive shear failure (Burrow et al., 2011)(Figure 2-9). Due to the repeat overstressing wheel loads, surface soil moves upwards and side wards, following the least resistance path to form “cumulative plastic deformation” (ballast pocket) or “progressive shear failure”. Burrow et al

(2011) suggested that progressive shear failure occurs where train induced cyclic stress levels are sufficiently high to cause the soil to be sheared and remoulded (Figure 2-9) but at stress levels below those causing massive shear. Loh & Nikraz (2012) also found that subgrade soil beneath railway tracks experiences stress of cyclic nature with the passing of train axles/wheels that can result in progressive shear failure at a stress level lower than its monotonic strength. The progressive shear failure can lead to deterioration of track-geometry conditions (i.e. track defects, which in turn will increase dynamic wheel loads because track defects increase rail and wheel contacting impact and accelerate deterioration). Heave of soil due to progressive failure at the subgrade-subballast interface also cause the water ponding in subgrade and escalate the subgrade progressive shear failure.

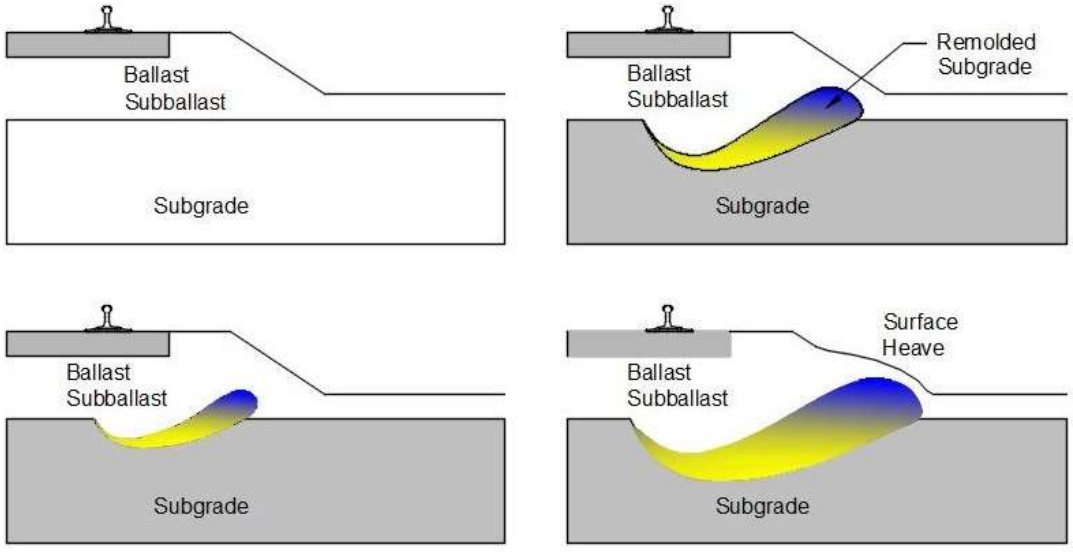

Figure 2-9 Subgrade progressive shear failure (Burrow et al., 2011)

Factors contributing to subgrade failures can be categorized into three groups: load factors, soil factors, and environmental factors (soil moisture and temperature) (Li & Selig, 1995). These three factors contribute progressive shear failure too.

The load factor is an external factor, which is a function of self-weight of rail structure and cyclic train loads. The self-weight of the structure can be considered to be key triggering factor that can be associated with massive shear failures for a high embankment and consolidation settlement of a rail track. However, the load factor of greatest concern is from repeated traffic loading. The subgrade behaves quite differently under a single static loading than under repeated traffic

loading, even though the magnitudes of individual axle loads may be the same. For example, the subgrade, particularly subgrades of fine-grained soils such as silt and clay, will exhibit lower strengths under repeated loadings than under a single loading. The subgrade settlement accumulated under smaller magnitudes of wheel loads with large numbers of repeated applications may be significantly larger than that generated under a single application of a larger dynamic wheel loading (Li & Selig, 1995).

The influence of soil type on the subgrade performance is strongly related to fine-grained soils (silt and clay) because of its lower strength and permeability, since the fine-grained soils that do not typically drain well are most susceptible to decrease in shear strength and stiffness with an increasing water content.

Almost every subgrade problem can be attributed to the high moisture content in the fine-grained soil subgrade. The presence of water in the subgrade can reduce the strength and stiffness of subgrade soils dramatically. A subgrade may become wet or saturated by the infiltration of water from the surface or from groundwater. The duration of water contact with a subgrade soil has significant influence on the resulting shear strength of the soil. A clay sub grade exposed to the air with occasional rain showers and dry periods may stay strong, whereas a subgrade covered by ballast and subballast (which cuts off evaporation) may get weak. The ballast and subballast allow water to penetrate, but they do not allow it to evaporate. As a result a subgrade that is not free-draining invariably can be saturated (Li & Selig, 1995).

Soil temperature is also of concern particularly during freezing and thawing cycles. Under certain combinations of temperature, soil suction, soil permeability, and availability of water, ice lenses will form when the soil freezes, causing ground heave. When the soil thaws again excess water from the ice lens will cause weakening of the soil.

The huge costs associated with the rail substructure maintenance can be significantly reduced if the PROGRESSIVE SHEAR FAILURE and its influence on the physical and mechanical characteristics of the railway foundation are well understood.

CHAPTER 3
LITERATURE REVIEW

This chapter provides a brief review about the mechanics of saturated and unsaturated soils that is relevant to the research topic.

3.1 The Basics of Soil Mechanics

3.1.1 Soil Mechanics

Soil mechanics is a discipline of civil engineering that can be used as a tool in interpreting the soil performance characteristics utilizing the engineering techniques of statics, dynamics, fluid mechanics, and other technologies. The soil composition, shear strength, compaction, hydraulic conductivity and consolidation are some of the key properties that are addressed for explaining soil sediments and other deposits behavior using soil mechanics. The field of soil mechanics is regarded as one of the major sciences for resolving problems related to geotechnical engineering, geology and geophysical engineering. These studies are important for civil engineers because several civil infrastructures are designed and constructed based on using the soil mechanics as a tool. The type of construction, type of equipment to be used, type of foundation, support material, and many other aspects of construction works are largely affected by the soil mechanics studies (Vandevelde & Basudhar, 2020).

3.1.2 Formation of Soils

Soil is a combination of minerals and organic elements that are in solid, gaseous, and aqueous form. Soil consists of particle layers that are different from the original materials in their physical, mineralogical, and chemical properties because of the interactions between the atmosphere and hydrosphere and other reasons. The particles of the soil are created from broken rocks that have been changed due to the chemical and environmental effects, including weather and erosion. Particles of soil are filled loosely, creating a soil formation that consists of pore spaces. Studying soil formation modes is important because it helps in determining properties of soil. Several such as the cohesion, adhesion, friction, acidity, and other related soil characteristics factors can easily be determined from various tests. However, we cannot draw any concrete

conclusions merely by conducting soil studies but we surely can narrow our research parameters by studying the basic characteristics of soil like color, texture, and nature of soil (Vandevelde & Basudhar, 2020).

3.1.3 Basic Characteristics of Soils

Soil consists of different phases of solid, liquid, and gas and its characteristics depend on the interacting behavior of these phases, and on the stress applied. The solid phase includes clay, non-clay minerals, and organic matter. They are categorized as clay, sand, and gravel based on their size. The liquid phase is primarily composed of water; however, it can contain organic compounds available from chemical spills, and wastes, while the gas phase is normally air. The size, form, chemical properties, compressibility, and load carrying capability of the soil particles are determined by soil mineralogy, which is a science related with the chemistry, structure, and physical properties of minerals. The structure of a soil depends upon the arrangement of particles, particle groups, pore spaces, and the composition. These basic characteristics determine the type of structure to be built and what external support measures, if any, has to be taken to make the structure last long and bear the effects of earthquake, water seepage, and other external factors (Vandevelde & Basudhar, 2020).

Soil mechanics studies are used to determine lateral earth pressure, bearing capacity of soil, and conduct slope stability analysis. These studies always help a civil engineer to design and construct better structures and indirectly these studies help in risk mitigation too because if we know beforehand how the soil mass is going to behave, we can take precautionary measures at the time of construction.

3.1.4 The soil shear strength

The shear strength of a soil mass is the internal resistance per unit area that the soil mass can offer to resist failure and sliding along any plane inside it. A geotechnical engineer must understand the nature of shearing resistance in order to analyze soil stability problems such as bearing capacity, slope stability, and lateral pressure on earth retaining structures (Das, 2001).

Mohr (1900) presented a theory for rupture in materials and concluded that a material fails because of a critical combination of normal stress and shearing stress, and not from either maximum normal or shear stress alone. Thus, the functional relationship between normal stress

and shear stress on a failure plane can be expressed by a curved line. For most soil mechanics problems, it is sufficient to approximate the shear stress on the failure plane as a linear function of the normal stress (Coulomb, 1776). This linear function can be written as

$$\tau_f = c + \sigma \tan \emptyset \qquad 3.1$$

where, c = cohesion

ϕ = angle of internal friction

σ = normal stress on the failure plane

τ_f = shear strength

The preceding equation is called the Mohr-Coulomb failure criterion.

In saturated soil, the total normal stress at a point is the sum of the effective stress (σ') and pore water pressure (u), or $\sigma = \sigma' + u$. The effective stress σ' is carried by the soil solids. The Mohr-Coulomb failure criterion, expressed in terms of effective stress as below:

$$\tau_f = c' + \sigma' \tan \emptyset' \qquad 3.2$$

where, c' = effective cohesion, and

ϕ' = angle of internal friction, based on effective stress.

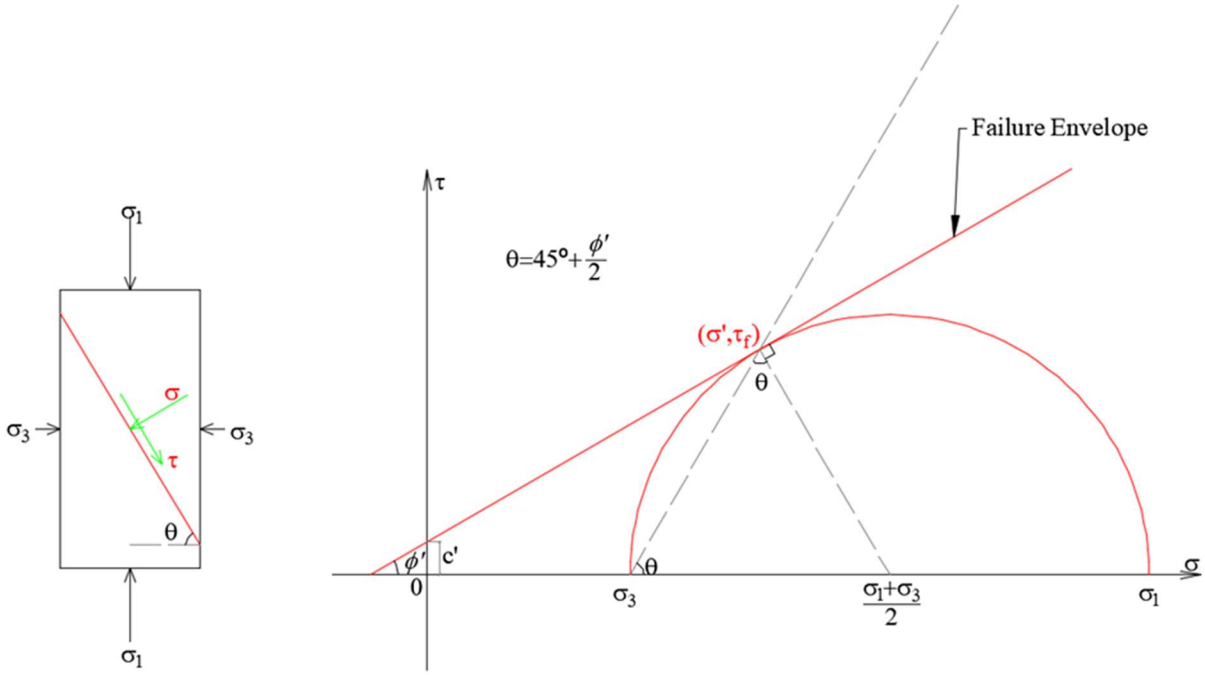

Figure 3-1 Mohr Coulomb shear failure criterion with Mohr circle of stress

Thus, Equation 3.1 and 3.2 are expressions of shear strength based on total stress and effective stress. The value of effective cohesion, c' for sand and inorganic silt is zero. For normally consolidated clays, effective cohesion c' can be approximated as zero. However, overconsolidated clays have values of effective cohesion c' that are greater than zero. The angle of friction, ϕ', is sometimes referred to as the drained angle of friction.

The significance of Equation 3.2 can be explained by referring to Figure 3-1, which shows stress on a soil mass and the plot of the failure envelope. If the magnitudes of σ' and τ on failure plane are plotted as a point on Figure 3-1 and if falls below the failure envelope, shear failure will not occur along the plane. If the effective normal stress and the shear stress on plane falls on the failure envelope, shear failure will occur along that plane. A state of stress on a plane represented by a point above the failure envelope cannot exist, because shear failure in a soil would have occurred already (Das, 2001).

3.2 Unsaturated Soil Mechanics

3.2.1 Introduction

Unsaturated soils contain both air and water phases in their pores. They can be either naturally occurring soils, such as those found in arid and tropical zones, or artificially created (man-made) soils such as those that are formed by compaction.

Fundamental principles pivotal to understanding the engineering behavior of saturated soils emerged with the concept of effective stress in the 1930s (Terzaghi, 1943). However, there was considerable interest in understanding the behavior of unsaturated soils along with saturated soils. This is documented through the research papers published in the First International Conference on Soil Mechanics and Foundation Engineering in 1936.

Theoretically based framework of stress state variables for interpreting the engineering behavior of an unsaturated soil was proposed 40 years later within the context of multiphase continuum mechanics (Fredlund & Morgenstern, 1977). Two stress state variables, namely; net normal stress, $(\sigma_n - u_a)$ and matric suction, $(u_a - u_w)$ which is the difference between the pore-air pressure, u_a and pore-water pressure u_w are used for explaining the behavior of unsaturated soils.

The behavior of unsaturated soils could be viewed as a natural extension of saturated soil behavior (Fredlund & Morgenstern, 1976).

The seven international conferences held in Paris, France (1995), Beijing, China (1998), Recife, Brazil (2002), Carefree, U.S.A (2006), Barcelona, Spain (2010), Sydney, Australia (2014), and Hong Kong, China (2018) have been fruitful to exchange the latest developments in the research and application of unsaturated soil mechanics. In recent years, there is an increased interest in the application of the mechanics of unsaturated soil into engineering practice.

3.2.2 Various Phases in Unsaturated Soils

Unsaturated soils contain both air and fluid phases in their pores. Soil in a state of saturated condition is commonly referred to as a two-phase mixture (i.e., solids and water), but an unsaturated soil includes two other independent phases (i.e., air and the contractile skin or the air–water interface) (Fredlund et al., 2012). The contractile skin acts like a thin membrane interwoven throughout the voids of the soil, acting as a partition between the air and water phases. It is the interaction of the contractile skin with the soil structure that causes an unsaturated soil to have a significant influence on its mechanical behavior (i.e., volume change and shear strength properties). The unsaturated soil properties change in response to the position of the contractile skin. It is important to view an unsaturated soil as a four-phase mixture for purposes of stress analysis, within the context of multiphase continuum mechanics (Fredlund & Morgenstern, 1976).

The contractile skin can be considered as part of the water phase with regard to changes in volume–mass soil properties but must be considered as an independent phase when describing the stress state and phenomenological behavior of an unsaturated soil (Fredlund et al., 2012). Numerous research studies on the nature of the contractile skin point toward its independent role in the mechanics of unsaturated soils. A surface tension of approximately 75 MN/m translates into a unit stress in the order of 140,000 kPa.

The soil suction is defined in terms of the free energy or the relative vapor pressure (relative humidity) of the soil moisture. A meniscus forms at the soil-air interface, due to the surface tension, resulting in reduced vapor pressure in the water. The vapor pressure decreases, becomes more negative, and the matric suction pressure increases as the radius of curvature of the

meniscus decreases. The size of the soil pores decreases with a decrease in soil particle size which then affects the size of the radius of curvature and consequently the matric suction pressure. The vapor pressure decreases as the degree of saturation decreases (Han et al., 2017).

Soil suction is a key factor that controls effective shear stress of unsaturated soils and is influenced by particle size distribution (PSD), soil type, fine particle percentage, soil fabric orientation, and drainage boundary conditions (Bishop, 1959). Rajeev et al. (2012) suggested that soil suction is highly sensitive to climate changes. In addition to soil suction, soil temperature has a significant influence on the track foundation failures in cold regions, as soil freezing and thawing can control permeability, stiffness, and strength (Wang et al. 2007).

The suction in the unsaturated soils can range from zero at the water table to a maximum tension of approximately 1,000,000 kPa under dry soil conditions (Fredlund et al. 2012). For the same range of suction, degree of saturation of the soil varies from 100% to zero. The suction in soils varies from zero to 1,000,000 kPa irrespective of the type of soil. The changes in soil suction result in distinct zones of saturation. The zones of saturation can be been defined in situ as well as in the laboratory through the use of soil–water characteristic curve as shown Figure 3-2 (Vanapalli et al. 1999).

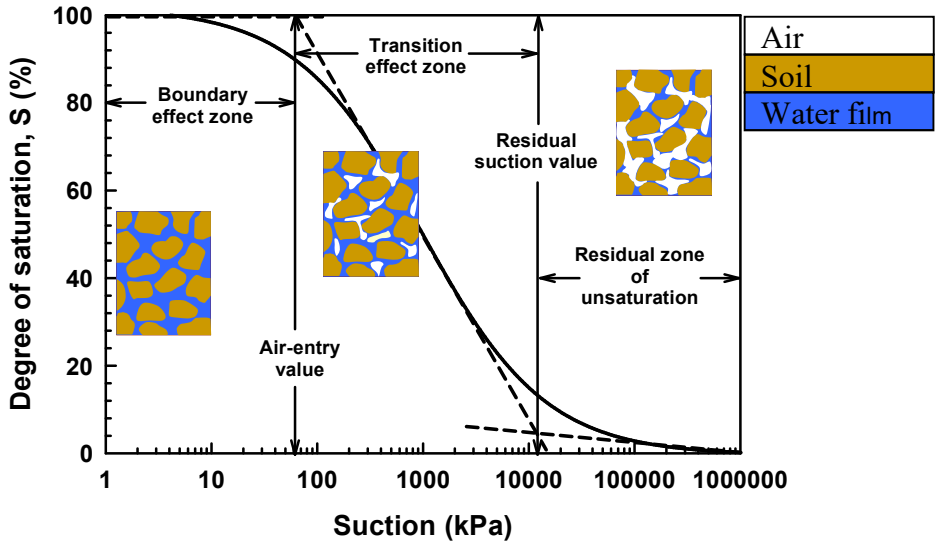

Figure 3-2 Soil–water characteristic curve and its various zones (modified after Vanapalli et al. 1999)

3.2.3 Soil Water Characteristic Curve

The Soil Water Characteristic Curve (SWCC) (Fredlund et al., 2012) defines the amount of water in a soil versus soil suction (Figure 3-2). The amount of water in the soil is commonly defined in more than one way and it is difficult to restrict the definition to a single variable. Three common variables used to define the amount of water in the soil are: gravimetric water content, w, volumetric water content, θ, and degree of saturation, S. This relationship is referred in the literature using different terms which include Soil Water Retention Curve (SWRC) or Soil Moisture Curve (SMC) or Soil-Water Characteristic Curve (SWCC) as used in this thesis.

The SWCC can be divided into three zones; namely, boundary effect, transition and residual zones (Vanapalli et al., 1999). Within the boundary effect zone, soil pores are saturated with capillary water under suction. It is likely there may be some air in the form of occluded bubbles, which is not continuous. As suction exceeds the air-entry suction, air starts to enter the largest soil pores and subsequently drain the capillary water out of the soil. In this stage of desaturation, both air phase and water phase are continuous; however, liquid phase flow and capillary effect tends to decrease with increasing suction. When suction exceeds the residual suction, the amount of capillary water and the contribution of capillary effect and suction towards the skeleton constitutive stress become negligible. Water transports in the soil pores only in the form of vapor as the water phase retreats to the micro-pores and becomes discontinuous in the residual zone of desaturation. In this stage, the rate of the desaturation of water becomes remarkably slower regardless of the large suction increase. This characteristic can be recognized from the flattened part of the SWCC at large suction values.

There is no unique SWCC but rather, there is an infinite number of scanning curves contained within a drying (desorption) boundary curve and an adsorption (wetting) boundary curve (Figure 3-3) (Fredlund et al., 2012). It is the primary drying and wetting curves that are of greatest relevance to unsaturated soil mechanics. The drying curve is easier to measure and is therefore the curve is generally measured in the laboratory. Most of the research studies published in the literature use the drying SWCC (Vanapalli et al., 2008). The scanning curves define the pathways between the boundary curves. However, for many geotechnical practical applications, a drying SWCC may be sufficient. Several models are available in the literature that takes into account of hysteresis. Several investigators have used SWCC as a tool in the prediction of

engineering properties of unsaturated soils such as the coefficient of permeability and the shear strength.

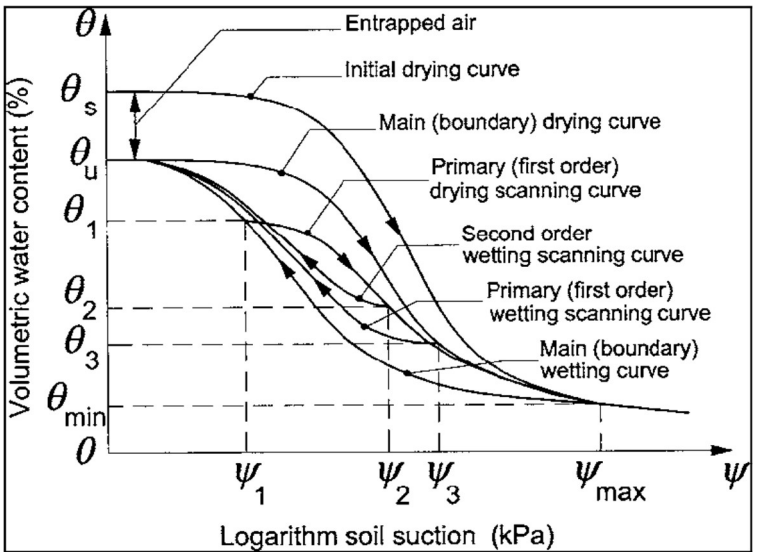

Figure 3-3 Bounding and scanning curves that comprisethe drying and wetting behavior of an unsaturated soil (Fredlund et al., 2012)

3.2.4 Shear Strength

Several investigators made an attempt to explain the unsaturated soils behavior using a single stress state variable. These equations proposed in the literature relate different stresses into a single stress variable through the inclusion of other soil properties. The best known single-valued relationship to describe effective stress in unsaturated soils is Bishop's equation (Bishop, 1959):

$$\sigma' = (\sigma - u_a) + \chi(u_a - u_w) \quad 3.3$$

where, σ' = effective stress and

χ = soil parameter related to degree of saturation, S which ranges from 0 to 1.

The shear strength constitutive relationship provides a mathematical equation relating the normal and shear components of the stress tensor. Any one of several shear strength failure criteria could be extended from saturated soil conditions to unsaturated soil conditions. The Mohr–Coulomb failure criterion was extended to embrace unsaturated soils by (Fredlund et al. 1978). In a general form, the shear strength equation can be written as follows:

$$\tau = c' + (\sigma_n - u_a)tan\emptyset' + (u_a - u_w)f_1 \quad 3.4$$

where, τ = shear strength;

c' = effective cohesion intercept;

σ_n = total normal stress on the failure plane at failure;

ϕ' = effective angle of internal friction;

f_1 = soil property function defining the relationship between shear strength and soil suction; the derivative of which [i.e., $df_1/d(u_a - u_w)$], gives the instantaneous rate of change in shear strength.

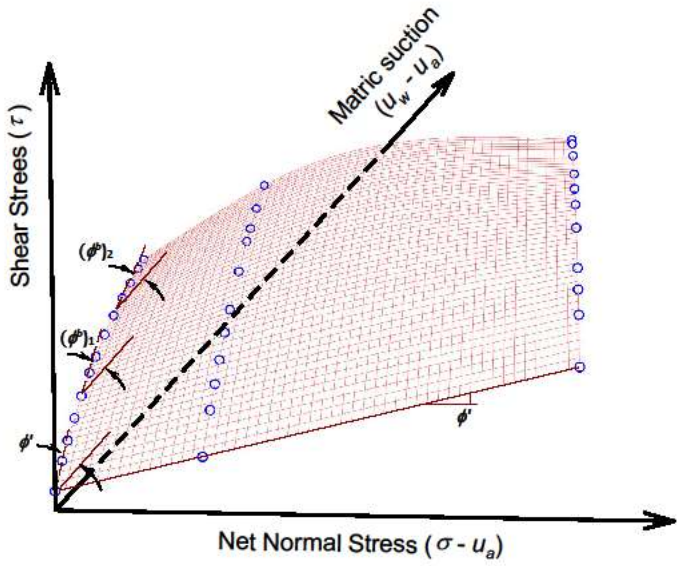

Figure 3-4 Extended Mohr-Coulomb failure surface written as a function of the stress state using Fredlund et al. 1978 equation

Figure 3-4 shows a three-dimensional constitutive surface with matric suction plotted perpendicular to the conventional two-dimensional Mohr–Coulomb plot. The shear strength parameters c', and ϕ' are presented as saturated soil constants; however, the soil property function, f_1, varies in response to the amount of water filling the voids of the soil (i.e., it is a function of matric suction) (Gan et al., 2006).

There is a relationship between the SWCC and the shear strength (Vanapalli et al., 1996) as shown in Figure 3-5.

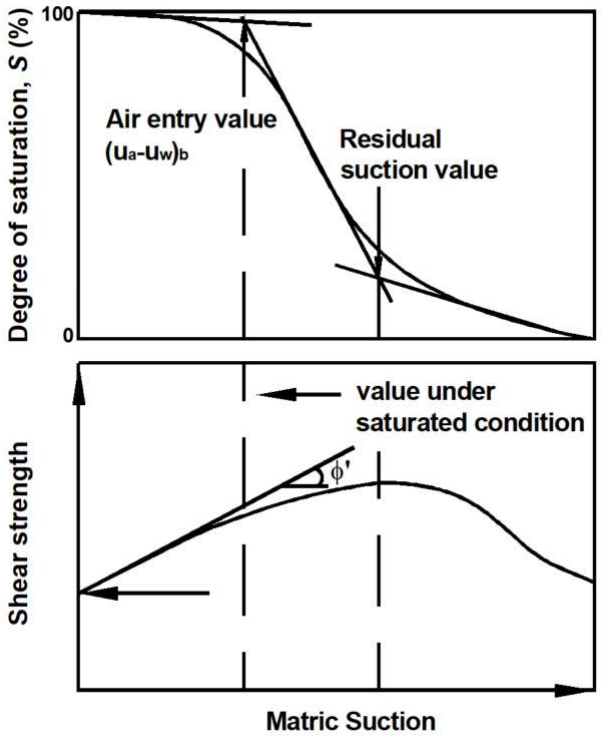

Figure 3-5 Curvature to the shear strength envelope with respect to matric suction (modified after Vanapalli et al. 1996)

The peak shear strength of an unsaturated soil bears a relationship to key points along the SWCC. Under low suction conditions (i.e., less than the air entry value of the soil), the derivative of f_1, tends to equal the tangent of the effective angle of internal friction of the saturated soil (i.e., tan ϕ') (Vanapalli et al., 1996). At high suction conditions (i.e., greater than residual soil suction), the derivative of f_1, has been shown to tend toward zero for several soils with varying silt and clay contents. Sandy soils have shown that the slope may even become negative at suctions greater than the residual value (Vanapalli et al., 1996).

A linear form of the general shear strength equation [i.e., 3.5] was published by Fredlund et al. 1978):

$$\tau = c' + (\sigma_n - u_a)tan\emptyset' + (u_a - u_w)tan\emptyset^b \quad 3.5$$

The linear form is more appropriate for limited ranges of matric suction, particularly for fine-grained soils. Some of the earlier unsaturated soils shear strength data sets (Bishop et al. 1960)

show a close fit to the linear equation (Fredlund et al., 2012). The linear form is also more convenient to use for shear strength solutions.

Vanapalli et al (1996) proposed a semi-empirical procedure based on the equation proposed by (Fredlund et al., 1978) to predict the variation of shear strength with respect to matric suction using the saturated shear strength parameters and the SWCC as given below.

$$\tau = c' + (\sigma_n - u_a)tan\emptyset' + (u_a - u_w)(S^K)tan\emptyset' \quad 3.6$$

where, S = the degree of saturation and

κ = is fitting parameter.

Several other empirical or semi-empirical procedures are available in the literature to predict or estimate the shear strength of unsaturated soils.

Most of data on shear strength of unsaturated soils appear to have been undertaken on soils that were initially compacted to an initial water content and density and then wetted such that the initial suction was allowed to come toward a zero value (Gan et al., 2006; Vanapalli et al., 1996). The soil specimens are then subjected to a series of increasing matric suctions along the desorption branch of the SWCC. Since there is hysteresis between the drying and wetting curve it would be anticipated that soils may exhibit a different shear strength envelope if first subjected to high matric suction conditions and then reduced to a series of suction values along the wetting curve.

Melinda et al. 2004 reported the shear strength results on a residual soil from Singapore tested along both the drying curve and the wetting curve. The results showed that the measured shear strengths along the drying curve are higher than those measured along the wetting curve. These results can be explained on the basis of the hysteresis of the SWCC that shows the matric suction having a greater cross-sectional area over which to act along the drying curve, for a specific suction. The difference in shear strength between drying and wetting conditions appears to be related to the magnitude of the drying and wetting hysteresis loop.

3.3 The nature of compacted subgrade

The soil shear strength and stiffness are two key properties that significantly influence the performance of subgrade. An increase in subgrade water content contributes to a decrease in

strength and stiffness of fine-grained soil, resulting in higher plastic deformation under cyclic train loads, consolidation settlement or massive shear failures.

The compacted subgrade soil is a typical example of an unsaturated soil with its moisture and suction influenced by the environmental factors. Moisture content of compacted pavement materials during their service life can fluctuate seasonally due to environmental factors such as surface infiltration and evaporation, freeze–thaw cycles, and variation of the ground water table (Han et al. 2017). As compacted soils are initially in an unsaturated state, their hydraulic and mechanical behavior should be interpreted within the framework of the mechanics of unsaturated soils using suction (s) as the primary stress-state variable (Fredlund et al. 2012; Sheng, 2011).

The stiffness - suction and shear strength - suction relationships for unsaturated soils are non-linear and sensitive to various factors such as the external stress, moisture regime, soil type, hydraulic hysteresis, soil structure, aging and testing technique. The soil-water characteristic curve (SWCC), which represents the moisture regime - suction relationship, is frequently used in the interpretation and prediction of the stiffness - suction and shear strength - suction relationships (Alonso et al. 1990; Fredlund & Rahardjo, 1993; Alonso et al., 2013; Gallipoli et al. 2003; Gens, 2010; Sawangsuriya et al. 2009; Thu et al. 2007).

Figure 3-6(a) and Figure 3-6(b) show an example, for a glacial till from Saskatchewan, Canada (liquid limit w_L = 35.5%, plastic index I_p = 18.7%, optimum moisture content w_{opt} = 16.3%), the SWCC and the peak shear strength (τ_p) - suction (s) relationship obtained from suction-controlled multistage direct shear tests under a net normal stress of 25 kPa (data from Vanapalli et al. 1996). The relationship between the SWCC and the τ_p shown in Figure 3-6(a) and Figure 3-6(b) is corroborated by the testing data of other soils from the literature on the relationships between the SWCC and the stiffness and shear strength properties.

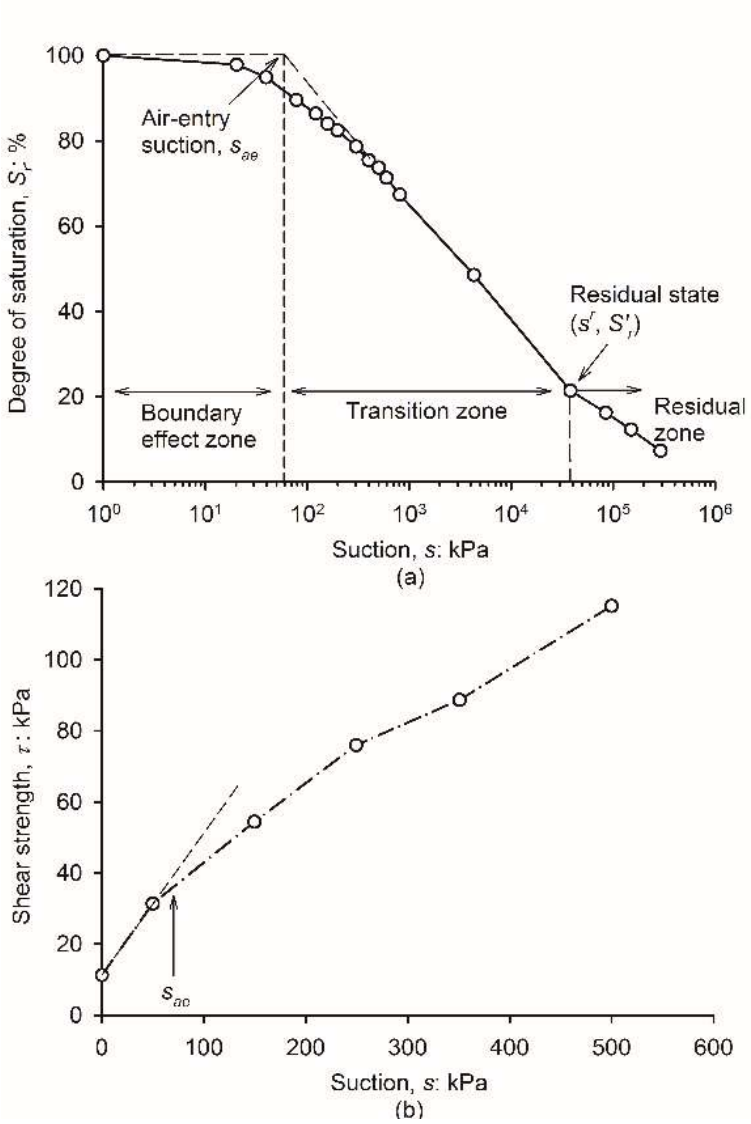

Figure 3-6 SWCC Curve and its relationship with shear strength (modified after Vanapalli et al., 1996)

It is well recognized from experimental investigations that the stiffness and shear strength properties exhibit non-linear evolution with suction and water degree of saturation (see Figure 3-6(b)) and also in (Cunningham et al. 2003; Escario & Saez, 1986; Jotisankasa et al. 2009; Lu & Kaya, 2014; Ng & Yung, 2008; Ng & Zhou, 2014; Oh et al., 2009; Sivakumar et al. 2013; Wheeler & Sivakumar, 1995). Such a behaviour can be related to the variation of the capillary water and its associated capillary effect and suction, which contributes to the changes in the skeleton constitutive stress and therefore, the stiffness and shear strength properties (Alonso et al. 2010; Baker & Frydman, 2009; Lu & Likos, 2006). Within the boundary effect zone, the soil

system stays in a stage of capillary saturation and can be treated as a continuum medium. The increasing suction fully contributes to the constitutive stress of the soil skeleton, resulting in a significant increase in the stiffness and shear strength properties. The contribution of suction becomes less efficient with further suction increase and the corresponding drainage of the capillary water in the transition zone, which results in a less significant increase in the stiffness and shear strength properties.

It should be noted that, apart from the suction, the physicochemical inter-particle forces such as the van der Waals and cementation forces also influence the mechanical properties (Baker & Frydman, 2009; Lu & Likos, 2006). The physicochemical inter-particle forces are different for different soil types. Their influence on the soil mechanical behaviour for natural soils may be secondary compared with that of suction within the lower suction range. At higher suction range, the influence of suction decreases with decreasing capillary water and the physicochemical inter-particle forces start to dominate. For example, the stiffness and shear strength for cohesionless soils such as gravels and sands usually decrease in the residual zone of desaturation due to the decrease in the contribution of the suction and the weak physicochemical inter-particle forces (Escario et al. 1989; Ghayoomi & McCartney, 2011; Oh et al. 2009; Wu et al. 1984). However, for cohesive soils, stiffness and shear strength behaviour in the high suction range varies for different soil types. Decreasing, constant or increasing trends of stiffness and shear strength behaviour are respectively reported for various soils (Cunningham et al. 2003; Escario et al. 1989; Geiser et al. 2006). It would be rather difficult to clearly determine or distinguish the boundary suction value or moisture regime where the influence of the physicochemical forces outweigh that of the suction. However, it is reasonable to assume, for natural soils, that the capillary effect and suction govern i) the mechanical behaviour of cohesionless soils over the whole suction range, and ii) the mechanical behaviour of cohesive soils in the lower suction range where liquid flow is typically predominant, especially the in-situ suction range which is typically between 0 kPa and 600 kPa (Cui & Delage, 1996; Khalili & Khabbaz, 1998; Vanapalli et al. 1996). Within higher suction range, physicochemical inter-particle forces should be taken into account, in addition to suction, for the reasonable interpretation of the mechanical behaviour of cohesive soils.

3.4 The Coefficient of Earth Pressure at Rest

3.4.1 Definition of Coefficient of Earth Pressure at Rest (K_0)

The coefficient of earth pressure at rest is a relationship between the in situ horizontal and vertical stress and usually expressed as a factor (Sivakumar et al. 2002). The relationship factor was first proposed by Donath in his 1891-paper for total stresses (Brooker & Ireland, 1965; Hamouche et al. 1995) as Equation 3.7

$$K_0 = \frac{\sigma_h}{\sigma_v} \qquad 3.7$$

where, K_0 is the coefficient of earth pressure at rest,

σ_v is vertical earth stress, and

σ_h is horizontal earth stress.

Considering the pore pressure, the horizontal and vertical effective stresses are used to express K_0', as seen in Equation 3.8 (Mesri & Castro, 1987; Mesri & Hayat, 1993; Schmertmann, 1983), and it will be used in this report as the coefficient of earth pressure at rest.

$$K_0' = \frac{\sigma'_h}{\sigma'_v} \qquad 3.8$$

where, K'_0 is the Coefficient of Earth Pressure at Rest,

σ'_v is vertical effective stress, and

σ'_h is horizontal effective stress.

The above Equation 3.8 has a conditions of no lateral deformation under vertical loading (Mesri & Hayat, 1993).

3.4.2 The previous study

Jaky (1944) presented a theoretical relationship between the K_0 value and the angle of internal friction ϕ' by analyzing a talus of a granular soil mass. In this study, the angle of repose of the talus was equal to the angle of internal friction of the granular soil, and the lateral pressure acting on a plane passing through the apex of the talus and perpendicular to the base was the lateral earth pressure at rest. He divided a talus of granular soil mass into two zones including the outer zone and the inner zone. In the outer zone, sliding planes were developed and stresses on the

planes were determined by the Rankine theory. In the inner zone, shear stress distribution on any horizontal plane was assumed to be a parabolic shape and decreased to zero at the center vertical plane of talus.

The relationship coefficient of earth pressure at rest as provided by Jaky (1944) is

$$K_0 = (1 + \frac{2}{3} sin\,\phi') \frac{1 - sin\,\phi'}{1 + sin\,\phi'} \quad 3.9$$

Mesri & Hayat, (1993) pointed out that a granular soil mass forming a talus was loose, normally consolidated and young, and therefore, Jaky's analysis corresponds to loose normally consolidated young granular soils that have not been densified.

Jaky (1948) dropped out the $(1 + \frac{2}{3} sin\,\phi')/(1 + sin\,\phi')$ in Eq.3.9, and the coefficient of earth pressure at rest of normally consolidated loose granular soils, generally used in engineering practice, becomes

$$K_0 = 1 - sin\,\phi' \quad 3.10$$

Nevertheless, Mayne & Kulhawy (1982; 1983) provide a summary of the effects of stress history on K_0, including data compiled from over 170 different soils tested and reported by many researchers. They conducted a statistical analysis of this data and determined relationships between at rest earth pressure and soil stress history. Based on these results, Jaky's formula Eq. 3.10 was found to have close agreement with the data for normally consolidated soil and deviated significantly for overconsolidated soil. Mayne & Kulhawy (1982; 1983) provided a relationship between K_0 and the overconsolidation ratio (OCR) that builds on Jaky's simplified formula as follows:

$$K_0 = (1 - sin\,\phi')OCR^{sin\,\phi'} \quad 3.11$$

Moreover, Feda (1984) objected that the same equation claims the dependence of K_0 on the strength parameter, although K_0 is a deformation parameter.

Cherubini et al (1990) found that values of K_0, calculated using Eq. 3.11, are 3.5% less than the average measured values, which is practically acceptable. Hanna & Al-Romhein (2008) compared the theoretical values predicted by Mayne & Kulhawy (1982; 1983) with experimental results conducted on well-graded dry silica sand. The comparison indicated that Mayne and Kulhawy's formula provided good agreement with the experimental results of the coefficient of

earth pressure at rest K_0 up to OCR = 3.0, whereas the theoretical values underestimated K_0 thereafter.

Despite its practical significance and attractive simplicity, Jaky's formula and its derivative (i.e., Eq. 3.9 and 3.11) claim the dependence of K_0 only on the soil internal friction angle, ϕ'. However, Feda (1984) proved theoretically that K_0 depends on soil deformation. The ignorance of soil deformation in calculating K_0 using Jaky's formula is considered a major deficiency, as stated by (Feda, 1984).

Massarsch (1986) proposed an empirical formula to estimate the K_0 of normal consolidated fine-grained soils:

$$K_0 = 0.44 + 0.42PI \qquad 3.12$$

where, PI is the plasticity index.

Guo (2010) found that the coefficient of earth pressure at rest K_0 of granular materials is not a unique function of neither the critical friction angle ϕ'_{cv} or the peak friction angle ϕ'_p. Instead, the effect of density and stress level on K_0 should not be neglected.

Zhao et al. (2010) conducted consecutive consolidated isotropically drained triaxial tests and concluded that the coefficient of the earth pressure at rest is not constant at high pressure, but shows an increasing trend as the consolidation stress increases. The methods of predicting K_0 values from the Jaky and Roscoe equations are not applicable for soils without cohesion with bilinear strength variations. The nonlinear characteristics of K_0 are related to the variation in the void ratio during compression. Zhao et al. (2010) also proposed linear functions for the calculation of K_0 values based on test results in order to interpret the rules of nonlinear variation for the coefficient of earth pressure at rest.

3.4.3 The factors influencing the value of coefficient of earth pressure at rest

The research of field and laboratory investigations of coefficient of earth pressure at rest, has made it clear that the value of coefficient of earth pressure at rest is affected by both the material properties of the soil and the stress history (Shin & Santamarina, 2009).

3.4.3.1 Effect of Stress History (Unloading and Reloading)

The horizontal stress is affected by the loading history of the deposit investigated according to (Hamouche et al. 1995; Shin & Santamarina, 2009; Sivakumar et al. 2002).

The relationship between the radial and axial stress for Reid-Bedford sand under repeated load and unload cycles is shown in Figure 3-7 (Al-Hussaini, 1981).

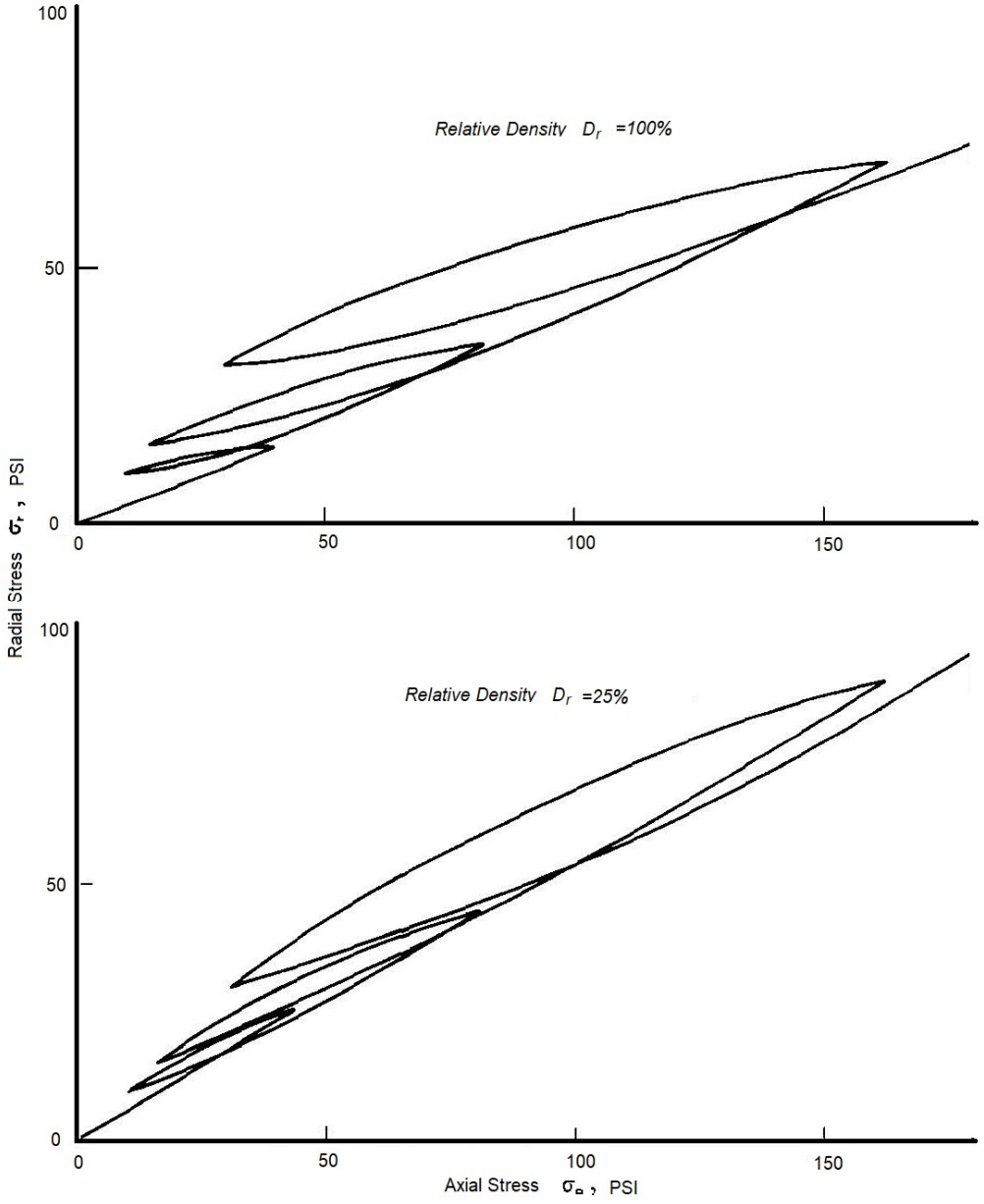

Figure 3-7 K_0, Relationship of radial versus axial stress for Reid-Bedford sand (Al-Hussaini, 1981)

The relationship for the first loading cycle may be approximated by a straight line. However, upon unloading, the relationship becomes nonlinear with a flatter curvature at the higher stress level, which then becomes concave downward with increasing slope as unloading continues. The relationship during first reloading is also nonlinear but concave upward with slope much flatter than the first loading cycle. This trend was similar for the dense specimen that exhibited a flatter slope than the loose specimen for any particular loading or unloading cycle. These results also indicate that the value of coefficient of earth pressure at rest is always lower on loading than unloading. It also indicates that the secant value of coefficient of earth pressure at rest increases with increasing number of cycles, which implies that coefficient of earth pressure at rest is dependent on stress history (Al-Hussaini, 1981).

Normally consolidated clay is often referred to a soil which only experienced primary loading, while overconsolidated clays have experienced preconsolidation pressures which are higher than the present overburden pressures due to unloading (Sivakumar et al. 2002). Many researchers consider overconsolidated clays has soils that have preconsolidation pressure higher than the present overburden pressure, regardless of what has caused the preconsolidation pressure. Sivakumar et al (2002, 2009) stated that the value of coefficient of earth pressure at rest is a constant during first loading that is horizontal stress and increases proportionally with vertical loading. However, during unloading process, the horizontal stress is no longer proportional and decreases with the vertical stress. The horizontal stress reduces at a slower rate than vertical stress, because the interparticle locking contributes a higher horizontal stress than the vertical stress.

The difference of coefficient of earth pressure at rest between loading and unloading is illustrated in Figure 3-8 (Sivakumar et al., 2002). For soil deposits with high overconsolidation values, with much higher preconsolidation pressure than the current loading, the horizontal stress is likely to be greater than the vertical stress. Hence, the value of coefficient of earth pressure at rest tend to increase with the overconsolidation ratio, OCR (Sivakumar et al. 2009). This has also been confirmed experimental studies by Hamouche et al. (1995).

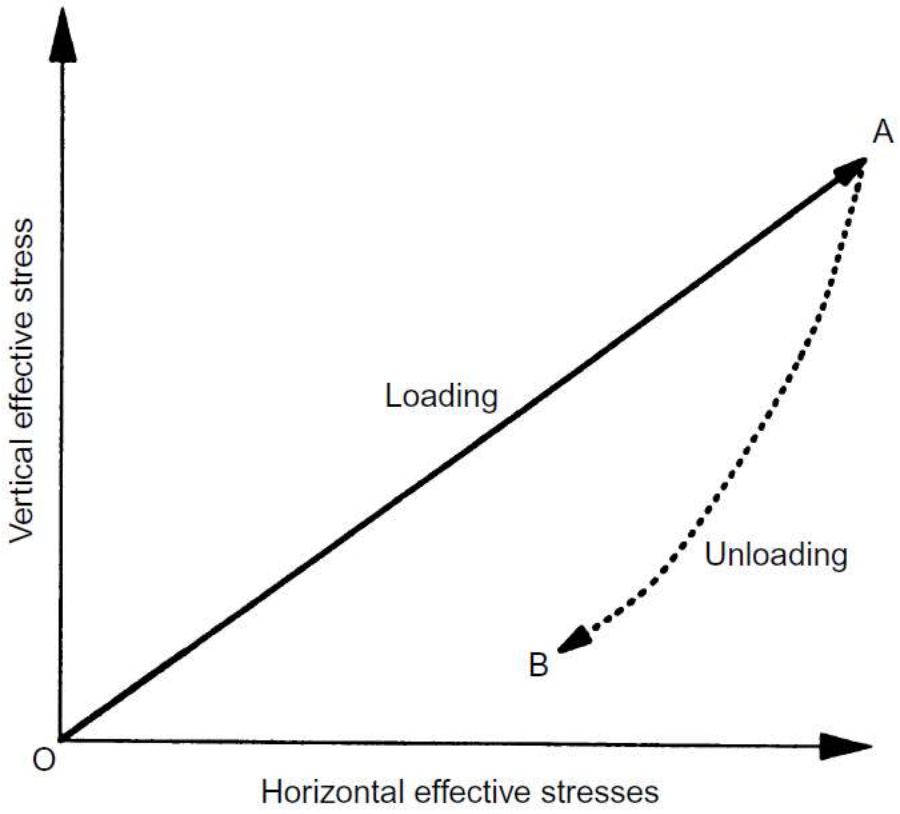

Figure 3-8 Variation of vertical and horizontal stresses during loading and unloading (Sivakumar et al. 2002)

OCR is defined in Equation 3.13 (Mayne & Kulhawy, 1982; 1983).

$$OCR = \frac{p'_c}{\sigma'_{v0}} \tag{3.13}$$

where, p'_c is the effective vertical preconsolidation pressure, and

σ'_{v0} is the current effective overburden pressure.

There is a clear link between coefficient of earth pressure at rest and OCR from several research studies (Keskin et al., 2004; Mayne & Kulhawy, 1982; 1983; Sivakumar et al., 2009). As over consolidation ratio increases, the coefficient of earth pressure at rest also increases.

One straightforward example of such overconsolidated materials are clays deposited towards the end of the last ice age in Norway (Gylland et al. 2013). As the ice melted (unloading) and the ground rebound, the clays deposited in the seabed were brought up to become continent.

Subsequent erosion resulted in further unloading of the overburden pressure and finally form overconsolidated clay materials.

3.4.3.2 Time Effects

As per the discussions summarized in earlier sections, the consolidation and overconsolidation characteristics influence the coefficient of earth pressure at rest. El-Emam (2011) suggested overconsolidation ratio of sandy soil is an important factor that affects the at-rest lateral earth force. However, consolidation characteristics are related to the time, due to this reason, time also has an effect on the coefficient of earth pressure at rest.

Several researchers concluded that significant aging effects occur in virtually all types of soils, including dry sands (Schmertmann, 1991; Tomás et al., 2007). These investigators found many examples that demonstrate soil aging over engineering times can cause a general 50 to 100% improvement effect in many key soil properties. These evidences indicate that most engineering-time age-strengthening effects are drove by in situ effective stresses and result from increased basic soil friction, including dilatancy effects, but not from increased cohesion. These effects include grain slippage, soil-structure dispersion, increased interlocking, and a postulated internal arching of stresses. These investigators differentiated between chemical time effects that include thixotrophy and mechanical time effects that include secondary compression and other effects. Schmertmann (1991) argued that both types of time effects resulted in an increased strength of the material and that both involve the flocculation and dispersion of particles. On the other hand, thixotrophy is most likely to occur during very low effective stresses whilst mechanical time effects will dominate under higher stresses. Hence, the mechanical time effects will be much more pronounced from an engineering practice point of view.

3.4.3.3 Chemical Changes

Mesri & Castro, (1987) confirmed that chemical changes can contribute to an increase in interparticle resistance, including cation exchange and the bonding of the soil fabric by components such as oxides, carbonates, silicates, and organic molecules. The increased resistance can be relatively small or strong that contribute to brittle links at particle contacts.

Bjerrum (1967) stated exchange of cations and cementation are the most important chemical bonding effects in the relatively young Norwegian clays. Exchange of cations is a direct

consequence of rainwater entering the clay. The basic factor governing the chemical stability of minerals in clay is the *pH* value of the pore water; any change reducing the *pH* value of the pore water will increase the rate of disintegration of the minerals, and vice-versa.

The geological and topographic conditions in Norway are such that as soon as a clay deposit rises above seawater level it will in almost all cases be subjected to a slow exchange of the original pore water by percolating rainwater. This will lead to a gradual removal of the Na^+ ions. This in itself has no great effect on the *pH* value, but rainwater contains dissolved O_2, and CO_2. CO_2, lowers the pH of the pore water and the O_2 coming into contact with organic matter forms humic acids which also reduce the *pH*-value. If this slow but persistent process advances to such an extent that the pH is reduced to a sufficiently low value, then a disintegration of feldspar, mica and chlorite will commence. The disintegration results in liberation of cations of higher order than Na^+ which collect on the surface of the clay particles. The effect of this base-exchange is to raise the plasticity of the clay and additional strength is developed. The disintegration also causes the liberation of other chemical compounds which tend to increase the *pH* and thereby prevent the process. The development of structural strength by exchange of Na^+ ions by ions of higher order thus requires a continuous supply of *pH*-reducing agents to the clay (Bjerrum, 1967).

The K^+ ions are liberated from the mineral lattice of feldspar and mica, two minerals which exist in all Norwegian clays. The K^+ ions are believed to be the dominant ones in the early phase of this process and govern the development of additional structural strength in the relatively young Norwegian clays (Bjerrum, 1967).

Fischer et al. (1978) investigated the process of cementation, in which sediments eventually develop from soils into rock under high pressure, also known as lithification. In clays exposed to this process, there exists additional chemical bonding in addition to the friction and cohesion found in uncemented clays. In addition, Fischer et al. (1978) also investigated the possibility of developing cementation in two normally consolidated samples of Drammen clay. The authors found that the strength of a normally consolidated clay increased with about 35 - 40 % as a consequence of the cementation process. For a stiff clay the change in engineering properties was essentially the same regardless of whether the preconsolidation originated from mechanical overconsolidation or cementation.

Thixotropy is a strength increasing process due to reversible changes in viscosity (Fioravante et al. 1998; Schmertmann, 1991). Thixotropic behaviour are able to stiffen with a great increase in strength over a short period of time and thereafter loose most of its strength and become a viscous fluid when exposed to some mechanical disturbance. Schmertmann (1991) argued that the process is the result of a dispersion-flocculation process occurring for instance during the deposition of sediments. Even when exposed to almost no effective stresses, particles will tend to accumulate due to attractive forces. Because of the low stress level, it takes almost no disturbance for the particles to break apart.

The interparticle force and soil structure of bentonite were notably affected by the salinity, whereas for kaolin and marine clay, the soil structure appeared insensitive to the pore fluid salinity (Yan & Chang, 2015). The K_0 coefficient and friction angle of kaolin and marine clay were barely affected by the pore fluid salinity. However, as the salt content increased, the K_0 coefficient of bentonite decreased significantly and the friction angle increased noticeably (Yan & Chang, 2015). The mineral type may play an important role in the relationship between the salt content and K_0 coefficient. Due to the difference in the material structure, different minerals have different sensitivities to the ion concentration. For soils that mainly consist of sensitive minerals (bentonite), the effect of the salt content on the K_0 coefficient and friction angle was significant (Yan & Chang, 2015). K_0 predicted using Jaky's formula was close to the measurement for kaolin regardless of its salt content. The prediction became less promising in marine clay, for which consistently underestimation was seen, and the prediction error appeared to increase with the increase in salt content. Jaky's formula gave a reasonable prediction of K_0 for bentonite at higher salinity. Prediction using the Atterberg limits failed in all cases, particularly for bentonite at low salinity (Yan & Chang, 2015).

3.4.3.4 Moisture change

Water table changes associated rainfall infiltration, evaporation or freezing can significantly influence the preconsolidation pressure (Tomás et al., 2007). When a material experiences drying, the loss of pore water will generate suction (Shin & Santamarina, 2009). During repeated wet and dry cycles, very fine soils may experience high effective stresses due to the suction. The effect of moisture is likely to mainly affect the first few meters of a soil deposit, where the existing preconsolidation due to overburden load is quite small (Tomás et al., 2007).

The laboratory tests performed by Abrantes & Pereira de Campos (2019) suggest the coefficient of earth pressure at rest (K_0) of the colluvium soil under saturated condition was equal to K_0 of 0.36. This value is higher than the average value of K_0 of 0.26, obtained under a suction of 10 kPa, following a loading path. This is in agreement with other studies in the literature that suggest the K_0 value decreases with an increase of suction or decrease of the degree of saturation.

Mahar & O'Neill (1983) investigated the geotechnical properties of dried clays and suggested that the suction process may generate cracks in the material. These cracks will lead to variable suction force, resulting in high variability in both preconsolidation pressure and undrained shear strength.

3.5 The Residual Shear Strength

The residual shear strength is the minimum strength that a soil can offer to large shear displacements under given effective normal stresses. It is the available shear strength of landslides which underwent large displacements on a slip surfaces (Scaringi & Di Maio, 2016). There is extensive research available in the literature during the past three decades for rational interpretation of the residual shear strength behavior (Mesri & Shahien, 2003). The residual shear strength parameters depend on the composition of both the solid skeleton and the pore fluid (Scaringi & Di Maio, 2016). In addition, several results reported in the technical literature, also suggest a dependence on the displacement rate, showing that the residual shear strength may increase, decrease or remain constant with the displacement rate.

3.5.1 Drained residual strength of cohesive soils

Lupini et al (1981) studied drained residual strength of cohesive soils and recognized three modes of residual shear behavior; namely, a turbulent mode, a transitional mode and a sliding mode. The mode depends on the dominant particle shape and the coefficient of interparticle friction.

The turbulent mode occurs when behaviour is dominated by rotund particles, or, possibly, in by platy particles in soils, when the coefficient of interparticle friction between these particles is high. Residual strength is typically high when no preferred particle orientation occurs and brittleness is due to dilatant behaviour only. The residual friction angle depends primarily on the

shape and packing of the rotund particles and not on the coefficient of interparticle friction. A shear zone, once formed, is a zone of different porosity only and it is considerably modified by subsequent stress history.

The sliding mode occurs when behaviour is dominated by platy, low-friction particles. A low strength shear surface of strongly orientated platy particles then develops. The residual friction angle depends primarily on mineralogy, pore water chemistry and on the coefficient of interparticle friction. A shear surface, once formed, is not significantly affected by subsequent stress history. Brittleness during first shearing is due primarily to preferred particle orientation.

The transitional mode occurs when there is no dominant particle shape, and involves turbulent and sliding behaviour in different parts of a shear zone. The properties of the soil in residual shear change progressively across the transitional range from those of turbulent shear to those typical of sliding shear. In this mode the residual friction angle is sensitive to small changes in grading of the soil, and the changes in grading required to cross this range entirely are typically small.

A soil which will fail internally in turbulent shear may fail at least partly in sliding if it is sheared against a smooth, hard interface.

The type of shearing mode can be determined by examining brittleness with a special sequence of loading and by examining the post-failure structure of the soil. The residual friction angle depends on the normal effective stress and this dependence is typically greatest for the sliding mode of behaviour.

The type of shearing mode to a much lesser extent and the magnitude of the residual strength correlate best with the granular void ratio of the soil defined as the ratio of the volume of platy particles plus voids to the volume of rotund particles. This correlation is not effective for the sliding mode and, if high friction platy particles are present, these may behave as rotund particles. The shape of clay mineral particles present is of great importance. The correlations of change in shearing mode with the granular void ratio depend on the relative size of the platy and rotund particles and on the grading of the rotund particles.

There are no unique correlations between residual strength and gradation or soil index properties. However, such correlations are valuable in studying the residual strength provided they are

investigated properly reflect changes in the more fundamental properties of particle shape, grading, mineralogy, pore water chemistry, etc.

3.5.2 Correlation for residual strength

Collotta et al. (1989) proposed correlation for residual strength evaluation in form of Eq. 3.14.

$$\sigma'_R = c'_R + \sigma'_{vc} \tan \phi'_R \qquad 3.14$$

where, σ'_R is the residual shear strength,

c'_R is residual apparent cohesion intercept,

ϕ'_R is residual friction angle, and

σ'_{VC} is vertical stress.

The suggested correlation confirms that the residual friction angle is influenced by both the clay fraction (CF) and the mineralogical composition of the clay. The mineralogy factor is indirectly reflected in the liquid limit (LL), and plasticity index (PI). So the proposed correlation relates residual friction angle to a parameter that combines CF, LL and PI.

3.5.3 Residual Shear Strength Mobilized in First-Time Slope Failures

Mesri & Shahien (2003) reviewed the long-term stability of stiff clay and clay shale slopes by re-analyzing 99 slope failures in 36 soft clays to stiff clays and clay shales. Some key conclusions from this study are summarized below.

1) Most stiff clays and clay shales are not homogeneous. They are usually stratified and may include hard to soft or permeable to impermeable layer interfaces, bedding planes and separations, laminations, or thin weak continuous seams.
2) Erosion and unloading, including removal of lateral support, lead to swelling, fissuring, and softening. The end result of softening is the fully softened condition with a shear strength equal to that of the normally consolidated mineralogical composition of the stiff clay or clay shale. Any state of stiff clay or clay shale before the fully softened condition is reached is said to be an “intact” condition. The intact condition is quite variable, because different degrees of fissuring and softening are possible. Stiff clay and shale masses may include sheared zones in which plate shaped clay mineral particles are parallel-oriented to the maximum extent possible in the direction of shearing. This is the residual condition.

3) The relationships between shear strength and effective normal stress for all conditions of stiff clays and shales—intact, fully softened, and residual—are curved, and there is no shear strength at zero effective normal stress. A convenient method for describing the nonlinear intact, fully softened, and residual shear strength envelopes is to employ secant friction angles, respectively, that are functions of the effective normal stress. There are some reliable empirical information based on secant fully softened and secant residual friction angles of stiff clays and clay-shale mineralogical compositions characterized by Atterberg's plasticity index in a practical range of effective normal stresses. However, caution should be exercised in the use of empirical correlations for friction angles because for certain stiff clay, shale, and mudstone compositions, sample preparation may have a significant effect on Atterberg limits. Also, the plasticity index of weak seams may be different from that of the scarp cutting across the laminations.
4) On reactivated slip surfaces of landslides in stiff clays and clay shales the residual condition has been reached, and the mobilized shear strength is equal to the residual shear strength from laboratory reversal direct shear or ring shear tests, independent of time after initial failure.
5) In first-time slope failures in unstratified stiff clays of low plasticity, the mobilized strength is equal to the intact strength from laboratory specimens because there is little post peak reduction in strength.
6) The fully softened shear strength is the lower bound for mobilized strength in first-time slope failures in homogeneous soft to stiff clay slopes and on the part of the slip surface cutting across bedding planes and laminations in stiff fissured clays and shales.
7) Part of the slip surface for first-time slope failures may be at the residual condition. In stiff clays and shales either the residual condition already exists along bedding planes and laminations before a cut is made or it develops by progressive deformation. Sufficient strain energy to reach the residual condition is available along nearly horizontal surfaces, including bedding planes and laminations. When shearing strain is localized in thin weak bands, and clay particles are already substantially oriented parallel to the direction of shearing, rather small displacements will cause the clay to reach the residual condition.
8) Delayed first-time failure of slopes in stiff clays and clay shales is caused by (i) time-dependent rise of pore water pressure toward the steady seepage condition, swelling,

decrease in effective stress and shear strength, (ii) fissuring and softening, and (iii) development and propagation of the residual condition into the slope on nearly horizontal surfaces, including layer boundaries, bedding planes and partings, laminations, or weak seams.

9) Selection of potential slip surfaces for stability analyses of natural and excavated slopes should be based on a knowledge of geology. Special attention should be directed toward structural features such as presheared surfaces produced by old landslides, tectonic or glacial deformation, or downslope creep, as well as to lithological details such as horizontal or subhorizontal bedding planes, laminations, and weak seams that are likely to drop to the residual condition after relatively small shear displacements, measured in millimeters or centimeters as opposed to meters as commonly assumed for homogeneous clays or across laminations. For existing slopes, locating the position and shape of the critical slip surface by trial and error may be aided by observations of movements. In the absence of well-defined weak surfaces, including pre-existing shear surfaces, the planar basal portion of the critical slip surface in stiff clays and shales should be selected parallel to the bedding and at the level of the base of the slope.

3.5.4 Residual shear strength of unsaturated soils via suction-controlled ring shear testing

Results from a comprehensive series of suction-controlled ring shear (RS) tests on statically compacted specimens of silty clayey sand (SC-SM) and silty sand (SM) soils were presented by (Hoyos et al. 2014). The experiments were conducted in a newly developed servo/suction-controlled RS apparatus that is suitable for testing unsaturated soils under large deformations via axis translation technique. The results reflect the important role played by matric suction on residual shear strength properties of unsaturated soils. For the range of net normal stresses and suction states investigated, the increase in residual shear strength with increasing suction was found to be virtually linear for SM soil, but significantly nonlinear for SC-SM soil. Multi-stage test results also appear to confirm that the residual shear strength of compacted soils is independent of both the pre-shearing and the suction histories undergone by the soil. Results, in general, suggest that a conceptual residual shear strength framework for unsaturated soils, similar to that postulated for peak shear strength, could eventually be devised as more experimental evidence of this kind is made available. Further investigations, including Environmental

Scanning Electron Microscopy (ESEM) technology, are necessary to correlate and further substantiate the observed phenomena with changes in soil particle gradation, aggregation and plasticity as the soil is subjected to suction controlled ring shearing.

3.5.5 Residual shear strength of fine-grained soils

The following conclusions are drawn by (Eid et al., 2015) based on the results of soil and interface shear testing at low effective normal stresses (between 3 and 6.7 kPa) using a modified torsional ring shear apparatus and the macroscale interface direct shear test device.

1) The secant residual friction angle of soil decreases with increasing liquid limit and clay-size fraction. These soil parameters have a similar effect on the measured interface residual friction angles that are also lower for smoother surfaces. The change in effective normal stresses within the range utilized in this study did not show a considerable effect on the measured residual friction angles of soils and interfaces;
2) For low effective normal stresses, the clay-size fraction, as an indication of particle size and shearing mode, has less influence on the measured residual friction angle than the influence of the liquid limit that indicates the clay mineralogy and particle shape;
3) Correlations were developed to help in estimating residual shear strength at low effective normal stresses for soil types similar to those utilized in the current study. These describe the secant residual friction angle as a function of soil liquid limit and clay-size fraction as well as plasticity index. Since the residual shear strength envelope of most fine-grained soils is known to be nonlinear especially at low effective stress ranges, the newly developed correlations can assist in avoiding significant underestimation of residual shear strength angles that would occur when using current correlations that are developed for high effective normal stress ranges. These also avoid overestimating the drained residual friction angles of such soil types when using residual strength expressions, the development of which is influenced by testing soils of distinct contents (i.e., foraminifera, faecal pellets, carbonates, allophane, or halloysite) at low effective normal stresses and consequently do not consider the effect of soil plasticity;

4) A correlation and a simple equation have been suggested for estimating the interface residual friction between fine grained soils and solid surfaces sheared at low effective normal stresses as a function of the surface average roughness of the solid surface and the soil residual friction angles. The residual interface efficiencies (i.e., the ratio between soil and interface friction angles) determined using the introduced correlation and equation compare well with those reported in the literature for high effective normal stresses, provided that the soil and interface residual shear strengths that are estimated at the same effective normal stress range are used for efficiency calculations;
5) Using the normalized roughness seems to be ineffective in developing a better correlation to estimate the residual interface efficiency for fine-grained soils. It is advocated that the surface roughness alone may not adequately characterize a given surface. Parameters such as hardness, yield strength, stress–strain behavior of solid material, and compatibility between soil particle size and interface surface roughness are likely to impact the overall interface frictional response observed at soil–solid interfaces. Further studies are warranted to explore these aspects.

3.5.6 Drained residual shear strength at effective normal stresses relevant to soil slope stability analyses

Eid et al. 2016 have undertaken to evaluate the results from a comprehensive torsional ring shear test program conducted to measure the drained residual shear strengths of clays, silts, mudstones, and shales at the wide range of effective normal stresses relevant to slope stability analyses. It was found that nonlinearity of the residual shear strength envelopes is most pronounced for effective normal stresses lower than 50 kPa. For effective stresses equal or higher than 200 kPa that are occasionally mobilized in slope failures, these envelopes can be approximated as straight lines. The influence of clay-size fraction, which is the governing factor in developing different shearing behaviors, on the measured residual friction angle decreased with decreasing the effective normal stress level.

The work led to the development of new residual shear strength correlations for sedimentary soils as a function of soil index parameters and a wide range of effective normal stress levels (i.e., 10 kPa to 400 kPa). This is a significant advancement since the currently available

correlations do not cover the residual strength at effective normal stresses lower than 50 kPa, and also between 100 kPa and 400 kPa. The new correlations are suitable for fine-grained materials with mostly plate-like clay particles. It is noted that, they would underestimate the drained residual friction angles of soils with distinct contents - such as carbonate soils, and soils that contain allophan, halloysite, or foraminifera - that are unlikely to have particle rearrangement towards some preferred orientation.

For shales, mudstones, and heavily over consolidated clays, the liquid limit and clay-size fraction used in developing the presented correlations were derived from a modified sample preparation procedure that involves ball-milling to disaggregate the particles of such indurated materials. To facilitate the use of the empirical shear strength correlations introduced herein, a set of new equations were developed – using previously published data - to convert the index parameters derived from the commonly used standard procedures to result in indices equivalent to those derived from the ball-milled sample preparation procedure.

The suitability of the new correlations in predicting the residual strength was verified through comparisons with back-calculated shear strength data reported in the literature as well as results yielded from similar existing correlations. It was revealed that accounting for the effect of normal stress is an important consideration in arriving at better predictions using such empirical correlations. New simple formula was generated to express the residual shear strength correlations developed in this study. The formula should facilitate incorporating the nonlinearity of the residual shear strength envelopes in slope stability software.

3.5.7 Influence of displacement rate on residual shear strength of clays

Shear tests under controlled displacement rates were carried out by (Scaringi & Di Maio, 2016) on a kaolin, a bentonite, on their mixtures with sand at various percentages, and on the clayey soil of the Costa della Gaveta earthflow. The range 10^{-4}-10^{2} mm/min of displacement rate was investigated. The results relative to the material mixed with distilled water show that the mixtures clay-sand with clay fraction $\geqslant$ 50% exhibit positive rate effects which increase with the clay fraction content. The rate effect becomes significant for displacement rate in the order of mm/min, with slight differences dependent on the used experimental shear apparatus. Results consistent with those of artificial mixtures are found on the Costa della Gaveta soil, the clay fraction of which is about 50%.

The results relative to the material mixed with NaCl solutions at various concentrations show that the rate effect increases with the pore solution concentration. Since the increase in salt concentration also makes the material void ratio decrease greatly, the observed strength improvement could be reasonably attributed to the increasing number of solid-solid contacts that probably endeavours the turbulent shearing mechanism.

The independence of residual shear strength on the displacement rate in the range 10^{-6}-10^{-1} has been confirmed by the results of shear tests performed under controlled shear stress conditions. This latter procedure can be promisingly improved for the evaluation of rate effects in a wider rate range.

3.5.8 Effect of shear rate on the residual shear strength of pre-sheared clays

Habibbeygi & Nikraz (2018) investigation the shear strength behaviour of a pre-sheared clay to examine the effect of shear rate on the residual shear strength. Based on the results of the ring shear tests, the following conclusions have been derived:

1) There is an immediate increase of residual strength in comparison with the slow residual strength when the shear rates increase. In fact, there is a positive rate effect on the residual strength at a small displacement.
2) The fast residual strength of pre-sheared clays increases with an increasing applied normal stress.
3) The peak residual strengths of the pre-sheared clay in the fast shear steps are dependent on the rates of shear displacement. The fast residual strengths increase the slow residual strength when the rates increase. Moreover, the maximum peak residual strength of the fast steps occurs at the displacement rates of 50 and 200 mm/min.
4) There is a drop in the fast residual strength on top of the increase in the displacement for all various shear rates and the applied normal stresses.
5) There is a positive and negative effect of displacement rate on the residual strength for the rates greater than 50 kPa, which requires more research on the shear behaviour of pre-sheared clayey soils at fast shearing conditions.

.

CHAPTER 4
SIMULATION OF PROGRESSIVE SHEAR FAILURE IN SUBGRADE

This chapter includes assumptions, equations, and programming for simulating the progressive shear failure and finding out shear failure plane.

4.1 Assumptions of progressive shear failure in Subgrade

Progressive shear failure is the plastic flow of the soil caused by overstressing at the subgrade surface under repeated loading. The subgrade soil gradually squeezes out from under the tie and then upward at the tie end, following the path of least resistance as shown in Figure 4-1 (Li et al., 2016). This is primarily a problem with fine-grained soils, particularly those with high clay content. The addition of more ballast above the subgrade squeeze zone results in an increase in ballast depth and a corresponding tendency for a reduction in stress at the subgrade level, which might improve subgrade stability. However, the depression in the subgrade surface will trap water that can further soften the subgrade.

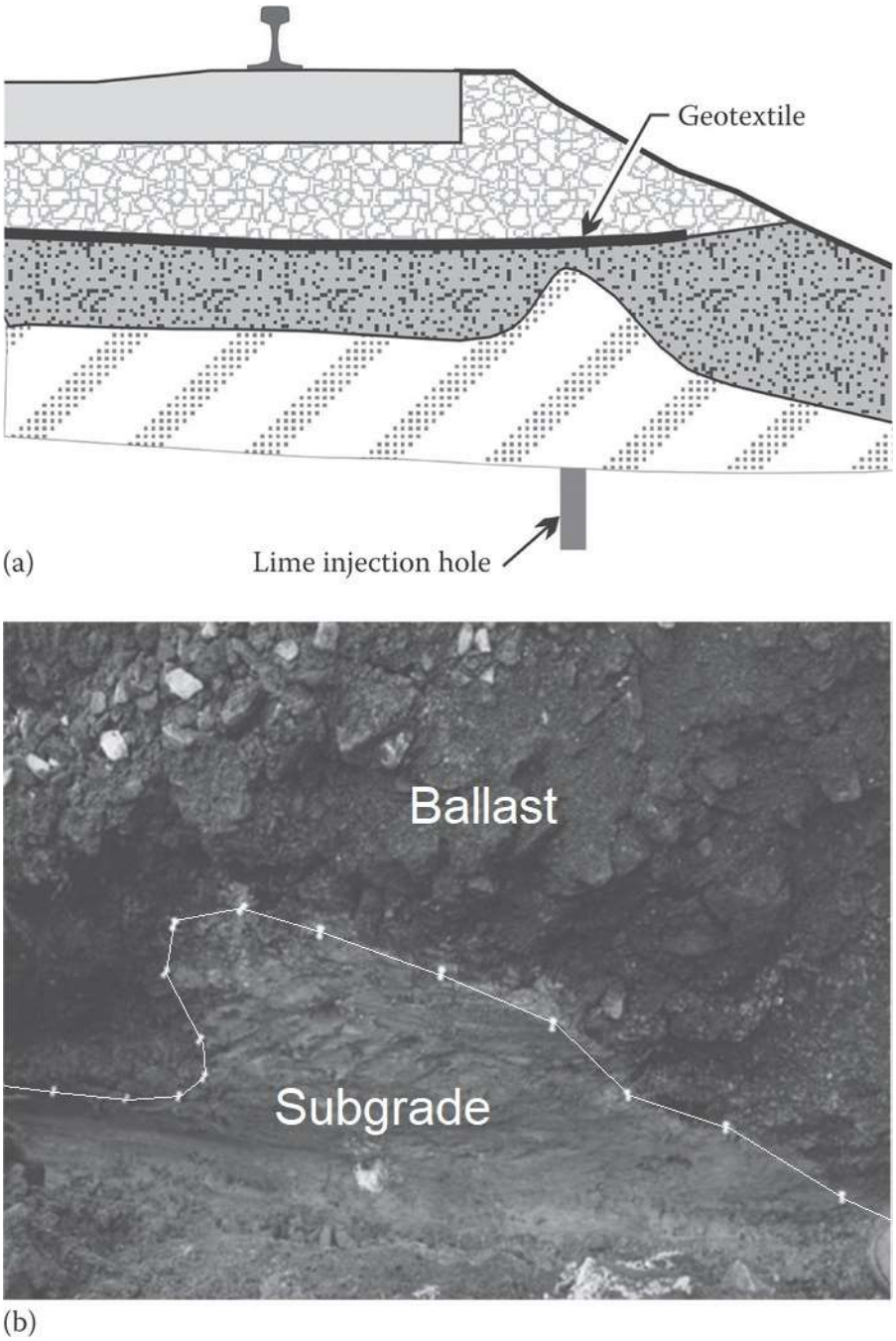

Figure 4-1 Subgrade squeeze at end of tie (Li et al., 2016):
(a) track cross section with a subgrade squeeze and
(b) subgrade squeeze and lime injection hole

The above descripted progression of progressive shear failure could be broken down and simulated with following steps.

1) The progressive shear failure typically initiates within a weak zone of the subgrade. Figure 4-2 shows series of elements on a typical shear failure plane within a railway subgrade. The elements 0 through 6 are zoomed-in and highlighted along a simulated failure plane. The stresses within these elements typically increase in the foundation due to an approaching train on the track, and the stresses decrease in the foundation when the train is leaving away on the track.
2) As the train approaches and contributes to a significant increase in the foundation stress, the (shear) stress within an element of the weak zone increases too. When stress exceeds the shear strength of the element, i.e. the shear stress in the element is above the Mohr Coulomb shear failure envelope (see Figure 3-1), the element will fail. We name this first failed element as primary element (i.e. element 0 shown in Figure 4-2). Figure 4-3a shows the shearing stress on the failed element.
3) In spite of the shear failure in the primary element, there is still some limited strength in the form of residual shear strength (see Figure 4-3a and Eq. 4.11 in Section 4.2) on failure plane. For this condition, there is an unbalanced shear stress (see Figure 4-3b and Eq. 4.13 in Section 4.2) which equals shear stress generated by train load minus the residual shear strength. This unbalanced shear stress will be transferred to the neighboring elements (or zones) -- the first element, i.e. the element 1 in Figure 4-2.
4) The first element, under the additional stress (i.e., unbalanced stress) from the primary element, has a new stress state (see Figure 4-3b & c).
5) As the train comes, the stress within the first element continues increase and may exceeds the shear strength of the soil (see Figure 3-1). Under such a scenario, the first element fails too under shear loading (see Figure 4-3a).
6) After first element fails, similar to the primary element, the unbalanced shear stress transfer to its neighboring secondary elements (i.e. see, the element 2 in Figure 4-2).
7) The shear stress within the elements typically increase with the train approaches closer. Due to this reason, the failure may extend to the second, third and fourth elements (i.e. element 2, 3, and 4 in Figure 4-2) as the stress increase. These increasing loads may contribute to the failure plane finally reaching the surface of Subgrade (see Figure 4-2).

8) The stresses in the elements decrease after the first pair of wheels of the train passes these elements (or weak zone), and the progressive shear failure plane will cease extension if the failure plan has not reached the surface of subgrade.

9) The stresses in the subgrade increase with the approach of the next pair of wheel loads. The above mentioned progressive shear failure continues with the repeated loads of passing train.

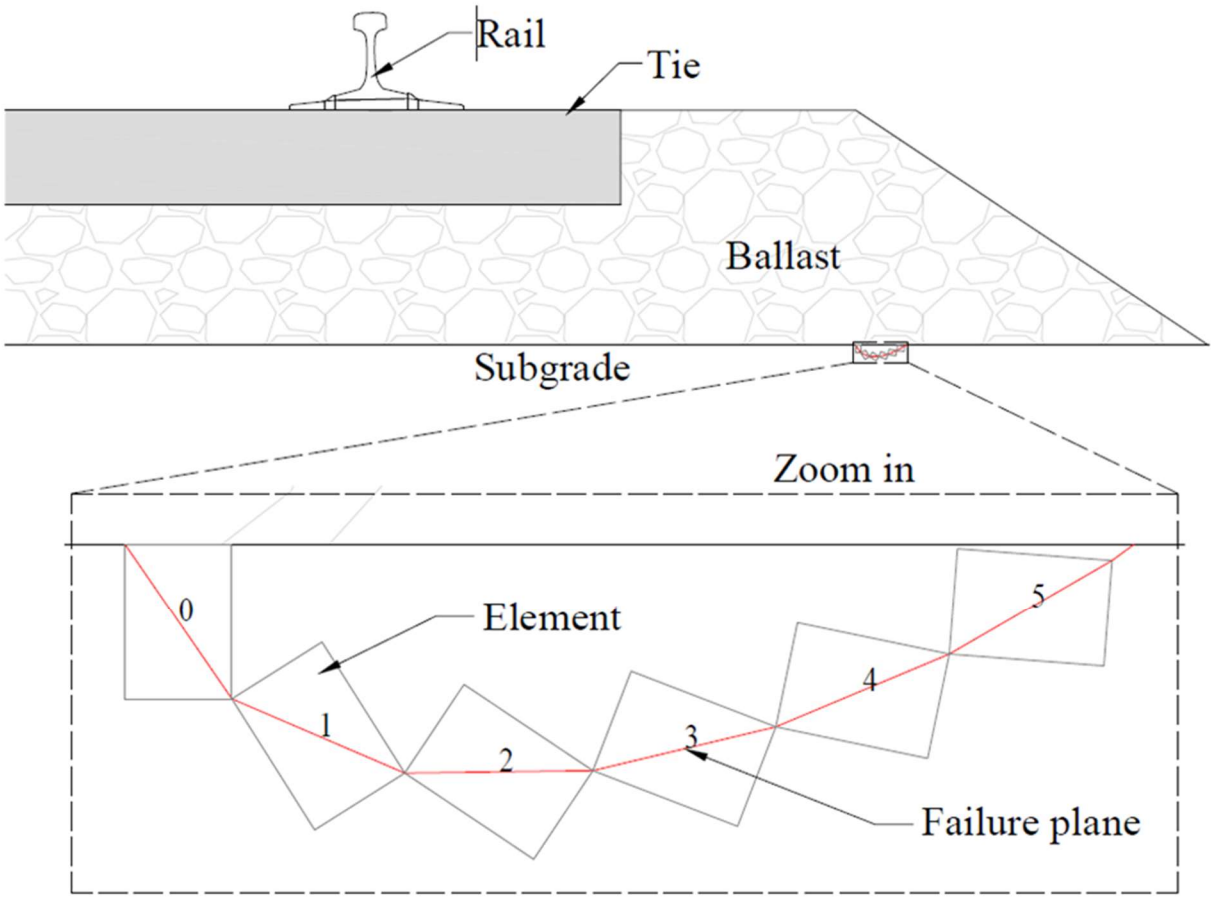

Figure 4-2 Failure elements and plane in Subgrade

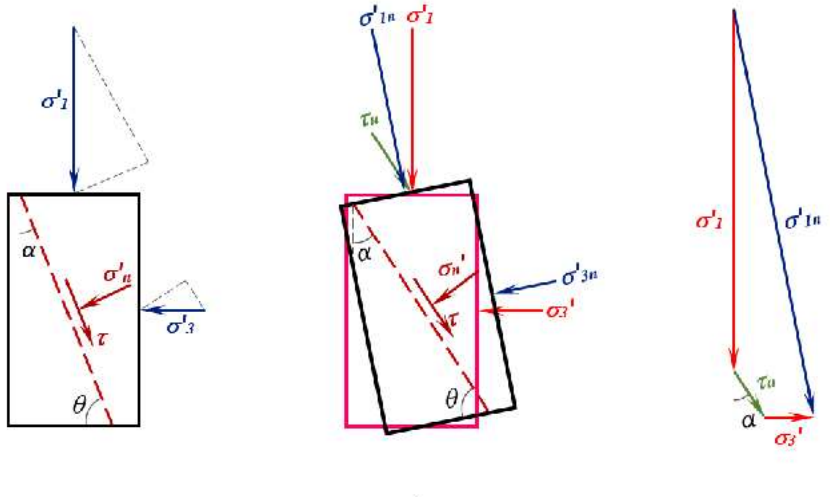

Figure 4-3 Failure element and its stresses:
a. Stress status and failure plane in an element.
b. New stresses status as the unbalanced shear stress from previous element is transferred in.
c. Calculating new major principle stress according to initial principle stresses and unballanced shear stress from previous element

4.2 Shear Failure Criterion and Stresses in Subgrade

During above described progression of progressive shear failure, element shear failure and stress transfer are calculate and simulated with the following equations summarized in this section.

1) Mohr-Coulomb failure criteria in terms of effective shear strength parameters (Figure 3-1):

$$\tau_f = c' + \sigma_f' \tan \phi' \qquad 4.1$$

where τ_f is shear strength at failure, c' is effective cohesion, σ_f' is effective stress at failure, and ϕ' is the effective stress friction angle.

This is a principle equation to identify the element failure.

2) Extension of Mohr-Coulomb failure criteria in unsaturated soil mechanics by (Vanapalli et al., 1996):

$$\tau = c' + (\sigma_n - u_a)tan\phi' + (\sigma_a - u_w)\Theta^k \tan \phi' \qquad 4.2$$

where τ is shear strength, $(\sigma_n - u_a)$ is the net normal stress, σ_n is the total net normal stress, u_a is the pore–air pressure, $(u_a - u_w)$ is the matric suction, u_w is the pore–water pressure, Θ is the degree of saturation and κ is fitting parameter.

The progressive shear failure can be considered mainly a subgrade surface failure (Li et al., 2016), so the variation of matric suction $(u_a - u_w)$ is small. To simplify the calculation of shear strength, we can ignore the variation of shear strength $(u_a - u_w)\Theta^K \tan\phi'$ contributed by matric suction and assume it is a constant in the progressive shear failure zone, so we consider it is part of apparent cohesion, c. i.e.

$$c = c' + (u_a - u_w)\Theta^K \tan\emptyset' \quad 4.3$$

Then, the Mohr-Coulomb failure equation (4.1) can be used to instead of equation (4.2) to study the progressive shear failure under unsaturated condition.

3) The normal and shear stresses at failure expressed with principal stresses:

Based on Mohr-Coulomb failure equation (3.2 or 4.1) and Figure 3-1, equation (4.4) and (4.5) could be derived on failure envelope. The normal and shear stressed at failure on failure plane can also be calculated with major and minor principal stresses.

$$\tau_f = \frac{\sigma_1' - \sigma_3'}{2} \sin 2\theta \quad 4.4$$

$$\sigma_f{}' = \frac{\sigma_1' + \sigma_3'}{2} + \frac{\sigma_1' - \sigma_3'}{2} \cos 2\theta = \sigma'_1 \cos^2\theta + \sigma'_3 \sin^2\theta \quad 4.5$$

where σ'_1 is the major principal stress, σ'_3 is the minor principal stress, θ is angle between direction of minor principal stress and shear failure plane (see Figure 3-1).

$$\theta = 45^\circ + \frac{\phi'}{2} \quad 4.6$$

4) Mohr-Coulomb failure envelope (criteria) expressed with principal stresses:

Mohr-Coulomb failure envelope (criteria) can also be expressed with major & minor principal stresses by substituting shear strength, τ_f, in Equation 4.1 with Equation 4.4 and substitute effective normal stress, σ'_f, in Equation 4.1 with Equation 4.5, to get the relationship Equation 4.7.

$$\sigma'_{f1} = \sigma'_{f3} \tan^2\theta + 2c' \tan\theta \quad 4.7$$

In other words, Equation 4.7 represents the relationship between major and minor principle stresses at failure.

5) The initial principal stresses on element:

The initial major principle stress (see Figure 4-2 and Figure 4-3a) can be calculated according to track load and weight of subgrade with following formula.

$$\sigma'_1 = p(d) + \rho g d \qquad 4.8$$

where, *p(d)* is vertical stress (or load of track) transferred to element in subgrade, ρ is density of subgrade material, *g* is standard gravity, *d* is depth of element to the top surface of subgrade.

The minor principal stress (see Figure 4-3) can be calculated with major principal stress according to following formula.

$$\sigma'_3 = K_0 \sigma'_1 \qquad 4.9$$

where, K_0 is the Coefficient of earth pressure at rest.

6) The effective normal stress on the shear plane after failure:

The normal stress on failure plane can be calculated with major and minor principal stresses by following formula. See Figure 4-3a.

$$\sigma_n' = \sigma'_1 \cos\theta + \sigma'_3 \sin\theta \qquad 4.10$$

7) The residual shear strength after failure:

$$\tau_r = K_r \sigma'_n = \sigma'_n tan\, \phi'_r \qquad 4.11$$

where, K_r *is* coefficient of residual friction,

ϕ'_r is residual effective friction angle,

$\phi'_r = 34° e^{-0{,}114 I_P}$ (Eid et al., 2015),

I_P is plastic index.

8) Shear stress (see Figure 4-3a) along the shear plane after failure:

$$\tau = \sigma'_1 \sin\theta - \sigma'_3 \cos\theta \qquad 4.12$$

9) Unbalanced shear stress (see Figure 4-3b) along the shear plane after failure:

$$\tau_u = \tau - \tau_r \quad (4.13)$$

10) New stresses status in element after previous element failed:

In the railway foundation, the major principal stress is not in the vertical direction (Li et al., 2016) (see Figure 2-8), but there are no experimental data to reveal the accurate direction of principal stresses. To simplify the calculation, assume the major principal stress is in the vertical direction in this thesis.

After previous element failed, the unbalanced shear stress transfer to its next element, so the stress status in next element is changed. The new major and minor principal stresses are:

$$\sigma'_{1n} = \sigma'_1 \cos\beta + \tau_u \cos(\alpha - \beta) + \sigma'_3 \sin\beta \quad (4.14)$$

$$\sigma'_{3n} = \sigma'_1 \sin\beta + \tau_u \sin(\alpha - \beta) + \sigma'_3 \cos\beta \quad (4.15)$$

where σ'_{1n} is the new major principal stress,

β is the angle between initial major principal stress σ'_1 and new major principal stress σ'_{1n},

α is the angle between initial major principal stress σ'_1 and unbalanced shear stress τ'_u.

The α can be calculated with θ, the angle between direction of major principal stress and failure plane. The α of the primary element can be calculated with following equation:

$$\alpha = 90° - \theta \quad (4.16)$$

β can be calculated with following equation:

$$\beta = \tan^{-1} \frac{\sigma_3 + \tau \sin\alpha}{\sigma_1 + \tau \cos\alpha} \quad (4.17)$$

4.3 Program of the Simulation

The computer program of progressive shear failure simulation is a Visual Basic program developed in the environment of AutoCAD based on above assumption in Section 4.1 and equations in Section 4.2. The full Code of the Program has around 500 lines.

The program facilitates an Input file which can feed the data for the program. An output file is generated to gather all the simulation results. In addition, the program is also capable of displaying the progressive shear failure planes in AutoCAD drawing.

The Code of the Program, An input file and two output files are provided in the Appendix and will be used in later sections to detail the program simulation. The input file is named as "Data.txt" for user to input the data required for the program running. Each inputted data is followed by a note or explanation. The output file "Output.txt" records the number of failed elements along failure plane during each simulation and final load or stress in the subgrade at end of each simulation.

CHAPTER 5
SIMULATION RESULTS OF PROGRESSIVE SHEAR FAILURE IN SUBGRADE

This chapter provides details of the required input data along with the other information for performing numerical simulations. The numerical simulation results are also analyzed and discussed.

5.1 Input Data and Subgrade Parameters

The input file provides source data for the simulation, including size of the element, geometry data of track, property parameters of ballast and subgrade, as well as stress distribution at bottom of the ballast. Appendix provides more details of a sample input file. The key data and parameters are discussed in this section.

5.1.1 The Density and Thickness of Ballast

According to specification of RailCorp and Australian Rail Track Corporation (Wilson, 2013), the particle density of ballast material shall not be less than 2500 kg/m^3, and the compacted bulk density of ballast material shall not be less than 1,400 kg/m^3. In addition, most railway specifications require the thickness of the ballast should not be less than 12” (300mm) from bottom of the tie, and the top width of ballast is 3.5m.

In this study, to simplify the calculations, track weight (including rail, plate, fastener, tie and ballast) is considered as ballast weight. A constant width, thickness and density of ballast are respectively taken 3.5m, 0.5m, and 2000kg/m^3.

5.1.2 The density of subgrade soil

Structural Engineering Resources (StructX, 2019) suggests following density ranges for different soil types (see Table 5-1).

Table 5-1 Density Ranges for Different Soil Types (kg/m^3)

	Dry Density		Submerged Density	
	Min.	Max.	Min.	Max.
Sand; clean / uniform / fine or medium	1346	2179	833	1169
Silt; uniform / inorganic	1297	2179	817	1169
Silty Sand	1410	2275	865	1265
Sand; Well-graded	1378	2371	849	1378
Silty Sand and Gravel	1442	2483	897	1474
Sandy or Silty Clay	1602	2355	609	1362
Silty Clay with Gravel; uniform	1842	2419	849	1426
Well-graded Gravel / Sand / Silt and Clay	2002	2499	993	1506
Clay	1506	2130	497	1137
Colloidal Clay	1137	2050	128	1057
Organic Silt	1394	2098	400	1105
Organic Clay	1297	2002	288	993

Progressive shear failure typically occurs in a subgrade constructed with fine grained soils that is nearly saturated. From the information of density values in the Table 5.1, a value of 1560 kg/m^3 was used as subgrade density in this thesis.

5.1.3 The effective cohesion of subgrade soil and matric suction, *c*

The cohesion is the non-frictional part of the soil shear strength which is independent of the normal stress.

Table 5-2 summarizes typical cohesive strength values from GEOL 615 course notes of Pennsylvania State University.

Table 5-2 The Cohesive strength (c) or (c prime)

Rock	10,000 kPa
Silt	75 kPa
Clay	10-20 kPa
Very soft clay	0- 48 kPa
Soft clay	48-96 kPa
Medium clay	96-192 kPa
Stiff clay	192-384 kPa
Very stiff clay	384-766 kPa
Hard clay	>766 kPa

In this thesis, the apparent cohesion includes effective cohesion along with the shear resistance arising from the contribution of matric suction (Equation 4.3). Since increasing effective cohesion or matric suction, increases the total shear strength of the soil, relatively small values of cohesion, c between 0 – 10 kPa are used.

5.1.4 The effective angle of friction of subgrade soil

In GEOL 615 course notes of Pennsylvania State University, following angle of internal friction has been used (Table 5-3).

Table 5-3 Angle of internal friction (ϕ) or (ϕ prime)

Rock	30°
Sand	30-40°
Gravel	35°
Silt	34°
Clay	20°
Loose sand	30-35°
Medium sand	40°
Dense sand	35-45°
Gravel with some sand	34-48°
Silt	26-35°

Geotechdata.info web (Geotechdata.info, 2013) lists typical values of angle of friction for different USCS (Unified Soil Classification System) soil types.

Table 5-4 Typical values of soil friction angle

Soil Description	USCS	Friction angle (°)		
		min	max	Specific value
Well graded gravel, sandy gravel, with little or no fines	GW	33	40	
Poorly graded gravel, sandy gravel, with little or no fines	GP	32	44	
Sandy gravels - Loose	(GW, GP)			35
Sandy gravels - Dense	(GW, GP)			50
Silty gravels, silty sandy gravels	GM	30	40	
Clayey gravels, clayey sandy gravels	GC	28	35	
Well graded sands, gravelly sands, with little or no fines	SW	33	43	
Well-graded clean sand, gravelly sands - Compacted	SW	-	-	38
Well-graded sand, angular grains - Loose	(SW)			33
Well-graded sand, angular grains - Dense	(SW)			45
Poorly graded sands, gravelly sands, with little or no fines	SP	30	39	
Poorly-garded clean sand - Compacted	SP	-	-	37
Uniform sand, round grains - Loose	(SP)			27
Uniform sand, round grains - Dense	(SP)			34
Sand	SW, SP	37	38	
Loose sand	(SW, SP)	29	30	
Medium sand	(SW, SP)	30	36	
Dense sand	(SW, SP)	36	41	
Silty sands	SM	32	35	
Silty clays, sand-silt mix - Compacted	SM	-	-	34
Silty sand - Loose	SM	27	33	
Silty sand - Dense	SM	30	34	
Clayey sands	SC	30	40	
Calyey sands, sandy-clay mix - compacted	SC			31
Loamy sand, sandy clay Loam	SM, SC	31	34	
Inorganic silts, silty or clayey fine sands, with slight plasticity	ML	27	41	
Inorganic silt - Loose	ML	27	30	
Inorganic silt - Dense	ML	30	35	

Inorganic clays, silty clays, sandy clays of low plasticity	CL	27	35	
Clays of low plasticity - compacted	CL			28
Organic silts and organic silty clays of low plasticity	OL	22	32	
Inorganic silts of high plasticity	MH	23	33	
Clayey silts - compacted	MH			25
Silts and clayey silts - compacted	ML			32
Inorganic clays of high plasticity	CH	17	31	
Clays of high plasticity - compacted	CH			19
Organic clays of high plasticity	OH	17	35	
Loam	ML, OL, MH, OH	28	32	
Silt Loam	ML, OL, MH, OH	25	32	
Clay Loam, Silty Clay Loam	ML, OL, CL, MH, OH, CH	18	32	
Silty clay	OL, CL, OH, CH	18	32	
Clay	CL, CH, OH, OL	18	28	
Peat and other highly organic soils	Pt	0	10	

The minimum angle of friction of soil in Table 5-4 is 17° and the maximum angle of friction is 44°. In this research, following these guidelines, the relatively smaller values of angle of friction 17-25° are used.

5.1.5 The coefficient of earth pressure at rest

Al-Hussaini (1981) tested values of K_0 for the sand using the LVDT clamp, swinging arms, the K_0 -belt with strain gages, and the burette method are presented in terms of initial relative densities in Table 5-5. The K_0 value are from 0.39 to 0.55.

Table 5-5 Values of K_0 for the sand tested by (Al-Hussaini, 1981)

LVDT Clamps		Swinging-Arms		K_0-Belt		Burette Method	
D_r, %	K_0	D_r, %	K_0	D_r, %	K_0	D_r, %	K_0
30.9	0.53	25.6	0.51	26.9	0.55	36.0	0.52
75.1	0.45	72.1	0.42	72.9	0.48	69.3	0.44
94.0	0.39	99.5	0.39	96.5	0.42	96.8	0.39

Note: D_r, Relative Density, %.

Wang et al (2018) used materials which are mixtures of mixed artificially by crushed sandstone and mudstone particles. The test materials are classified as well-graded sand (SW). The test results of K_0 values are listed in Table 5-6 with coefficient of determination R^2, which are calculated from the experimental data. The K_0 value ranges from 0.242 to 0.381, with a mean value of 0.300. And the R^2 value ranges from 0.976 to 0.999, with a mean value of 0.989.

Table 5-6 Experimental Values of Coefficient K_0

No.	Mudstone particle content by weight of test material (%)	Initial dry bulk density of test specimen ρ_d (g/cm^3)	Coefficient of earth pressure at rest K_0	R^2 of fitting straight line
1	80	1.7	0.365	0.996
2	80	1.7	0.375	0.991
3	80	1.7	0.378	0.998
4	80	1.7	0.381	0.989
5	80	1.8	0.313	0.988
6	80	1.8	0.320	0.991
7	80	1.8	0.323	0.986
8	80	1.8	0.329	0.993
9	80	1.9	0.264	0.994
10	80	1.9	0.274	0.997
11	80	1.9	0.277	0.988
12	80	1.9	0.281	0.999
13	80	2.0	0.242	0.993
14	80	2.0	0.244	0.991
15	80	2.0	0.252	0.997
16	80	2.0	0.254	0.986
17	80	1.8	0.253	0.998
18	80	1.8	0.262	0.977
19	80	1.8	0.256	0.985
20	80	1.8	0.269	0.991

21	80	1.8	0.271	0.997
22	80	1.8	0.281	0.991
23	80	1.8	0.285	0.985
24	80	1.8	0.292	0.976
25	80	1.8	0.358	0.992
26	80	1.8	0.367	0.985
27	80	1.8	0.372	0.976
28	80	1.8	0.381	0.988
29	80	1.8	0.319	0.991
30	80	1.8	0.326	0.996
31	80	1.8	0.331	0.985
32	80	1.8	0.346	0.979
33	0	1.8	0.281	0.993
34	0	1.8	0.299	0.991
35	0	1.8	0.289	0.987
36	0	1.8	0.287	0.998
37	20	1.8	0.252	0.990
38	20	1.8	0.269	0.978
39	20	1.8	0.259	0.986
40	20	1.8	0.264	0.997
41	40	1.8	0.265	0.988
42	40	1.8	0.281	0.991
43	40	1.8	0.271	0.976
44	40	1.8	0.275	0.995
45	60	1.8	0.315	0.989
46	60	1.8	0.297	0.982
47	60	1.8	0.307	0.986
48	60	1.8	0.310	0.994
49	100	1.8	0.298	0.989
50	100	1.8	0.316	0.991

51	100	1.8	0.304	0.982
52	100	1.8	0.306	0.988
Mean			0.300	0.989

The subgrade which experienced progressive failure are mostly saturated fine grained soil, so K_0 values 0.25 ~ 0.4 are used in the present study.

5.1.6 The coefficient of friction on failure plane K_r

Tiwari & Marui (2005) collected 82 soil samples from existing landslide areas, slope failure areas, debris flow areas, and the volcanic eruption areas to investigate the influence of the mineralogical composition of the soil in various disaster areas. These details are summarized in Table 5-7.

Table 5-7 Index Properties, Mineralogical Composition, and residual friction angle of Natural Samples (Tiwari & Marui, 2005)

Sampling site	No	LL	PI	CF	Massive minerals	Kaolinite	Mica	Smectite	ϕ'_R
Landslide area									
Okimi	1	75.0	38.0	30.2	81.0	3.9	0.1	15.0	15.0
Okimi	2	82.0	39.1	32.2	82.0	2.8	0.2	15.0	16.0
Okimi	3	78.0	38.0	30.1	81.0	3.9	0.1	15.0	16.0
Okimi	4	66.7	21.9	17.5	84.0	1.9	0.1	14.0	22.0
Okimi	5	71.0	35.0	30.2	79.0	4.9	0.1	16.0	14.0
Okimi	6	72.3	37.1	31.1	79.0	4.8	0.2	16.0	14.0
Okimi	7	76.0	36.0	30.8	82.0	2.9	0.1	15.0	16.0
Okimi	8	68.1	34.6	28.8	78.0	5.9	0.1	16.0	12.0
Okimi	9	84.0	52.9	45.2	75.0	2.9	0.1	22.0	11.0
Okimi	10	69.2	31.0	26.3	78.0	6.9	0.1	15.0	12.0
Okimi	11	81.4	43.9	37.5	77.0	2.9	0.1	20.0	11.0
Okimi	12	78.2	25.8	20.5	76.0	9.0	0.1	15.0	12.0
Okimi	13	75.5	25.6	21.5	77.0	7.9	0.1	15.0	12.0
Okimi	14	77.2	49.5	38.2	77.0	4.9	0.1	18.0	10.0
Okimi	15	66.0	31.0	27.7	79.4	4.5	0.6	15.5	12.5

Okimi	16	55.0	18.0	19.5	85.3	3.5	1.0	10.2	18.8
Yosio	1	86.3	47.1	28.2	77.0	5.0	0.0	18.0	10.0
Yosio	2	89.0	41.9	37.5	73.0	8.0	0.0	19.0	10.0
Yosio	3	73.0	35.3	22.1	74.9	7.7	1.6	15.8	10.1
Yosio	4	64.0	34.1	19.2	74.2	6.9	1.2	17.7	12.7
Yosio	5	68.0	38.2	28.2	75.6	5.4	0.4	18.6	9.8
Yosio	6	69.0	40.0	27.2	76.4	7.0	0.7	15.9	9.8
Yosio	7	51.0	19.0	21.8	80.0	6.1	0.2	13.7	10.7
Mukohidehara	1	71.5	36.4	21.2	84.0	7.0	0.0	9.0	19.0
Mukohidehara	2	55.8	32.6	20.5	85.0	6.0	0.0	9.0	18.0
Mukohidehara	3	70.0	38.0	24.0	72.6	11.2	0.9	15.3	8.9
Mukohidehara	4	65.0	34.0	22.0	72.3	7.3	0.8	19.6	10.7
Mukohidehara	5	61.0	15.0	20.0	84.6	2.8	0.5	12.1	16.2
Mukohidehara	6	53.0	26.0	14.0	85.7	2.0	1.9	10.4	19.3
Engyoji	1	91.3	50.5	32.8	73.0	10.0	0.0	17.0	10.0
Engyoji	2	94.6	62.4	33.2	74.0	8.0	0.0	18.0	10.0
Engyoji	3	69.0	38.0	27.5	75.0	4.5	2.5	18.0	9.8
Engyoji	4	62.0	29.0	19.9	78.8	5.2	2.6	13.4	12.8
Engyoji	5	59.0	19.0	20.0	85.1	3.5	1.4	10.0	17.6
Iwagami	1	96.2	48.0	32.2	78.0	6.0	1.0	15.0	12.0
Iwagami	2	94.7	59.2	33.5	78.0	6.0	0.0	16.0	12.0
Iwagami	3	63.0	32.0	24.8	75.9	14.5	1.9	7.7	17.1
Iwagami	4	71.0	38.0	26.2	77.8	10.8	0.3	11.1	11.2
Iwagami	5	64.0	21.0	23.0	70.5	3.9	1.7	23.8	11.1
Tsuboyama	1	79.8	36.3	40.2	75.0	8.0	0.0	17.0	10.0
Tsuboyama	2	100.0	68.3	42.8	76.0	6.0	0.0	18.0	10.0
Tsuboyama	3	120.0	65.5	42.0	73.7	3.9	1.7	20.7	10.9
Tsuboyama	4	108.0	66.2	41.2	73.6	8.7	2.2	14.4	14.7
Tsuboyama	5	58.0	29.2	21.3	86.5	3.8	0.4	9.3	19.2
Landslide area									

Hirayama	1	57.0	17.0	10.0	76.9	3.1	1.8	18.1	12.7
Hirayama	2	57.0	23.0	2.8	75.0	4.4	1.8	17.7	10.4
Takao	1	61.0	24.0	18.0	85.4	3.2	1.4	10.0	18.1
Takao	2	55.0	27.0	6.5	84.0	4.1	0.9	11.0	17.6
Hotenji	1	82.0	51.0	31.0	82.0	6.0	2.2	9.8	15.2
Hotenji	2	84.0	31.0	22.0	84.8	3.2	1.7	10.3	14.0
Heito	1	54.0	19.0	10.0	74.6	6.9	1.8	16.5	12.9
Heito	2	56.0	28.0	5.4	80.7	11.7	1.0	6.6	25.7
Utsunomata	1	49.0	9.0	5.0	80.9	6.7	5.6	6.8	26.7
Utsunomata	2	41.0	6.0	2.9	83.7	0.0	11.7	4.6	28.9
Utsunomata	3	83.0	54.0	51.0	76.4	7.0	1.4	15.2	11.0
Utsunomata	4	41.2	29.9	10.0	83.6	5.1	7.3	4.0	28.7
Utsunomata	5	46.8	30.3	10.0	80.8	4.8	8.1	6.3	23.1
Utsunomata	6	67.7	27.5	17.0	79.3	3.5	0.2	17.0	14.4
Utsunomata	7	72.3	29.9	17.0	81.5	4.1	0.3	14.1	17.2
Utsunomata	8	55.6	38.6	12.0	72.1	6.2	0.5	21.2	8.3
Utsunomata	9	56.8	34.3	16.0	70.2	7.0	0.4	22.4	7.8
Tunnel	1	36.0	10.0	10.0	92.0	5.2	0.7	1.4	29.0
Tunnel	2	35.0	8.0	6.0	93.9	1.6	0.0	1.6	29.0
Tukuche		26.0	8.0	5.0	94.0	0.0	3.0	0.0	31.0
Slope failure area									
Karamatsu	1	77.2	20.7	16.2	84.0	14.0	0.0	2.0	25.6
Karamatsu	2	57.0	17.3	15.2	84.0	14.0	0.0	2.0	25.8
Heito		57.3	12.7	11.2	89.0	5.0	0.0	6.0	23.4
Tsukidate	1	36.0	5.0	9.0	90.6	3.0	0.2	6.2	23.3
Tsukidate	2	45.0	19.0	13.0	89.2	3.1	1.6	5.5	25.5
Tsukidate	3	47.0	9.0	6.5	92.3	2.6	1.4	3.7	28.0
Debris flow area									
Urakawa	1	36.4	9.6	0.4	91.8	3.0	0.0	5.2	28.4
Urakawa	2	31.1	11.1	1.0	88.0	4.0	0.0	8.0	24.9

Urakawa	3	54.0	23.5	2.4	89.0	3.0	0.0	8.0	24.4
Urakawa	4	48.6	16.6	4.3	91.0	3.0	0.0	5.0	30.1
Urakawa	5	42.7	16.1	4.2	91.5	3.2	0.0	5.3	29.0
Urakawa	6	32.0	4.5	1.8	89.5	3.0	0.0	7.5	23.6
Urakawa	7	35.0	6.0	2.3	88.0	4.0	0.0	8.0	21.1
Urakawa	8	36.0	5.5	3.9	87.9	3.9	0.0	8.2	21.4
Volcanic area									
Usu	1	65.8	42.6	6.7	85.0	3.0	0.0	12.0	21.3
Usu	2	44.6	20.7	10.9	87.0	3.0	0.0	10.0	23.2
Usu	3	37.9	15.4	7.0	87.0	4.0	0.0	9.0	23.7
Usu	4	47.8	21.9	8.9	82.0	0.0	0.0	18.0	17.8
Average		63.8	29.8	19.8	81.2	5.3	1.0	12.4	17.1

Note: All units except ϕ'_R are in % and ϕ'_R is in degrees; LL=liquid limit; PI=plasticity index; CF=clay fraction.

The residual friction angles of Natural Samples (Tiwari & Marui, 2005) vary from 7.8° to 31°, average 17.1°.

Fifty four landslides through sedimentary fine-grained materials (i.e., clays, marls, mudstones, and shales) were chosen by (Eid et al., 2016) from the large number of reactivated landslides reported in the literature as case histories (Table 5-8).

Table 5-8 Reactivated landslides and reported soil residual shear strength correlations (Eid et al., 2016)

No.	Site	Stratum	ϕ'_R(°)
1-5	Chiusi della Verna (5 slides), Tuscany, Italy	Clay shale	11.7-15.6 (av.= 13.2)
6	River Beas Valley, India	Siwalik rock	18-20
7	Jackfield, Shropshire, UK	Carboniferous mudstone	17.1
8	St. Martino Valley, Italy	Weathered marl	17
9	Weirton,West Virginia, USA	Colluviume	16
10	St. Cristoforo, Italy	Lugagnano clay	11.5
11	Mam Tor, Berbyshire, UK	Edale shale	14

12-19	Seattle Freeway (8 slides), Seattle, USA	Lawton clay	13.6-16.5 (av.=15.3)
20	Walton's Wood, Staffordshire, UK	Carboniferous mudstone	13.5-15.5
21	Lyme Regis, UK	Lower Lias clay	11.2
22	Bury Hill, Staffordshire, UK	Etruria marl	12
23	Burderop Wood, Swindon, UK	Gault clay	13.3
24	Hodson, Swindon, UK	Gault clay	14
25	Folkestone Warren, slip W4, Kent, UK	Gault clay	7.7-9.4
26	Barnsdale, Leicestershire, UK	Upper Lias clay	10.4
27	Hambleton, Leicestershire, UK	Upper Lias clay	10.3
28	Uppingham, Leicestershire, UK	Upper Lias clay	16.2
29	Gretton, Northamptonshire, UK	Upper Lias clay	13.5
30	Daventry, Northamptonshire, UK	Upper Lias clay	13
31	Rockingham, Northamptonshire, UK	Upper Lias clay	13.9
32	Weedon, Northamptonshire, UK	Upper Lias clay	14.2
33	Wansford, Cambs, UK	Upper Lias clay	9.8
34	Wardley, Leicestershire,UK	Upper Lias clay	14.9
35	Endcombe, UK	Atherfield clay	13.7
36	Patney-Chirton, UK	Gault clay	11.9
37	Petrofka, Saskatchewan, Canada	Bedrock clay	5.7
38	Spinney Hill, Saskatchewan, Canada	Clay shale	8.7
39	Denholm, Saskatchewan, Canada	Bedrock clay	6.7
40	Hadleigh, (slip surf. 2&3), Essex, UK	Brown London clay	13.2
41	Hadleigh, (slip surf. 5), Essex, UK	Brown London clay	13.3
42	Hadleigh, (slip surf. 8), Essex, UK	Brown London clay	13.5
43	Hadleigh, (slip surf. 12), Essex, UK	Brown London clay	13.2
44	Guildford, Surrey, UK	Brown London clay	10.9
45	Beacon Hill, Herne Bay, Kent, UK	Brown and Blue London clay	14.1-14.8
46-47	Queen's Avenue, (1966,1970), Herne Bay, Kent, UK	Brown and Blue London clay	12.3-12.5

48-51	Miramar, (1953, 1956, 1966, 1970), Hern Bay, Kent, UK	Brown and Blue London clay	10.8-12.3
52	San Diego, California, USA	Santiago claystone	7.5
53	Portuguese Bend, California, USA	Altamira bentonitic tuff	6.5
54	Gardiner Dam, Saskatchewan, Canada	Bearpaw Shale	9.8

For each considered case history (Eid et al., 2016) investigated the soils summarized in Table 5-8 for slope stability analyses and suggested the residual friction angles vary from 5.7° to 20°, with an average value of 13.7°.

In this thesis, residual friction angles 5° ~ 20° were used use for angle of internal friction on failure plane and K_r values from 0.05 ~ 0.35 were used.

5.1.7 The Stress Distribution in Railway Subgrade

The stress distribution variation under ballast is typically "W" shape (see Figure 5-1 and Figure 5-2), which is referred to as normal spreading load. In some scenarios, under the action of cyclic wheel loads and vibration, a few large ballast particles may punch into subgrade as a point load and contribute to the progressive shear failure. For this reason, in the study, two different types of load, namely, point load and normal spreading are considered.

The point load is that stress concentrated on one or a few of particles of ballast in a small area and stress is typically small in the surrounding domain of the stress concentrated area.

The normal spreading load is the stress that distribute normally in subgrade without major stress concentration. This is typically to Figure 2-8, Figure 5-1and Figure 5-2.

Leshchinsky (2012) and Leshchinsky & Ling (2013) have investigated the effects of geocell confinement on ballasted embankments when encountering a soft subgrade, weaker ballast, or varying reinforcement stiffness values.

A series of 6 large-scale model tests of ballasted railroad embankments were conducted by (Leshchinsky, 2012; Leshchinsky & Ling, 2013) in the laboratory. The material properties used in the analysis are summarized in Table 5-9.

Table 5-9 Model material properties (Leshchinsky & Ling, 2013)

Properties	Ballast	Subballast	Subgrade	Geocell	Tie plates	Ties
Mass Density, γ (kg/m^3)	1520	1520	1700	1500	2000	2000
Elastic modulus, E (MPa)	2	2	20	2070	200,000	30,000
Poisson's Ratio, v	0.35	0.35	0.35	0.35	0.3	0.25
Internal Angle of Friction, ϕ (°)	45	45	-	-	-	-
Angle of Dilation, ψ (°)	15	15	-	-	-	-

The wheel load chosen for the analysis in the present study conservative in order to demonstrate track behavior under the worst conditions possible (Leshchinsky & Ling, 2013). This load corresponds to two wheels, each having a wheel load of 22.4 kN (50,000 lbs or 25 tons, USACE Railroad Design Manual).

A series of simulations were performed by on displacements, stresses and strains in railway subgrade in order to determine the effects of geocell stiffness, ballast strength, and foundation compressibility. 6 types of Geocell Stiffness (MPa) were used in the study, which are 100, 500, 1000, 2070, 100000, 200000 MPa. Similar values are suggested by Leshchinsky & Ling, 2013

The Figure 5-1 is Subgrade stress distribution below geocell-reinforced embankment overlying very soft foundation (2 MPa).

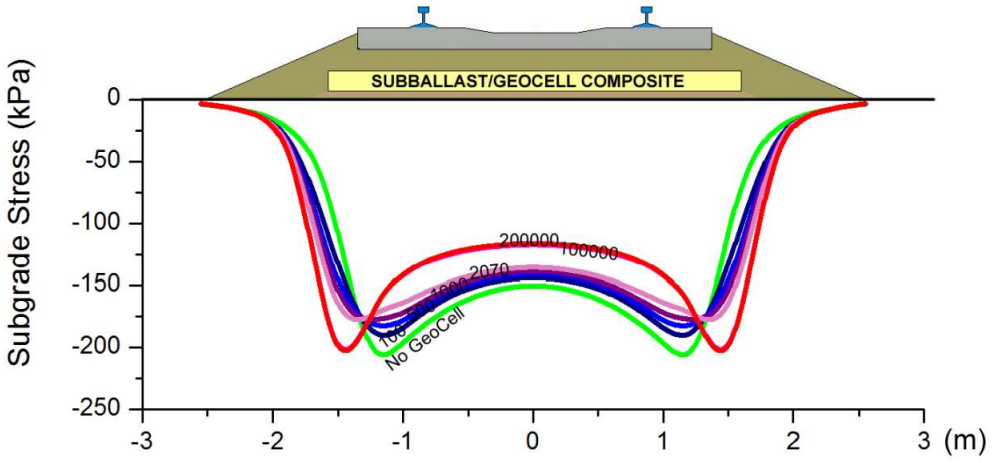

Figure 5-1 Subgrade stress distribution below geocell-reinforced embankment overlying very soft foundation (2 MPa) (Leshchinsky, 2012).

The Figure 5-2 is Subgrade stress distribution below geocell-reinforced embankment overlying soft foundation (20 MPa).

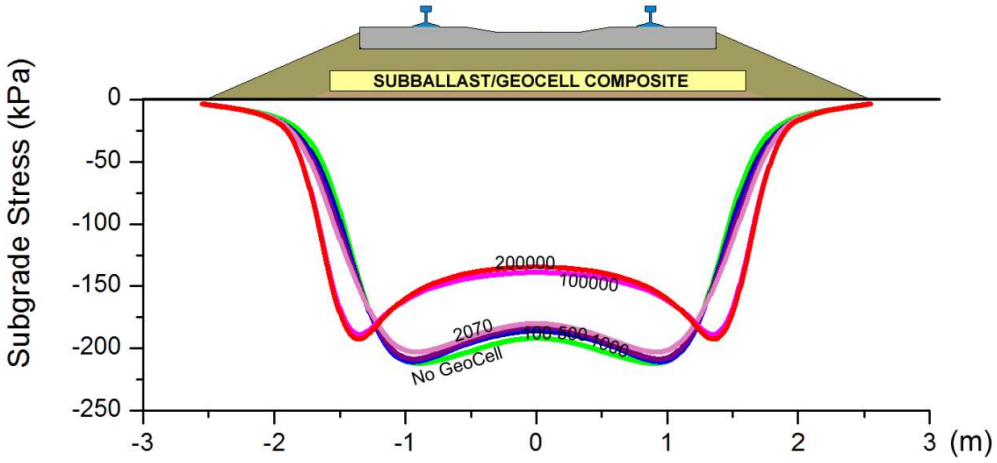

Figure 5-2 Subgrade stress distribution below geocell-reinforced embankment overlying soft foundation (20 MPa) (Leshchinsky, 2012).

Although the stress distribution in subgrade presented in Figure 2-8 is more rational, but it is difficult to accurately digitalize it. For this reason, in this thesis, the N Geocell values and pattern of stress distribution in subgrade of soft soils shown in Figure 5-1 is used for representing the normal spreading load.

To the best of the knowledge of the author, there are no experimental studies results in the literature to provide guidance on the likely maximum point load (or stress) that arises in railway tracks. This value is difficult or measure or estimate. For this reason, a value of 420 kPa, is considered as stress associated with a point load with a safety factor of 2 as shown Figure 5-1.

5.2 Result of Simulation for Point Load

Based on selected input data of four key soil properties, which include the effective angle of friction, effective cohesion, coefficient of earth pressure at rest, and the coefficient of residual friction on failure plane, 1400 simulations have been conducted. In these simulations, the effective angle of friction of subgrade soils was varied from 17° to 25° with increments of 2° (i.e., ϕ' = 17°, 19°, 21°, 23°, 25°), the effective cohesion values was varied from 1 kPa to 10 kPa

with increments of 1 kPa (i.e., c' = 1, 2, 3, 4, 5, 6, 7, 8, 9, 10 kPa) , the coefficient of earth pressure at rest was varied from 0.25 to 0.4 with increments of 0.05 (i.e., K_o = 0.25, 0.3, 0.35, 0.4), and the coefficient of residual friction on failure plane was varied from 0.05 to 0.35 with increments of 0.05 (i.e., K_r = 0.05, 0.1, 0.15, 0.2, 0.25, 0.3, 0.35) (i.e., total 5 x 10 x 4 x 7 = 1400 simulations). Some typical results of the simulations under point load are summarized in the Table 5-10 (see detail results in Appendix).

Table 5-10 Some typical results of simulation under point load

No of simulation	Angle of friction	Cohesion	Coefficient of earth pressure at rest	Coefficient of residual friction	Number of elements	Final Load
	ϕ'	c'	K_0	K_r	No.	P
	°	kPa				%
75	25	5	0.3	0.05	7	18
255	25	1	0.3	0.1	200	20
260	25	2	0.3	0.1	47	48
265	25	3	0.3	0.1	23	41
270	25	4	0.3	0.1	11	27
275	25	5	0.3	0.1	8	25
280	25	6	0.3	0.1	6	21
285	25	7	0.3	0.1	6	25
290	25	8	0.3	0.1	5	23
295	25	9	0.3	0.1	5	26
300	25	10	0.3	0.1	5	29
475	25	5	0.3	0.15	8	29
521	17	5	0.35	0.15	8	35
522	19	5	0.35	0.15	8	35
523	21	5	0.35	0.15	8	35
524	23	5	0.35	0.15	7	32
525	25	5	0.35	0.15	6	31
625	25	5	0.25	0.2	10	35

675	25	5	0.3	0.2	9	40
725	25	5	0.35	0.2	7	43
775	25	5	0.4	0.2	1	256
875	25	5	0.3	0.25	9	48
1075	25	5	0.3	0.3	9	58
1275	25	5	0.3	0.35	10	82

In the program, three conditions are set to end the each simulation of progressive shear failure.

(i) The limit number of elements for one progressive shear failure is 200.

(ii) The maximum stress (final load) in an element is limited to 200% of input stress (load).

(iii) The failure plane reaches the surface of subgrade. Therefore, in table 1, there are many simulations which its number of elements is 200 or its final load is 200%.

In Table 5-10, the number of elements is the number of failed elements along failure plane during each simulation. The final load is the percentage of maximum load or stress in the subgrade at end of each simulation.

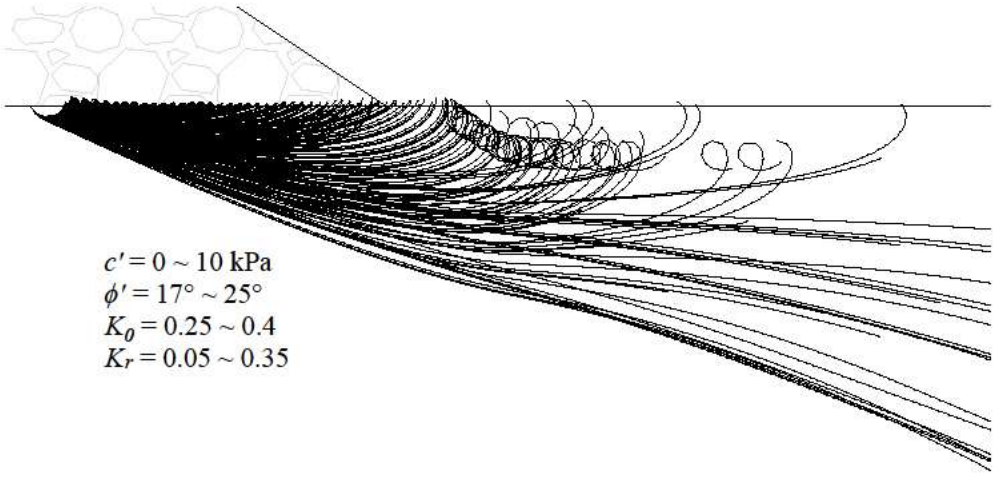

Figure 5-3 Failure planes of simulation for point load

Among the 1400 results of simulation for the point load, there are 77 simulations its number of element is 0; that represent the subgrade material is so weak and fail under self-weight according to Mohr-coulomb criteria, so these cases do not exist in the reality. There are 21 simulations its

number of element is 200; that represent the subgrade material is weak and failure plane extends inside subgrade, so it is not progressive shear failure but displacement or settlement. There are 88 simulations its final load is 200%; that represent the subgrade material is weak and failure plane extends inside subgrade until the load reaches 200% input load. There are 49 simulations its final load is greater than 200%; that represent the subgrade material is strong and failure does not occur under input load. The other 1165 simulations are progressive shear failure.

The simulation results show a few failure planes that are curled at end of failure plane. Such a behavior may be associated with some limitations in simulation program. This is most likely due to not considering the principle stresses rotation in the element under wheel load and displacements after element fails associated with the stress changes.

5.2.1 Effect of Angle of Friction

The Figure 5-4 shows the five failure planes for angle of friction, ϕ' from 17° to 25° while the effective cohesion, c' of subgrade is 5 kPa, the coefficient of earth pressure at rest, K_0 is 0.35, and the coefficient of residual friction, K_r is 0.15.

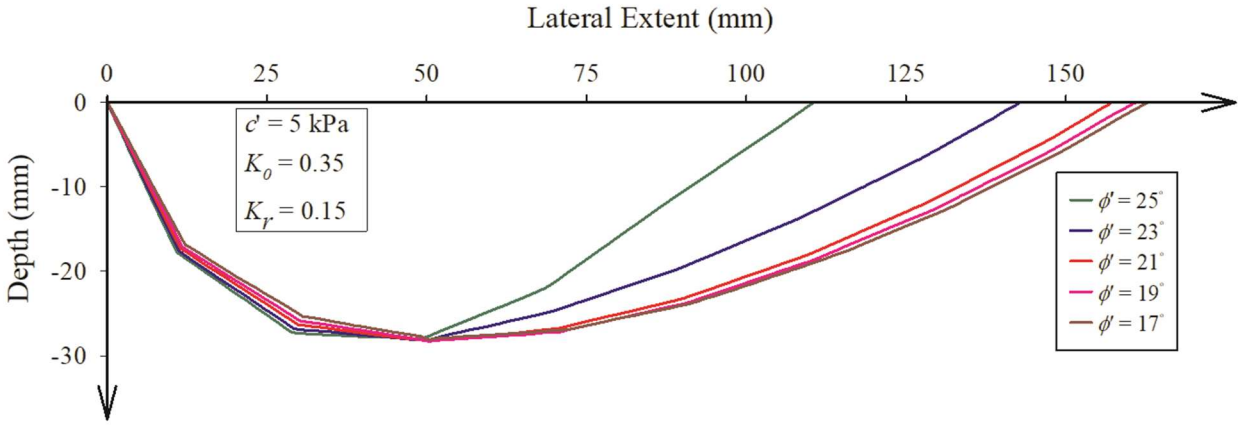

Figure 5-4 Effect of Angle of Friction to progressive shear failure

From this figure and the results summarized in Table 5-10, it can be observed that the failure planes progress rapidly and reach the surface of subgrade (i.e. lesser number of failed elements) with an increase in the angle of friction. The final (failure) load or stress increases slightly with an increase in the angle of friction, ϕ' value used for the subgrade. As expected, the possibility of

progressive shear failure reduces by using a subgrade soil with a higher angle of friction, ϕ' value.

5.2.2 Effect of Subgrade Effective Cohesion

The Figure 5-5 shows ten failure planes for the subgrade with effective cohesion, *c'* values varying from 1 kPa to 10 kPa for a soil with an angle of friction ϕ' value of 25°, the coefficient of earth pressure at rest, K_0 value of 0.3, and the coefficient of residual friction K_0 value of 0.1.

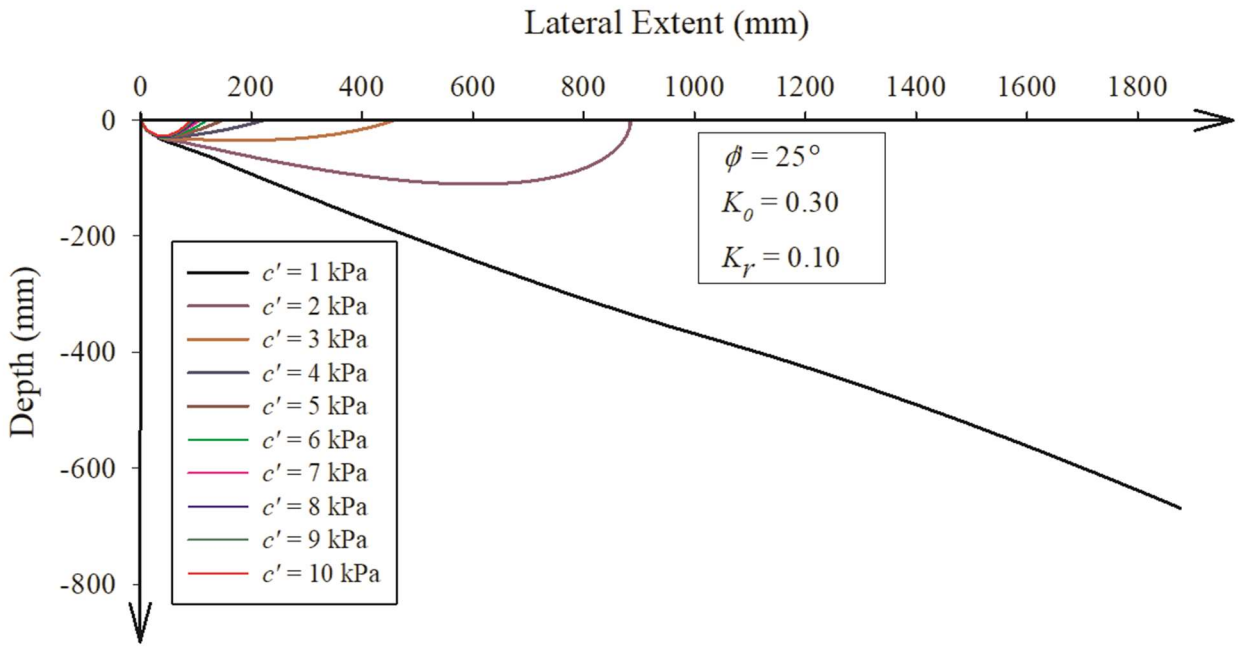

Figure 5-5 Effect of Subgrade Effective Cohesion to progressive shear failure

From Figure 5-5 and Table 5-10, we can see when the effective cohesion, *c'* of subgrade is 1 kPa, the failure plane goes out and down into subgrade with an around 20° angle to the horizontal direction, and does not return up to the surface of subgrade. For effective cohesion, *c'* value of subgrade is 2 kPa, the failure plane goes down initially, then slowly turns up, and finally it reaches the surface of subgrade where is out of ballast area after 47 failed elements. When the cohesion of subgrade is 3 kPa the failure plane turns up quicker than when the effective cohesion *c'* of 2 kPa, and reaches the surface of subgrade after 23 failed elements. When the cohesion of subgrade is 4 kPa the failure plane turns up even quicker and reach the surface of subgrade after

11 failed elements. Similarly, for the cohesion of subgrade from 5 kPa to 10 kPa, the failure plane reaches the surface of subgrade earlier and closer to primary failure element with lesser failed elements, as the cohesion increases.

The final (failure) load or stress increase and the number of failed elements decrease as the cohesion increase. In other words, increasing the effective cohesion of subgrade can reduce the risk of progressive shear failure in subgrade.

5.2.3 Effect of Coefficient of Earth Pressure at Rest

Figure 5-6 shows four failure planes for the coefficient of earth pressure at rest, K_0 value varying from 0.25 to 0.4 while the effective cohesion c' of subgrade is 5 kPa, the angle of friction ϕ' value is 25°, and the coefficient of residual friction, K_r is 0.2.

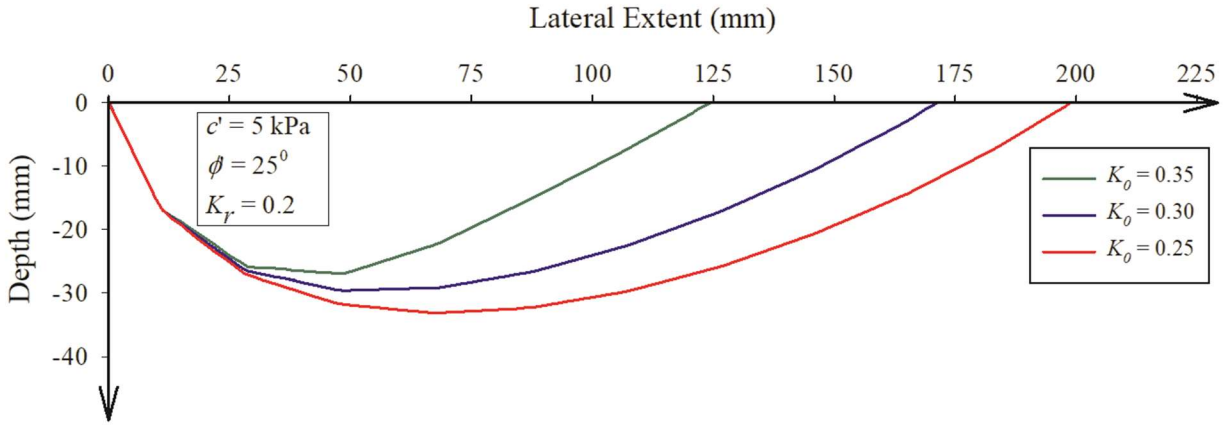

Figure 5-6 Effect of Coefficient of Earth Pressure at Rest to progressive shear failure

From Figure 5-6 and Table 5-10, we can see when the coefficient of earth pressure at rest, K_0 is 0.25 the failure plane extends down initially, then turns up, and finally reaches the surface of subgrade after 10 failed elements. When the coefficient of earth pressure at rest, K_0 is 0.3, the failure plane extends shorter than the coefficient of earth pressure at rest, K_0 is 0.25, and reaches the surface of subgrade after 9 failed elements. Similarly, when the coefficient of earth pressure at rest K_0 is 0.35, the failure plane goes up quicker than the coefficient of earth pressure at rest K_0 is 0.3, and reaches the surface of subgrade after 7 failed elements. However, when the coefficient of earth pressure at rest, K_0 is 0.4, the primary element does not fail until the load (or stress) is 2.56 times over the applied point load (or stress) in subgrade. This simulation result suggests the

failure would not occur normally when the coefficient of earth pressure at rest K_0 is greater than 0.4. This is because at higher values of K_0 there is more confinement which offers more resistance in the development of failure plane. Therefore, increasing the coefficient of earth pressure at rest K_0 value can reduce the risk of progressive shear failure in the subgrade.

5.2.4 Effect of Coefficient of Friction on Failure Plane

The Figure 5-7 shows seven failure planes for the coefficient of residual friction, K_r values varying from 0.05 to 0.35 on failure plane for a soil with an effective cohesion, c' value of subgrade is 5 kPa, and the angle of internal friction is 25°, and the coefficient of earth pressure at rest K_0 value is 0.3.

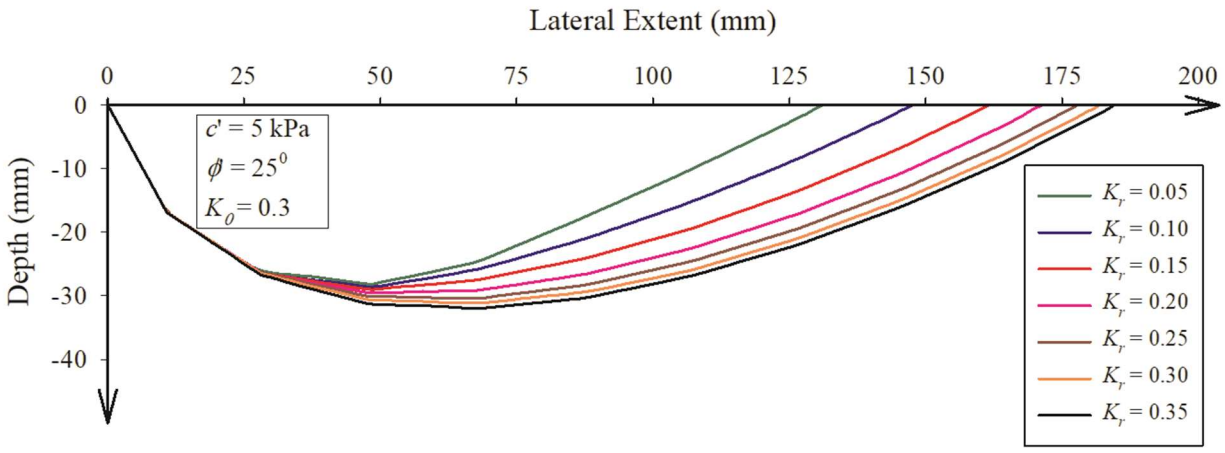

Figure 5-7 Effect of Coefficient of residual Friction on Failure Plane

From Figure 5-7 and Table 5-10, similar to analyses of results summarized earlier, all failure planes extend down initially, then turns up, and finally reaches the surface of subgrade after 7 to 10 failed elements. These simulation results suggest as the coefficient of residual friction, K_r on failure plane increase from 0.05 to 0.35, along the shear failure plane, the number of failed elements increase from 7 to 10, and the final load factor increase from 18% to 82%. These simulation results are consistent with the expected behavior which suggest that an increase in the coefficient of residual friction, K_r value on failure plane can reduce the risk of progressive shear failure in the subgrade.

5.3 Result of Simulation for normal spreading load

The typical load or stress on surface of subgrade, which is referred to as normal spreading load can be assumed as shown in Figure 5-1 and Figure 2-8. Based on selected input data which were summarized in earlier sections, 1400 simulation were conducted. Some typical results of these simulations are summarized in Table 5-11 (see detailed results in Appendix). In addition, Figure 5-8 summarizes the various failure planes.

From Figure 5-8 and Table 5-11, it can be observed, under normal spreading load, almost all the failure planes go down and then spread out in subgrade with an angle of 12° ~ 32° to the horizontal direction after the first several elements. They never turn up to the surface of subgrade, except when the cohesion or suction stress are 3 ~ 5 kPa. Some failure planes that turn up towards the surface of subgrade under the toe of ballast however do not reach the surface of subgrade.

Table 5-11 Some typical results of the simulation under normal spreading load

No of simulation	Angle of friction	Cohesion	Coefficient of earth pressure at rest	Coefficient of residual friction	Number of elements	Final Load
	ϕ'	C	K_0	K_r	No.	P
	°	kPa				%
5	25	1	0.25	0.05	0	0
10	25	2	0.25	0.05	200	7
11	17	3	0.25	0.05	200	101
12	19	3	0.25	0.05	168	200
13	21	3	0.25	0.05	143	200
14	23	3	0.25	0.05	132	200
15	25	3	0.25	0.05	126	200
20	25	4	0.25	0.05	93	200
25	25	5	0.25	0.05	80	200
30	25	6	0.25	0.05	67	200
35	25	7	0.25	0.05	60	200
40	25	8	0.25	0.05	54	200
45	25	9	0.25	0.05	50	200
50	25	10	0.25	0.05	47	200
65	25	3	0.3	0.05	92	200
115	25	3	0.35	0.05	40	200
165	25	3	0.4	0.05	1	310
215	25	3	0.25	0.1	146	200
415	25	3	0.25	0.15	135	200
615	25	3	0.25	0.2	109	200
815	25	3	0.25	0.25	90	200
1015	25	3	0.25	0.3	70	200
1215	25	3	0.25	0.35	54	200

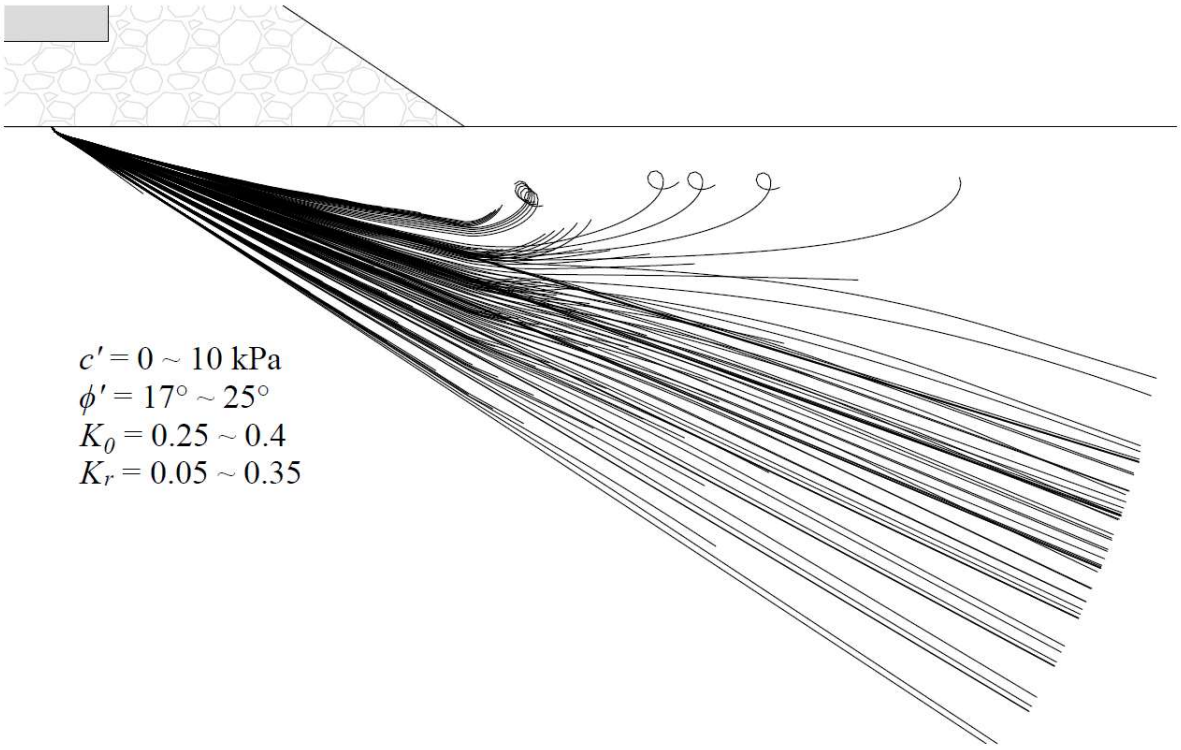

Figure 5-8 Failure planes under normal spreading load

5.3.1 Effect of Stress Distribution to Progressive Shear Failure

Comparing to the Figure 5-3 and the Figure 5-8, no failure plane finally reaches the surface of subgrade under normal spreading load although some failure planes turn up toward the surface of subgrade while many failure planes reach the surface of subgrade under point load. In other words, under the normal spreading load distribution, the progressive shear failure would not occur although many elements have failed but failure planes have not reached the surface of subgrade. However, under the point load, the progressive shear failure would occur when the failure planes reach the surface of subgrade.

5.3.2 Effect of Matric Suction

As per discussions summarized in Section 4.2 2) and Equation 4.3, for the cohesionless soil, the effective cohesion $c' = 0$, so c directly involves as the effect of matric suction.

The Figure 5-9 shows ten failure planes for the subgrade with effective cohesion, c' values varying from 1 kPa to 10 kPa for a soil with an angle of friction ϕ' value of 25°, the coefficient of earth pressure at rest, K_0 value of 0.25, and the coefficient of residual friction K_0 value of 0.05.

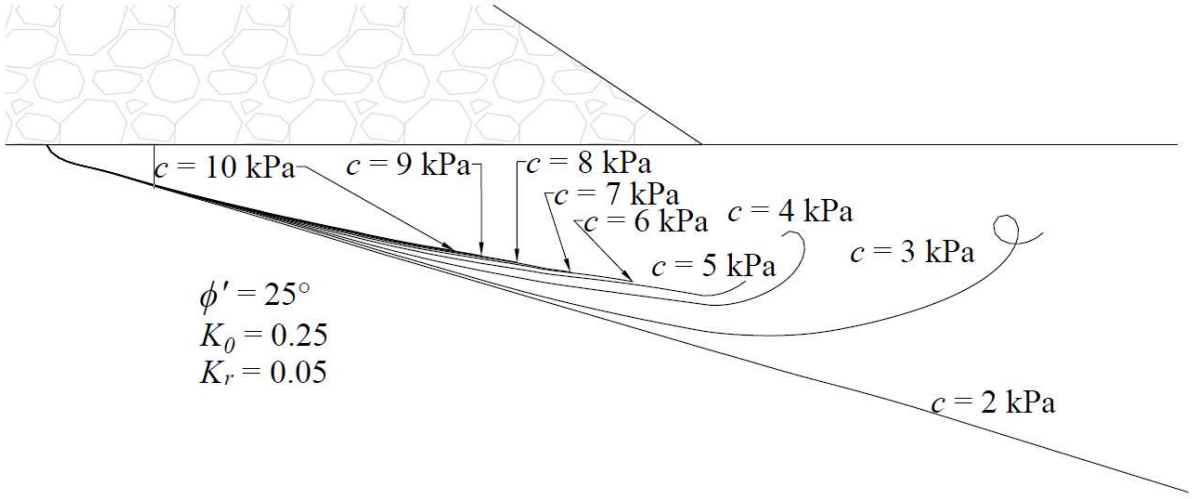

Figure 5-9 Effect of Matric Suction to Progressive Shear Failure

From Figure 5-9 and Table 5-11, we can see, all the failure plane goes down and out in subgrade with an angle of around 15° to the horizontal direction. As the suction increases, the angle of failure plane to the horizontal direction become smaller, and the number of failed elements become smaller too. So, increasing the cohesion or suction of subgrade can reduce the risk of progressive shear failure in subgrade.

5.3.3 Effect of frication angle, cohesion and coefficient of earth pressure at rest

According to Eq. 3.7 and 4.7, in this study, $\sigma'_3 = K_0\sigma'_1$. If $\sigma'_1 > \sigma'_3 \tan^2\theta + 2c'\tan\theta$, the element will fail. Or if $K_0 > \frac{\sigma'_1 - 2c'\tan\theta}{\sigma'_1 \tan^2\theta}$, the element will not fail. For cohesionless soil, the c' = 0, then if $K_0 > \frac{1}{\tan^2\theta}$, the progressive shear fail will not occur.

According to Leshchinsky & Ling (2013) and Leshchinsky (2012) (as summarized in Figure 5-1), the maximum stress under bottom of ballast is 210 kPa. Considering the safety factor of 2 as for point load, we use 420 kPa as vertical (major principal) stress σ_1'. Therefore, we can calculate the relationship of friction angle ϕ', cohesion c' and coefficient of earth pressure at rest K_0 at critical condition of shear failure as in Table 5-12 and Figure 5-10.

Table 5-12 The relationship of frication angle ϕ', cohesion c' and coefficient of earth pressure at rest K_0 at critical condition of shear failure

ϕ' (°)	11	12	13	14	15	16	17	18	19	20	21	22	23	24	25
c' (kPa)	0.98	0.99	1.01	1.03	1.05	1.06	1.08	1.10	1.12	1.13	1.15	1.17	1.19	1.20	1.22
0	0.45	0.42	0.39	0.36	0.33	0.31	0.28	0.26	0.24	0.22	0.20	0.18	0.16	0.15	0.13
1	0.45	0.42	0.39	0.36	0.33	0.30	0.28	0.26	0.24	0.22	0.20	0.18	0.16	0.15	0.13
2	0.45	0.42	0.38	0.36	0.33	0.30	0.28	0.25	0.23	0.21	0.19	0.18	0.16	0.14	0.13
3	0.45	0.41	0.38	0.35	0.33	0.30	0.28	0.25	0.23	0.21	0.19	0.17	0.16	0.14	0.13
4	0.44	0.41	0.38	0.35	0.32	0.30	0.27	0.25	0.23	0.21	0.19	0.17	0.16	0.14	0.13
5	0.44	0.41	0.38	0.35	0.32	0.29	0.27	0.25	0.23	0.21	0.19	0.17	0.15	0.14	0.12
6	0.44	0.40	0.37	0.34	0.32	0.29	0.27	0.25	0.22	0.20	0.19	0.17	0.15	0.14	0.12
7	0.43	0.40	0.37	0.34	0.31	0.29	0.26	0.24	0.22	0.20	0.18	0.17	0.15	0.13	0.12
8	0.43	0.40	0.37	0.34	0.31	0.29	0.26	0.24	0.22	0.20	0.18	0.16	0.15	0.13	0.12
9	0.43	0.39	0.36	0.34	0.31	0.28	0.26	0.24	0.22	0.20	0.18	0.16	0.15	0.13	0.12
10	0.42	0.39	0.36	0.33	0.31	0.28	0.26	0.24	0.21	0.20	0.18	0.16	0.14	0.13	0.12
11	0.42	0.39	0.36	0.33	0.30	0.28	0.25	0.23	0.21	0.19	0.17	0.16	0.14	0.13	0.11
12	0.42	0.38	0.35	0.33	0.30	0.28	0.25	0.23	0.21	0.19	0.17	0.16	0.14	0.13	0.11
13	0.41	0.38	0.35	0.32	0.30	0.27	0.25	0.23	0.21	0.19	0.17	0.15	0.14	0.12	0.11
14	0.41	0.38	0.35	0.32	0.29	0.27	0.25	0.23	0.21	0.19	0.17	0.15	0.14	0.12	0.11
15	0.41	0.38	0.35	0.32	0.29	0.27	0.24	0.22	0.20	0.18	0.17	0.15	0.13	0.12	0.11
16	0.40	0.37	0.34	0.32	0.29	0.27	0.24	0.22	0.20	0.18	0.16	0.15	0.13	0.12	0.10
17	0.40	0.37	0.34	0.31	0.29	0.26	0.24	0.22	0.20	0.18	0.16	0.15	0.13	0.12	0.10
18	0.40	0.37	0.34	0.31	0.28	0.26	0.24	0.22	0.20	0.18	0.16	0.14	0.13	0.11	0.10
19	0.39	0.36	0.33	0.31	0.28	0.26	0.23	0.21	0.19	0.18	0.16	0.14	0.13	0.11	0.10
20	0.39	0.36	0.33	0.30	0.28	0.25	0.23	0.21	0.19	0.17	0.16	0.14	0.12	0.11	0.10

Note: Row 1 are the values of friction angle ϕ' in degree
Row 2 are the value of angle of shear failure plane θ in radian
Colon 1 are the value of cohesion c' in kPa, including suction
All the other cell are value of coefficient of earth pressure at rest K_0

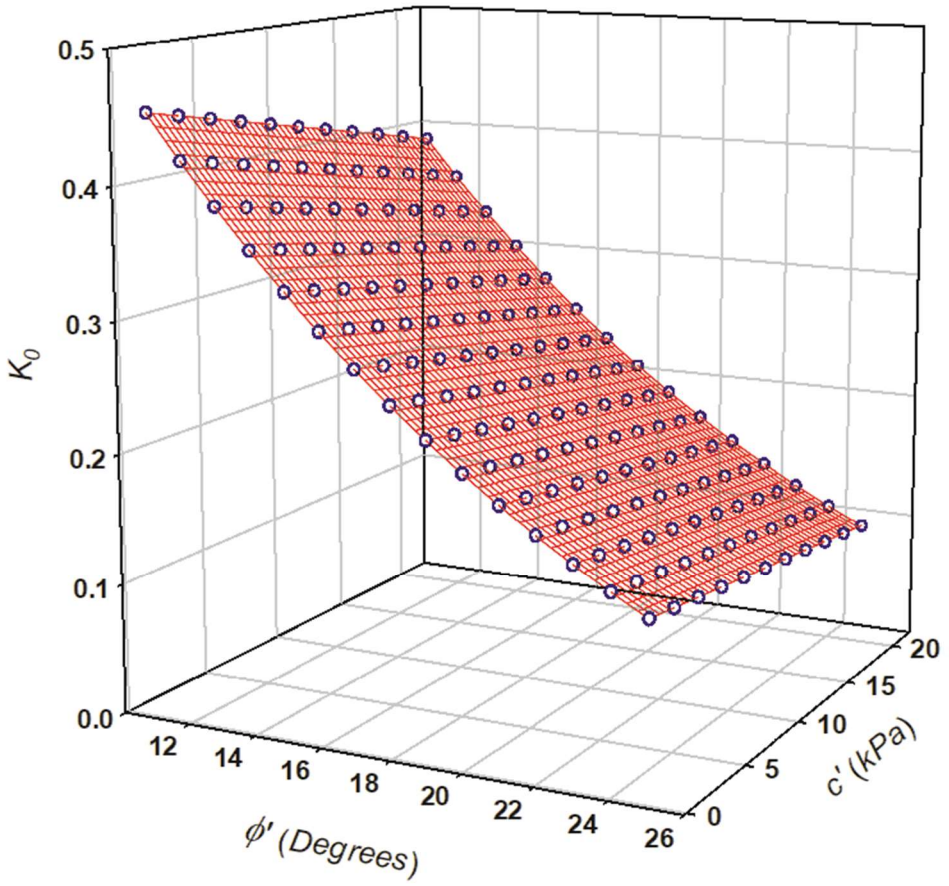

Figure 5-10 The relationship of frication angle ϕ', cohesion c' and coefficient of earth pressure at rest K_0 at critical condition of shear failure

In the Figure 5-10, if the relationship of friction angle ϕ', cohesion c' and coefficient of earth pressure at rest K_0 is above the critical surface, the shear failure would not occur; if the relationship is beneath the critical surface, the shear failure would occur, and it may develop into the progressive shear failure.

5.4 Sensitivity of element size

Figure 5-11 shows nine failure planes for the element is 0.02m, 0.05m and 0.1m, and the angle of friction is 17°, 21° and 25° while the effective cohesion, c' of subgrade is 2 kPa, the coefficient of earth pressure at rest, K_0 is 0.35, and the coefficient of residual friction, K_r is 0.1.

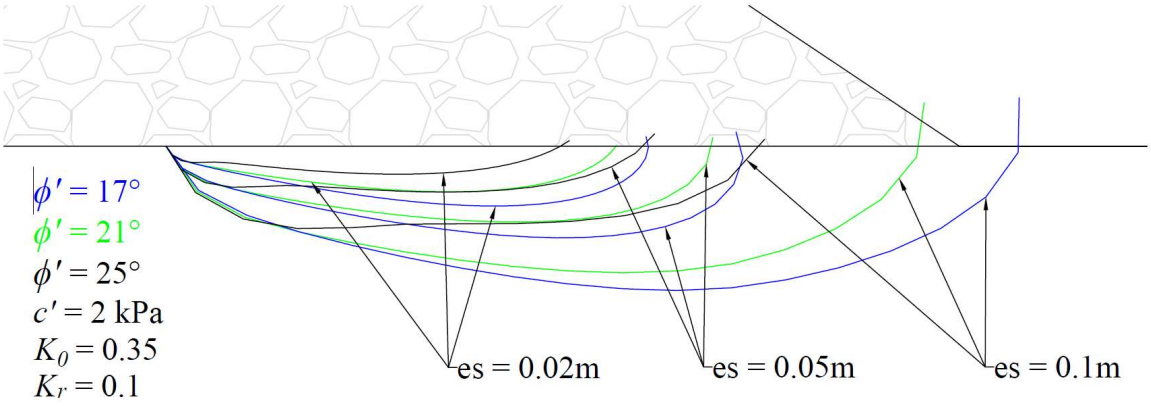

Figure 5-11 Sensitivity of element size

From Figure 5-11, we can see, as the element size increases, the failure plane goes down into subgrade deeper and extends longer, but the change of failure plane shape is not proportional to the increase of element size. Although the element size increases 2.5 times from 0.02m to 0.05m, the length of failure plane only increases 20%. When the element size increases 2 times from 0.05m to 0.1m, the length of failure plane increases 38%. So the element size does have an effect on simulation of progressive shear failure and shape of failure plane.

CHAPTER 6
CONCLUSIONS AND SUGGESTIONS FOR THE FUTURE RESEARCH

This chapter summarizes conclusions from the present study; in addition, recommendations for railway subgrade design and construction and suggestions for the future research are provided.

6.1 Conclusions

1) A first of its kind and novel numerical simulations of progressive shear failure in railway subgrade is undertaken in this study extending Mohr-Coulomb failure criteria considering the effect of matric suction within the framework of unsaturated soil mechanics. This is a rational approach to investigate progressive shear failure in the railway foundation subgrade taking account of the influence of soil suction in the railway subgrade.
2) Load (or stress) distribution has significant effects to progressive shear failure. The risk of progressive shear failure is low under the normal spreading load distribution. However, the ballast is constituted of uniformly large size granular material without any cohesion; under cyclic wheel load and vibration, the stress distribution under bottom of ballast has a high possibility to spread unevenly over surface of subgrade and form stress concentration, and have high risk of progressive shear failure.
3) The angle of internal friction, cohesion or suction, coefficient of earth pressure at rest, and coefficient of residual friction on failure plane have significant effects to progressive shear failure. Increasing the angle of friction of subgrade, increasing the cohesion (or matric suction) of subgrade, increasing the coefficient of earth pressure at rest, and increasing the coefficient of friction on failure plane, all can reduce the risk of progressive shear failure in subgrade.
4) There is a relationship among frication angle, cohesion or suction, and coefficient of earth pressure at rest. If $K_0 > \frac{\sigma'_1 - 2c' \tan\theta}{\sigma'_1 \tan^2\theta}$, both the shear failure and progressive shear

failure would not occur. This is a valuable guideline that can be followed in the design of railway tracks to alleviate railway subgrade failure.

6.2 Recommendations for Subgrade Design and Maintenance

6.2.1 Reduce the uneven stress distribution in railway subgrade

Leshchinsky (2012) suggested use of geocell to constrain lateral movement of ballast to achieve a more even distribution of stress on the surface of subgrade. Increasing thickness of ballast and adding subballast layer (Sayeed & Shahin, 2018), as well as well-tamping and maintenance of ballast, can also contribute to even stress distribution over top of subgrade.

6.2.2 Use geotextile

Burrow et al. (2011) recommended placing a layer of geotextile between subgrade and ballast (or subballast). Geotextile can separate ballast (or subballast) from subgrade materials and prevent the ballast particles sinking into subgrade. Geotextile can serve as effective filters to keep fine soil in subgrade in place but drain the water away. Geotextile can also serve as lateral reinforce to reduce lateral movement of ballast and subgrade materials.

6.2.3 Use high-qualified materials for subgrade

Use materials for subgrade with high friction angle, high cohesion (or matric suction), high coefficient of earth pressure at rest, and high coefficient of residual friction, or with optimum combination of friction angle, cohesion (or matric suction), coefficient of earth pressure at rest, and coefficient of residual friction to ensure the shear failure would not occur in subgrade.

6.2.4 Use various methods

Use various methods (Dong et al. 2018; Esmaeili & Khajehei, 2016; Milne et al., 2018) to increase the angle of friction, cohesion (or matric suction), coefficient of earth pressure at rest, and coefficient of residual friction of subgrade during railway construction and maintenance. The results of this study also consistent with the suggestions of these researchers.

6.3 Suggestion for the Future Research

The program developed for this research for simulating progressive shear failure had consumed a significant amount of time. Due to this reason, it was not possible to undertaken experimental studies in a laboratory environment and provide validations with numerical simulations of progressive shear failure in railway subgrade. It is important to undertake experimental studies in a laboratory environment along with field studies to validate the program developed through the present study.

The improvement of the simulations of progressive shear failure with Mohr-Coulomb failure criteria and finite element method (FEM) by considering the soil displacement and stress changes would be valuable.

In the present study, Mohr-Coulomb failure criteria is used. The simulations of progressive shear failure should also be compared with other soil failure theories to understand the strengths and limitations of the proposed approach presented in this thesis.

BIBLIOGRAPHY

Abrantes, L. G., & Pereira de Campos, T. M. (2019). Evaluation of the coefficient of earth pressure at rest (K0) of a saturated-unsaturated colluvium soil. *E3S Web of Conferences*, *92*, 1–6. https://doi.org/10.1051/e3sconf/20199207006

Al-Hussaini, M. (1981). Comparison of Various Methods for Determining Ko. *American Society for Testing and Materials*, 78–93.

Alonso, E. E., Gens, A., & Josa, A. (1990). A constitutive model for partially saturated soils. *Geotechnique*, *40*(3), 405–430. https://doi.org/10.1680/geot.1991.41.2.273

Alonso, E. E., Pereira, J. M., Vaunat, J., & Olivella, S. (2010). A microstructurally based effective stress for unsaturated soils. *Geotechnique*, *60*(12), 913–925. https://doi.org/10.1680/geot.8.P.002

Alonso, E. E., Pinyol, N. M., & Gens, A. (2013). Compacted soil behaviour: Initial state, structure and constitutive modelling. *Geotechnique*, *63*(6), 463–478. https://doi.org/10.1680/geot.11.P.134

Baker, R., & Frydman, S. (2009). Unsaturated soil mechanics. Critical review of physical foundations. *Engineering Geology*, *106*(1–2), 26–39. https://doi.org/10.1016/j.enggeo.2009.02.010

Bishop, A. W. (1959). The principle of effective stress. *Teknisk Ukeblad*, *106*, 859–863.

Bjerrum, L. (1967). Engineering geology of norwegian normally-consolidated marine clays as related to settlements of buildings. *Geotechnique*, *17*(2), 83–118. https://doi.org/10.1680/geot.1967.17.2.83

Boler, H., Mishra, D., Hou, W., & Tutumluer, E. (2018). Understanding track substructure behavior: Field instrumentation data analysis and development of numerical models. *Transportation Geotechnics*, *17*(July), 109–121. https://doi.org/10.1016/j.trgeo.2018.10.001

Brooker, E. W., & Ireland, H. O. (1965). Earth Pressures at Rest Related to Stress History. *Canadian Geotechnical Journal*, *II*(I), 1–15. https://doi.org/DOI: 10.1139/t65-001

Burrow, M. P. N., Ghataora, G. S., & Evdorides, H. (2011). Railway Foundation Design Principles. *Journal of Civil Engineering and Architecture*, *5*(3), 224–232.

Cherubini, C., Giasi, C. I., & Guadagno, F. M. (1990). Coefficient of pressure at rest in Subapenninc blue clays in Matera (Southern Italy). *Proc 6th International Congress International Association of Engineering Geology*, *2*, 1163–1169.

Collotta, T., Cantoni, R., Pavesi, U., Ruberl, E., & Moretti, P. C. (1989). A correlation between residual friction angle, gradation and the index properties of cohesive soils. *Geotechnique*, *39*(2), 343–346. https://doi.org/10.1680/geot.1989.39.2.343

Cui, Y. J., & Delage, P. (1996). Yielding and plastic behaviour of an unsaturated compacted silt. *Geotechnique*, *46*(2), 291–311. https://doi.org/10.1680/geot.1996.46.2.291

Cunningham, M. R., Ridley, A. M., Dineen, K., & Burland, J. B. (2003). The mechanical behaviour of a reconstituted unsaturated silty clay. *Geotechnique*, *53*(2), 183–194. https://doi.org/10.1680/geot.2003.53.2.183

Dareeju, B. S. S. S. (2017). *Performance Evaluation of Unsaturated Rail Track Foundations Under Cyclic Moving Wheel Load*. Queensland University of Technology (QUT).

Das, B. M. (2001). Shear strength of soils. In M. Vezilich (Ed.), *Advanced Soil Mechanics* (5th ed.). BilL Stenqttist. https://doi.org/10.1201/9781351215183-9

Dey, A., Valsa, S., & Nainegali, L. S. (2010). *Reinforced Earth Design of Embankments and Cuts in Railways Department of Civil Engineering Indian Institute of Technology Kanpur* (Issue August).

Dong, K., Connolly, D. P., Laghrouche, O., Woodward, P. K., & Alves Costa, P. (2018). The stiffening of soft soils on railway lines. *Transportation Geotechnics*, *17*(August), 178–191. https://doi.org/10.1016/j.trgeo.2018.09.004

Eid, H. T., Amarasinghe, R. S., Rabie, K. H., & Wijewickreme, D. (2015). Residual shear strength of fine-grained soils and soil–solid interfaces at low effective normal stresses. *Canadian Geotechnical Journal*, *52*(2), 198–210. https://doi.org/10.1139/cgj-2014-0019

Eid, H. T., Rabie, K. H., & Wijewickreme, D. (2016). Drained residual shear strength at effective

normal stresses relevant to soil slope stability analyses. *Engineering Geology*, *204*, 94–107. https://doi.org/10.1016/j.enggeo.2016.02.003

El-Emam, M. (2011). Experimental and numerical study of at-rest lateral earth pressure of overconsolidated sand. *Advances in Civil Engineering*, *2011*. https://doi.org/10.1155/2011/524568

Escario, V., Juca, J. F. T., & Coppe, M. S. (1989). Strength and deformation of partly saturated soils. *Proc 12th International Conference on Soil Mechanics and Foundation Engincering*, *13*, 43–46.

Escario, V., & Suez, J. (1986). The shear strength of partly saturated soils. *Geotechnique*, *36*(3), 453–456. https://doi.org/10.1680/geot.1987.37.4.523

Esmaeili, M., & Khajehei, H. (2016). Mechanical behavior of embankments overlying on loose subgrade stabilized by deep mixed columns. *Journal of Rock Mechanics and Geotechnical Engineering*, *8*(5), 651–659. https://doi.org/10.1016/j.jrmge.2016.02.006

Feda, J. (1984). Ko-coeflicient of sand in triaxial apparatus. Technical note. *J Geotech Engng Div ASCE*, *110*(NGT4), 519–524.

Fioravante, V., Jamiolkowski, M., Lo Presti, D. C. F., Manfredini, G., & Pedroni, S. (1998). Assessment of the coefficient of the earth pressure at rest from shear wave velocity measurements. *Geotechnique*, *48*(5), 657–666. https://doi.org/10.1680/geot.1998.48.5.657

Fischer, K. P., Andersen, K. H., & Moum, J. (1978). Properties of an Artificially Cemented Clay. *Canadian Geotechnical Journal*, *15*(3), 322–331. https://doi.org/10.1139/t78-030

Fredlund, D. G., & Morgenstern, N. R. (1976). Constitutive Relations for Volume Change in Unsaturated Soils. *Canadian Geotechnical Journal*, *13*(3), 261–276. https://doi.org/10.1139/t76-029

Fredlund, D. G., & Morgenstern, N. R. (1977). Stress state variables for unsaturated soils. *J Geotech Engng Div ASCE*, *103*(NGT5), 447–466. https://doi.org/10.1016/B978-0-444-98950-5.50008-3

Fredlund, D. G., Morgenstern, N. R., & R. A. WIDGE. (1978). The shear strength of unsaturated

soils. *Canadian Geotechnical Journal*, *15*, 313–321.

Fredlund, D. G., & Rahardjo, H. (1993). Soil mechanics for unsaturated soils. In *John Wiley & Sons, Inc.* https://doi.org/10.1016/0267-7261(93)90011-f

Fredlund, Delwyn G., Rahardjo, H., & Fredlund, M. D. (2012). Unsaturated Soil Mechanics in Engineering Practice. In *JOHN WILEY & SONS, INC.* https://doi.org/10.1002/9781118280492

Gallage, C., Dareeju, B., Dhanasekar, M., & Ishikawa, T. (2016). Effects of Principal Stress Axis Rotation on Unsaturated Rail Track Foundation Deterioration. *Procedia Engineering*, *143*(Ictg), 252–259. https://doi.org/10.1016/j.proeng.2016.06.032

Gallipoli, D., Gens, A., Sharma, R., & Vaunat, J. (2003). An elasto-plastic model for unsaturated soil incorporating the effects of suction and degree of saturation on mechanical behaviour. *Geotechnique*, *53*(1), 123–135. https://doi.org/10.1680/geot.2003.53.1.123

Gan, J. K. M., Feuerharmel, C., & Rahardo, H. (2006). Determination of the shear strength parameters of two unsaturated colluvium soils using the direct shear test. *Geotechnical Special Publication*, *147*, 1181–1190. https://doi.org/10.1061/40802(189)96

Geiser, F., Laloui, L., & Vulliet, L. (2006). Elasto-Plasticity of Unsaturated Soils: Laboratory Test Results on a Remoulded Silt. *Soils and Foundations*, *46*(5), 545–556. http://www.mendeley.com/research/geology-volcanic-history-eruptive-style-yakedake-volcano-group-central-japan/

Gens, A. (2010). Soil-environment interactions in geotechnical engineering. *Geotechnique*, *60*(1), 3–74. https://doi.org/10.1680/geot.9.P.109

Geotechdata.info. (2013). *Soil friction angle*. Geotechdata.Info. http://www.geotechdata.info/parameter/angle-of-friction.html

Ghayoomi, M., & McCartney, J. S. (2011). Measurement of small-strain shear moduli of partially saturated sand during infiltration in a geotechnical centrifuge. *Geotechnical Testing Journal*, *34*(5), 503–513. https://doi.org/10.1520/GTJ103608

Guo, P. (2010). Effect of density and compressibility on K0 of cohesionless soils. *Acta*

Geotechnica, *5*(4), 225–238. https://doi.org/10.1007/s11440-010-0125-0

Gylland, A., Long, M., Emdal, A., & Sandven, R. (2013). Characterisation and engineering properties of Tiller clay. *Engineering Geology*, *164*, 86–100. https://doi.org/10.1016/j.enggeo.2013.06.008

Habibbeygi, F., & Nikraz, H. (2018). Effect of shear rate on the residual shear strength of pre-sheared clays. *Cogent Geoscience*, *4*(1), 1–9. https://doi.org/10.1080/23312041.2018.1453989

Hamouche, K. K., Leroueil, S., Roy, M., & Lutenegger, A. J. (1995). In situ evaluation of K0 in eastern Canada clays. *Canadian Geotechnical Journal*, *32*(4), 677–688. https://doi.org/10.1139/t95-067

Han, Z., Vanapalli, S. K., & Zou, W. L. (2017). Integrated approaches for predicting soil-water characteristic curve and resilient modulus of compacted fine-grained subgrade soils. *Canadian Geotechnical Journal*, *54*(5), 646–663. https://doi.org/10.1139/cgj-2016-0349

Hanna, A., & Al-Romhein, R. (2008). At-Rest Earth Pressure of Overconsolidated Cohesionless Soil. *Journal of Geotechnical and Geoenvironmental Engineering*, *134*(3), 408–412. https://doi.org/10.1061/(ASCE)1090-0241(2008)134

Hendry, M. T., Martin, C. D., & Barbour, S. L. (2013). Measurement of cyclic response of railway embankments and underlying soft peat foundations to heavy axle loads. *Canadian Geotechnical Journal*, *50*(5), 467–480. https://doi.org/10.1139/cgj-2012-0118

Hoyos, L. R., Velosa, C. L., & Puppala, A. J. (2014). Residual shear strength of unsaturated soils via suction-controlled ring shear testing. *Engineering Geology*, *172*, 1–11. https://doi.org/10.1016/j.enggeo.2014.01.001

Indraratna, B. (2016). 1st Ralph Proctor Lecture of ISSMGE. Railroad performance with special reference to ballast and substructure characteristics. *Transportation Geotechnics*, *7*, 74–114. https://doi.org/10.1016/j.trgeo.2016.05.002

Indraratna, B., Salim, W., & Rujikiatkamjorn, C. (2011). Advanced rail geotechnology - Ballasted track. In *Advanced Rail Geotechnology - Ballasted Track*. https://doi.org/10.1201/b10861

Jotisankasa, A., Coop, M., & Ridley, A. (2009). The mechanical behaviour of an unsaturated compacted silty clay. *Geotechnique*, *59*(5), 415–428. https://doi.org/10.1680/geot.2007.00060

Jovanovic, S. (2016). Maintenance - the key driver of railway infrastructure costs. *SEETO Transport Infrastructure Forum, Transport: A Driver of Growth.*, 43. http://www.seetoint.org/wp-content/uploads/downloads/2016/03/Maintenance-the-key-driver-of-railway-infrastructure-costs-Mr.-Stasha-Jovanovic1.pdf

Keskin, S. N., Tekinsoy, M. A., & Uzundurukan, S. (2004). The Effects of Over Consolidation Radio and Effective Stresses on the Earth Pressure Coefficient at Rest of Clayey Soils. *Digest*, 947–961.

Khalili, N., & Khabbaz, M. H. (1998). A unique relationship for χ for the determination of the shear strength of unsaturated soils. *Geotechnique*, *48*(5), 681–687. https://doi.org/10.1680/geot.1998.48.5.681

Leshchinsky, B. A. (2012). *Enhancing Ballast Performance using Geocell Confinement*. Columbia University.

Leshchinsky, B. A., & Ling, H. I. (2013). Numerical modeling of behavior of railway ballasted structure with geocell confinement. *Geotextiles and Geomembranes*, *36*, 33–43. https://doi.org/10.1016/j.geotexmem.2012.10.006

Li, D. (2018). 25 years of heavy axle load railway subgrade research at the Facility for Accelerated Service Testing (FAST). *Transportation Geotechnics*, *17*(August), 51–60. https://doi.org/10.1016/j.trgeo.2018.09.003

Li, D., Hyslip, J., Sussmann, T., & Chrismer, S. (2016). Railway Geotechnics. In *Taylor & Francis Group, LLC*. CRC Press.

Li, D., & Selig, E. T. (1995). Evaluation of railway subgrade problems. *Transportation Research Record*, *1489*, 17–25.

Loh, H. (2011). *Behaviour of Railway Track Subgrade under Cyclic Loading* (Issue November). Curtin University November.

Loh, R. B. H., & Nikraz, H. R. (2012). Effective stress method on threshold stress of clay under high rate cyclic loading. *5th Asia-Pacific Conference on Unsaturated Soils 2012*, *2*, 511–515.

Lu, N., & Kaya, M. (2014). Power law for elastic moduli of unsaturated soil. *Journal of Geotechnical and Geoenvironmental Engineering*, *140*(1), 46–56. https://doi.org/10.1061/(ASCE)GT.1943-5606.0000990

Lu, N., & Likos, W. J. (2006). Suction Stress Characteristic Curve for Unsaturated Soil. *Journal of Geotechnical and Geoenvironmental Engineering*, *132*(2), 131–142. https://doi.org/10.1061/(ASCE)1090-0241(2006)132

Lupini, J. F., Skinner, A. E., & Vaughan, P. R. (1981). The drained residual strength of cohesive soils. *Geddmique*, *31*(2), 181–213.

Massarsch, K. R. (1986). Lateral earth pressure at rest in clay. *Proc 4th International Geotechnical Semtuar, Field Instrumentation and In-Situ Measurements, Singapore,* 203–209.

Mayne, P. W., & Kulhawy, F. H. (1983). Closure to "Ko-OCR Relationships in Soils." *Journal of Geotechnical Engineering*, *109*(6), 867–869.

Melinda, F., Rahardjo, H., Han, K. K., & Leong, E. C. (2004). Shear Strength of Compacted Soil under Infiltration Condition. *Journal of Geotechnical and Geoenvironmental Engineering*, *130*(8), 807–817. https://doi.org/10.1061/(ASCE)1090-0241(2004)130

Mesri, G., & Castro, A. (1987). Cα/Cc concept and K0 during secondary compression. *Journal of Geotechnical Engineering*, *113*(3), 230–247.

Mesri, G., & Hayat, T. M. (1993). The coefficient of earth pressure at rest. *Canadian Geotechnical Journal*, *30*(4), 647–666. https://doi.org/10.1139/t93-056

Mesri, G., & Shahien, M. (2003). Residual shear strength mobilized in first-time slope failures. *Journal of Geotechnical and Geoenvironmental Engineering*, *129*(1), 12–31. https://doi.org/10.1061/(ASCE)1090-0241(2003)129:1(12)

Miller, G. A., Teh, S. Y., Li, D., & Zaman, M. M. (2000). Cyclic Shear Strength of Soft Railroad

Subgrade. *J. Geotech. Geoenviron. Eng.*, *126*(1090-0241/00/0002-0139–0147), 139–147.

Milne, D., Le Pen, L., Watson, G., Thompson, D., Powrie, W., Hayward, M., & Morley, S. (2018). Monitoring and repair of isolated trackbed defects on a ballasted railway. *Transportation Geotechnics*, *17*(August), 61–68. https://doi.org/10.1016/j.trgeo.2018.09.002

Ng, C. W. W., & Yung, S. Y. (2008). Determination of the anisotropic shear stiffness of an unsaturated decomposed soil. *Geotechnique*, *58*(1), 23–35. https://doi.org/10.1680/geot.2008.58.1.23

Ng, C. W. W., & Zhou, C. (2014). Cyclic behaviour of an unsaturated silt at various suctions and temperatures. *Geotechnique*, *64*(9), 709–720. https://doi.org/10.1680/geot.14.P.015

Oh, W. T., Vanapalli, S. K., & Puppala, A. J. (2009). Semi-empirical model for the prediction of modulus of elasticity for unsaturated soils. *Canadian Geotechnical Journal*, *46*(8), 903–914. https://doi.org/10.1139/T09-030

Railisa. (2018). *RAIL TRANSPORT IN THE WORLD*. Union Internationale Des Chemins de Fer (UIC). https://uic.org/support-activities/statistics/

Rajeev, P., Chan, D., & Kodikara, J. (2012). Ground-atmosphere interaction modelling for long-term prediction of soil moisture and temperature. *Canadian Geotechnical Journal*, *49*(9), 1059–1073. https://doi.org/10.1139/T2012-068

Sánchez, M., Wang, D., Briaud, J. L., & Douglas, C. (2014). Typical geomechanical problems associated with railroads on shrink-swell soils. *Transportation Geotechnics*, *1*(4), 257–274. https://doi.org/10.1016/j.trgeo.2014.07.002

Sawangsuriya, A., Edil, T. B., & Bosscher, P. J. (2009). Modulus-suction-moisture relationship for compacted soils in postcompaction state. *Journal of Geotechnical and Geoenvironmental Engineering*, *135*(10), 1390–1403. https://doi.org/10.1061/(ASCE)GT.1943-5606.0000108

Sayeed, M. A., & Shahin, M. A. (2018). Design of ballasted railway track foundations using numerical modelling. Part I: Development1. *Canadian Geotechnical Journal*, *55*(3), 353–368. https://doi.org/10.1139/cgj-2016-0633

Scaringi, G., & Di Maio, C. (2016). Influence of Displacement Rate on Residual Shear Strength of Clays. *Procedia Earth and Planetary Science*, *16*, 137–145. https://doi.org/10.1016/j.proeps.2016.10.015

Schmertmann, J. H. (1983). A Simple Question About Consolidation. *Ournal of Geotechnical Engineering*, *109*(1), 119–122.

Schmertmann, J. H. (1991). The mechanical aging of soils. *Journal of Geotechnical Engineering*, *117*(9), 1288–1330.

Sheng, D. (2011). Review of fundamental principles in modelling unsaturated soil behaviour. *Computers and Geotechnics*, *38*(6), 757–776. https://doi.org/10.1016/j.compgeo.2011.05.002

Shin, H., & Santamarina, J. C. (2009). Mineral dissolution and the evolution of k0. *Journal of Geotechnical and Geoenvironmental Engineering*, *135*(8), 1141–1147. https://doi.org/10.1061/(ASCE)GT.1943-5606.0000053

Sivakumar, V., Doran, I. G., Graham, J., & Navaneethan, T. (2002). Relationship between K0 and overconsolidation ratio: A theoretical approach. *Geotechnique*, *52*(3), 225–230. https://doi.org/10.1680/geot.2002.52.3.225

Sivakumar, V., Kodikara, J., O'Hagan, R., Hughes, D., Cairns, P., & McKinley, J. D. (2013). Effects of confining pressure and water content on performance of unsaturated compacted clay under repeated loading. *Geotechnique*, *63*(8), 628–640. https://doi.org/10.1680/geot.10.P.103

Sivakumar, V., Navaneethanf, T., Hughes, D., & Gallagher, G. (2009). An assessment of the earth pressure coefficient in overconsolidated clays. *Geotechnique*, *59*(10), 825–838. https://doi.org/10.1680/geot.8.P.033

StructX. (2019). *Density Ranges for Different Soil Types*. https://structx.com/Soil_Properties_002.html

Terzaghi, K. (1943). Theoretical Soil Mechanics. In *John Wiler and Sons Inc* (Eighth). John Wiler and Sons Inc.

Thu, T. M., Rahardjo, H., & Leong, E. C. (2007). Elastoplastic model for unsaturated soil with incorporation of the soil-water characteristic curve. *Canadian Geotechnical Journal*, *44*(1), 67–77. https://doi.org/10.1139/T06-091

Tiwari, B., & Marui, H. (2005). A new method for the correlation of residual shear strength of the soil with mineralogical composition. *Journal of Geotechnical and Geoenvironmental Engineering*, *131*(9), 1139–1150. https://doi.org/10.1061/(ASCE)1090-0241(2005)131:9(1139)

Tomás, R., Domenech, C., Mira, A., Cuenca, A., & Delgado, J. (2007). Preconsolidation stress in the Vega Baja and Media areas of the River Segura (SE Spain): Causes and relationship with piezometric level changes. *Engineering Geology*, *91*(2–4), 135–151. https://doi.org/10.1016/j.enggeo.2007.01.006

Vanapalli, S. K., & Fredlund, D. G. (1999). Empirical procedures to predict the shear strength of unsaturated soils. *11 Asian Regional Conference on Soil Mechnics and Geotechnical Engineering*, 93–96.

Vanapalli, S. K., Fredlund, D. G., Pufahl, D. E., & Clifton, A. W. (1996). Model for the prediction of shear strength with respect to soil suction. In *Canadian Geotechnical Journal* (Vol. 33, Issue 3, pp. 379–392). https://doi.org/10.1139/t96-060

Vanapalli, S. K., Nicotera, M. V., & Sharma, R. S. (2008). Axis translation and negative water column techniques for suction control. *Geotechnical and Geological Engineering*, *26*(6), 645–660. https://doi.org/10.1007/s10706-008-9206-3

Vandevelde, J., & Basudhar, P. K. (2020). *The Basics of Soil Mechanics in Civil Engineering*. Bright Hub Engineering.

Wang, D. yan, Ma, W., Niu, Y. hong, Chang, X. xiao, & Wen, Z. (2007). Effects of cyclic freezing and thawing on mechanical properties of Qinghai-Tibet clay. *Cold Regions Science and Technology*, *48*(1), 34–43. https://doi.org/10.1016/j.coldregions.2006.09.008

Wang, J., Yang, Y., Bai, J., Hao, J. Y., & Zhao, T. L. (2018). Coefficient of Earth Pressure at Rest of a Saturated Artificially Mixed Soil from Oedometer Tests. *KSCE Journal of Civil Engineering*, *22*(5), 1691–1699. https://doi.org/10.1007/s12205-017-1811-3

Wheeler, S. J., & Sivakumar, V. (1995). An elasto-plastic critical state framework for unsaturated soil. *Geotechnique*, *45*(1), 35–53. https://doi.org/10.1680/geot.1995.45.1.35

Wikipedia. (2020). *Rail transport*. Wikipedia, the Free Encyclopedia. https://en.wikipedia.org/wiki/Rail_transport

ESC 240 BALLAST Version 2.4, Railcorp Transport 11 (2013).

Wu, S., Gray, D. H., & Richart, F. E. (1984). Capillary effects on dynamic modulus of sands and silts. *Journal of Geotechnical Engineering*, *110*(9), 1188–1203. https://doi.org/10.1061/(ASCE)0733-9410(1987)113:7(793)

Yan, W. M., & Chang, J. (2015). Effect of pore water salinity on the coefficient of earth pressure at rest and friction angle of three selected fine-grained materials. *Engineering Geology*, *193*, 153–157. https://doi.org/10.1016/j.enggeo.2015.04.025

Zhao, X., Zhou, G., Tian, Q., & Kuang, L. (2010). Coefficient of earth pressure at rest for normal, consolidated soils. *Mining Science and Technology*, *20*(3), 406–410. https://doi.org/10.1016/S1674-5264(09)60216-7

APPENDIX

for

The thesis of

SIMULATION OF PROGRESSIVE SHEAR FAILURE IN RAILWAY FOUNDATION

1. CODE OF THE PROGRAM

```
    Const g As Double = 9.81              'Gravity
    Dim nlp As Integer          'the number of stress points
    Dim lp(50, 1) As Double         'Stress location (horizontal distance to track center)and Stress
    Dim rb As Double          'the density of Ballast including track
    Dim wb As Double          'the width of top of Ballast
    Dim hb As Double          'the thickness of Ballast
    Dim mlp As Integer              'the max stress point
    Dim se As Double          'the size of element
    Dim rd As Double          'the density of subgrade soil
    Dim c As Double          'the effective cohesion of subgrade soil
    Dim phi As Double          'the effective angle of friction of soil in Degree
    Dim theta As Double             'the angle of failure plane to Major priciple stress in Radiant
    Dim K0 As Double          'the lateral earth pressure at rest
    Dim Kr As Double          'the coefficient of friction on failure plane
    Dim LayerName As String         'the name of layer


Sub MainPFS()
    Const ForReading = 1, ForWriting = 2, ForAppending = 3
    Const TristateUseDefault = -2, TristateTrue = -1, TristateFalse = 0
    Dim cfs As Object
    Dim gf As Object
    Dim of As Object
    Dim sl As String

    Dim i As Integer            'For loop
    Dim z0 As Double            'temporary max load stress
    Dim cS As Double, cE As Double, cI As Double         'the start, end and interval of effective cohesion of subgrade
soil
    Dim phiS As Double, phiE As Double, phiI As Double       'the start, end and interval of effective angles of
friction of soil in Degree
    Dim K0S As Double, K0E As Double, K0I As Double         'the start, end and interval coefficients of lateral earth
pressures at rest
    Dim KrS As Double, KrE As Double, KrI As Double         'the start, end and interval coefficients of friction on
failure plane

    'Open the data file and read data
    Set cfs = CreateObject("Scripting.FileSystemObject")
    'Set gf = cfs.GetFile("C:\Users\xudon\Documents\Uottawa\PhdThesis\Programme\Data-L.txt")
    Set gf = cfs.GetFile("C:\Users\xudon\Documents\Uottawa\PhdThesis\Programme\Data.txt")
    Set of = gf.OpenAsTextStream(ForReading, TristateUseDefault)
    sl = of.ReadLine
    rb = Left(sl, 10)
    sl = of.ReadLine
    wb = Left(sl, 10)
    sl = of.ReadLine
    hb = Left(sl, 10)
    sl = of.ReadLine
    sl = of.ReadLine
    nlp = Left(sl, 10)
    nlp = nlp - 1
```

```
Let z0 = 0
For i = 0 To nlp                'Read the stress on top of subgrade
   sl = of.ReadLine
   lp(i, 0) = Left(sl, 10)
   sl = of.ReadLine
   lp(i, 1) = Left(sl, 10)
   If lp(i, 1) >= z0 Then
      z0 = lp(i, 1)
      mlp = i             'the max stress point
   End If
Next i
'MsgBox mlp & "-" & lp(mlp, 0) & "-" & lp(mlp, 1)           'For watching.

sl = of.ReadLine            'Space line
sl = of.ReadLine
se = Left(sl, 10)
sl = of.ReadLine
rd = Left(sl, 10)
sl = of.ReadLine
cS = Left(sl, 10)
sl = of.ReadLine
cE = Left(sl, 10)
sl = of.ReadLine
cI = Left(sl, 10)
sl = of.ReadLine
phiS = Left(sl, 10)
sl = of.ReadLine
phiE = Left(sl, 10)
sl = of.ReadLine
phiI = Left(sl, 10)
sl = of.ReadLine
K0S = Left(sl, 10)
sl = of.ReadLine
K0E = Left(sl, 10)
sl = of.ReadLine
K0I = Left(sl, 10)
sl = of.ReadLine
KrS = Left(sl, 10)
sl = of.ReadLine
KrE = Left(sl, 10)
sl = of.ReadLine
KrI = Left(sl, 10)
of.Close


'Open the output file and write the result
'Set gf = cfs.CreateTextFile("Output.txt", True)
Set gf = cfs.CreateTextFile("C:\Users\xudon\Documents\Uottawa\PhdThesis\Programme\Output.txt", True)


'Simulation

'Loop for a range of coefficients of friction on failure plane
Kr = KrS
Do
   'Loop for a range of the coefficients of lateral earth pressures at rest
```

```
    K0 = K0S
    Do

      'Loop for a range of the effective cohesion of subgrade soil
      c = cS
      Do

        'Loop for a range of the effective angles of friction subgrade soil
        phi = RadF(phiS)            'Convert degree to radiant
        Do
          theta = ThetaF(phi)
          Let LayerName = "phi" & DegF(phi) & "-c" & c & "-K" & K0 & "-Kr" & Kr
          AddLayer (LayerName)

          'write the result to output fole
          gf.Write ("phi  ")
          gf.Write (Str(DegF(phi)) & Chr(9))
          gf.Write ("c  ")
          gf.Write (Str(c) & Chr(9))
          gf.Write ("K0  ")
          gf.Write (Str(K0) & Chr(9))
          gf.Write ("Kr  ")
          gf.Write (Str(Kr) & Chr(9))

          Call OnePFS(gf)

          gf.Write (Chr(13))

          phi = phi + RadF(phiI)
        Loop Until phi > RadF(phiE + 0.01)

        c = c + cI
      Loop Until c > cE + 0.1

      K0 = K0 + K0I
    Loop Until K0 > K0E + 0.01

    Kr = Kr + KrI
  Loop Until Kr > KrE + 0.01

  gf.Close

End Sub


Public Sub OnePFS(gf As Object)

  Dim i, j As Integer           'For loop

  Dim xza(200, 2) As Double     'location (x,z) and angle of failure plane of the element
  Dim lpsr As Double          'the ratio of start failure load to max load (or stress)
  Dim x0 As Double, z0 As Double      'temporary distances on x & z
  Dim svs As Double, svd As Double      'the vertical static and dynamic stresses in the original element
  Dim so1 As Double, so3 As Double      'the priciple stresses in the original element
  Dim sn1 As Double, sn3 As Double      'the priciple stresses in the new element at failure
  Dim tau As Double, sn As Double      'the normal stress and shear stress on failure plane
```

```
Dim s1f As Double      'the major principle stress at failure
Dim rtau As Double      'the unbalanced shear stress after failure plane
Dim alpha As Double          'the new major principal stress direction of the element in Radiant
Dim beta As Double           'the turning angle of two adjient failure planes in Radiant


'Calculate the location (x,z) and angle of first failure plane or element
'The first element
xza(0, 0) = lp(mlp, 0)
xza(0, 1) = 0
xza(0, 2) = 2 * Atn(1) - theta

'The second element
xza(1, 0) = xza(0, 0) + se * Sin(xza(0, 2))
xza(1, 1) = xza(0, 1) + se * Cos(xza(0, 2))
Call DrawPline(xza(0, 0), xza(0, 1), xza(1, 0), xza(1, 1), "0")

svs = SigmavF(xza(0, 0), xza(0, 1))
'so3 = SigmahF(svs)             '!!! not consider dynamic load yet.
so1 = 2 * c * Tan(theta) / (1 - K0 * (Tan(theta)) ^ 2)
so3 = K0 * so1

svd = so1 - svs
If svd < 0 Then
   'MsgBox "Warning!!! The first element fails at static load"
   lpsr = 0
   i = 0
   GoTo 100
   'Exit Sub
Else
   lpsr = svd / lp(mlp, 1)
End If


For i = 1 To 199           'Calculate each faied element

   Do
      lpsr = lpsr + 0.0001          'Load increase or Train approach

      For j = 0 To i - 1

         'Calculate the initial (original) principal stress in element
         svd = lpsr * SigmadF(xza(j, 0))
         svs = SigmavF(xza(j, 0), xza(j, 1))
         so1 = svd + svs
         'so3 = SigmahF(svs)             '!!! not consider dynamic load yet.
         so3 = SigmahF(so1)

         'Calculate the normal and shear stress on failure plane

         If j < 1 Then
            beta = 0
            rtau = 0
         Else
            beta = xza(j, 2) - xza(j - 1, 2)
         End If
```

```
            sn = SigmanF(so1, so3, xza(j, 2)) + rtau * Sin(beta)
            tau = TauF(so1, so3, xza(j, 2)) + rtau * Cos(beta)
            rtau = tau - Kr * sn

        Next j


        'Calculate the initial (original) principal stress in element
        svd = lpsr * SigmadF(xza(i, 0))
        svs = SigmavF(xza(i, 0), xza(i, 1))
        so1 = svd + svs
        'so3 = SigmahF(svs)             '!!! not consider dynamic load yet.
        so3 = SigmahF(so1)
        'Calculate the new principal stress in element
        x0 = so3 + rtau * Sin(xza(i - 1, 2))
        z0 = so1 + rtau * Cos(xza(i - 1, 2))
        sn1 = Sqr(z0 ^ 2 + x0 ^ 2)
        'Calculate the new major principal stress direction of the element
        alpha = Atn(x0 / z0)
        If z0 < 0 Then
            alpha = alpha + 4 * Atn(1)
        End If
        sn3 = so1 * Sin(alpha) + so3 * Cos(alpha) - rtau * Sin(xza(i - 1, 2) - alpha)
        'sn3 = so1 * Sin(alpha) + so3 * Cos(alpha)
        'Calculate the new major principal stress at failure
        s1f = Sigma1F(sn3)

        If lpsr > 2# Then
            Exit For
        End If

    Loop Until sn1 > s1f

    'MsgBox Str(i) & Chr(13) & Chr(10) & Str(lpsr)         'For watching.
    xza(i, 2) = alpha + 2 * Atn(1) - theta
    xza(i + 1, 0) = xza(i, 0) + se * Sin(xza(i, 2))
    xza(i + 1, 1) = xza(i, 1) + se * Cos(xza(i, 2))

    Call DrawPline(xza(i, 0), xza(i, 1), xza(i + 1, 0), xza(i + 1, 1), CStr(i))

    If xza(i + 1, 1) <= 0 Then
        Exit For
    End If

Next i

'MsgBox "Elements  " & i        'For watching.
'MsgBox "Final Load  " & Int(lpsr * 100) & Chr(37)       'For watching.

100    'write the result to output fole
    gf.Write ("No  ")
    gf.Write (Str(i) & Chr(9))
    gf.Write ("Load  ")
    gf.Write (Str(Int(lpsr * 100)) & Chr(37))
```

```
End Sub


'Convert degree to radiant
Function RadF(deg As Double) As Double
   RadF = Atn(1) * deg / 45
End Function


'Convert radiant to degree
Function DegF(rad As Double) As Double
   DegF = 45 * rad / Atn(1)
End Function


'Calculate the angle of failure plane
Function ThetaF(phi As Double) As Double
   ThetaF = Atn(1) + phi / 2
End Function


'Calculate the major principal stress with minor principal stress at failure
Function Sigma1F(Sigma3 As Double) As Double
   Sigma1F = Sigma3 * (Tan(theta)) ^ 2 + 2 * c * Tan(theta)
End Function


'Calculate the shear stress on failure plane with major and minor principal stresses
Function TauF(Sigma1 As Double, Sigma3 As Double, alpha As Double) As Double
   TauF = Sigma1 * Cos(alpha) - Sigma3 * Sin(alpha)
End Function


'Calculate the normal stress on failure plane with major and minor principal stresses
Function SigmanF(Sigma1 As Double, Sigma3 As Double, alpha As Double) As Double
   SigmanF = Sigma1 * Sin(alpha) + Sigma3 * Cos(alpha)
End Function


'Calculate the vertical load stress on Subgrade
Function SigmadF(x As Double) As Double

   If x <= lp(0, 0) Then
      'MsgBox "Warning!!! The load location out of range"
      SigmadF = lp(0, 1)
      Exit Function
   End If

   If x >= lp(nlp, 0) Then
      'MsgBox "Warning!!! The load location out of range"
      SigmadF = lp(nlp, 1)
      Exit Function
   End If

   For i = 1 To nlp
```

```
        If x < lp(i, 0) Then
            Exit For
        End If
    Next i
    'SigmadF = lp(i - 1, 1) + (lp(i, 1) - lp(i - 1, 1)) * (x - lp(i - 1, 0)) / (lp(i, 0) - lp(i - 1, 0))
    SigmadF = lp(i - 1, 1)

End Function


'Calculate the vertical static stress increase Sigmav in Subgrade
Function SigmavF(x As Double, z As Double) As Double
    Dim sz As Double
    If x <= wb / 2 Then
        sz = (rb * hb + rd * z) * g
    ElseIf x <= wb / 2 + hb * 2 Then
        sz = (rb * (hb - x / 2 + wb / 4) + rd * z) * g
    Else
        sz = rd * z * g
    End If

    SigmavF = sz / 1000
End Function


'Calculate the lateral stress Sigma3 in Subgrade
Function SigmahF(sz As Double) As Double
    SigmahF = sz * K0
End Function


Public Sub AddLayer(strLayerName As String)

    Dim objLayer As AcadLayer

    If "" = strLayerName Then
        Exit Sub        ' exit if no name entered
    End If

    On Error Resume Next        ' handle exceptions inline

    'check to see if layer already exists
    Set objLayer = ThisDrawing.Layers(strLayerName)

    If objLayer Is Nothing Then
        Set objLayer = ThisDrawing.Layers.Add(strLayerName)

        If objLayer Is Nothing Then         ' check if obj has been set
            'MsgBox "Unable to Add '" & strLayerName & "'"
        Else
            'MsgBox "Added Layer '" & objLayer.Name & "'"
        End If
    Else
        'MsgBox "Layer already existed"
    End If
```

```
    On Error GoTo 0        'Disables any error handler

End Sub


Public Sub DrawPline(xs As Double, ys As Double, xe As Double, ye As Double, noe As String)
    Dim pline As AcadPolyline
    Dim Points(0 To 5) As Double

    'Define the 2D polyline points
    Points(0) = xs
    Points(1) = -ys
    Points(2) = 0

    Points(3) = xe
    Points(4) = -ye
    Points(5) = 0

    'Create a line in model space
    Set pline = ThisDrawing.ModelSpace.AddPolyline(Points)
    pline.Layer = LayerName

  Call DrawElement(xs, ys, xe, ye, noe)

End Sub


Public Sub DrawElement(xs As Double, ys As Double, xe As Double, ye As Double, noe As String)
  Dim line As AcadLine
  Dim text As AcadText
  Dim StartPoint(0 To 2) As Double
  Dim EndPoint(0 To 2) As Double
  Dim x1, y1, x2, y2, aa, bb, cc, dd, bc As Double

  'Calculate the other two corner coordinates of the Element with quadratic equation of one unknown
  dd = xs ^ 2 - xe ^ 2 + ys ^ 2 - ye ^ 2 + se ^ 2 * ((Cos(theta)) ^ 2 - (Sin(theta)) ^ 2)
  aa = (xs - xe) ^ 2 + (ys - ye) ^ 2
  bb = 2 * (ys - ye) * (xe * ys - xs * ye) + dd * (xs - xe)
  cc = (xs ^ 2 + ys ^ 2 - se ^ 2 * (Sin(theta)) ^ 2) * (ys - ye) ^ 2 - dd * ys * (ys - ye) + dd ^ 2 / 4

  bc = bb ^ 2 - 4 * aa * cc
  If bc < 0 Then
    'MsgBox "Error with quadratic equation"
    Exit Sub
  End If

  'Calculate the third corner coordinates of the Element
  If ys > ye Then
    x1 = (bb + Sqr(bc)) / aa / 2
  Else
    x1 = (bb - Sqr(bc)) / aa / 2
  End If

  y1 = (dd / 2 - (xs - xe) * x1) / (ys - ye)

  'Calculate the fourth corner coordinates of the Element
```

```
  x2 = xs + xe - x1
  y2 = ys + ye - y1

  'Create the first line of element in model space
  StartPoint(0) = xs
  StartPoint(1) = -ys
  StartPoint(2) = 0
  EndPoint(0) = x1
  EndPoint(1) = -y1
  EndPoint(2) = 0
  Set line = ThisDrawing.ModelSpace.AddLine(StartPoint, EndPoint)
  line.Layer = LayerName

  'Create the second line of element in model space
  StartPoint(0) = xe
  StartPoint(1) = -ye
  StartPoint(2) = 0
  Set line = ThisDrawing.ModelSpace.AddLine(StartPoint, EndPoint)
  line.Layer = LayerName

  'Create the third line of element in model space
  EndPoint(0) = x2
  EndPoint(1) = -y2
  EndPoint(2) = 0
  Set line = ThisDrawing.ModelSpace.AddLine(StartPoint, EndPoint)
  line.Layer = LayerName

  'Create the fourth line of element in model space
  StartPoint(0) = xs
  StartPoint(1) = -ys
  StartPoint(2) = 0
  Set line = ThisDrawing.ModelSpace.AddLine(StartPoint, EndPoint)
  line.Layer = LayerName

  'Insert the No of element in model space
  StartPoint(0) = (xs + xe) / 2
  StartPoint(1) = -(ys + ye) / 2
  StartPoint(2) = 0
  Set text = ThisDrawing.ModelSpace.AddText(noe, StartPoint, 0.002)
  text.Layer = LayerName

End Sub
```

2. INPUT FILE

```
2000        'the density of Ballast including track, kg/m3
3.5         'the width of top of Ballast, m
0.5         'the thickness of Ballast, m

40          'the number of stress points
0           'Stress location (horizontal distance to track center), m
151         'Stress, kPa
0.08        'Stress location (horizontal distance to track center)
151         'Stress
0.15        'Stress location (horizontal distance to track center)
152         'Stress
0.23        'Stress location (horizontal distance to track center)
154         'Stress
0.3         'Stress location (horizontal distance to track center)
156         'Stress
0.36        'Stress location (horizontal distance to track center)
158         'Stress
0.41        'Stress location (horizontal distance to track center)
160         'Stress
0.47        'Stress location (horizontal distance to track center)
163         'Stress
0.54        'Stress location (horizontal distance to track center)
167         'Stress
0.63        'Stress location (horizontal distance to track center)
173         'Stress
0.72        'Stress location (horizontal distance to track center)
180         'Stress
0.81        'Stress location (horizontal distance to track center)
188         'Stress
0.89        'Stress location (horizontal distance to track center)
```

196 'Stress
0.95 'Stress location (horizontal distance to track center)
202 'Stress
0.99 'Stress location (horizontal distance to track center)
205 'Stress
1.03 'Stress location (horizontal distance to track center)
207 'Stress
1.05 'Stress location (horizontal distance to track center)
207 'Stress
1.08 'Stress location (horizontal distance to track center)
206 'Stress
1.11 'Stress location (horizontal distance to track center)
202 'Stress
1.14 'Stress location (horizontal distance to track center)
197 'Stress
1.17 'Stress location (horizontal distance to track center)
190 'Stress
1.2 'Stress location (horizontal distance to track center)
181 'Stress
1.24 'Stress location (horizontal distance to track center)
168 'Stress
1.28 'Stress location (horizontal distance to track center)
151 'Stress
1.31 'Stress location (horizontal distance to track center)
134 'Stress
1.35 'Stress location (horizontal distance to track center)
115 'Stress
1.39 'Stress location (horizontal distance to track center)
97 'Stress
1.44 'Stress location (horizontal distance to track center)
79 'Stress

```
1.48      'Stress location (horizontal distance to track center)
65        'Stress
1.53      'Stress location (horizontal distance to track center)
51        'Stress
1.57      'Stress location (horizontal distance to track center)
42        'Stress
1.62      'Stress location (horizontal distance to track center)
34        'Stress
1.67      'Stress location (horizontal distance to track center)
28        'Stress
1.75      'Stress location (horizontal distance to track center)
21        'Stress
1.8       'Stress location (horizontal distance to track center)
17        'Stress
1.87      'Stress location (horizontal distance to track center)
13        'Stress
1.93      'Stress location (horizontal distance to track center)
11        'Stress
2.0       'Stress location (horizontal distance to track center)
9         'Stress
2.13      'Stress location (horizontal distance to track center)
6         'Stress
2.5       'Stress location (horizontal distance to track center)
0         'Stress

0.02      'the size of element, m
1560      'the density of subgrade soil, kg/m3
1         '1 the start effective cohesion of subgrade soil, kPa
10        '10 the end effective cohesion of subgrade soil, kPa
1         '1 the interval of effective cohesion of subgrade soil, kPa
17        '17 the start effective angle of friction of soil in Degree
```

```
25          '25 the end effective angle of friction of soil in Degree
2           '2 the interval of effective angle of friction of soil in Degree
0.25        '0.25 the start Coefficient of earth pressure at rest
0.4         '0.4 the end Coefficient of earth pressure at rest
0.05        '0.05 the interval of Coefficient of earth pressure at rest
0.05        '0.05 the start coefficient of friction on failure plane
0.35        '0.35 the end coefficient of friction on failure plane
0.05        '0.05 the interval of coefficient of friction on failure plane
```

3. RESULT OF SIMULATION FOR POINT LOAD

No of simulation	Angle of friction	Cohesion	Coefficient of earth pressure at rest	Coefficient of residual friction	Number of elements	Final Load
	ϕ'	c'	K_0	K_r	No.	P
	°	kPa				%
1	17	1	0.25	0.05	0	0
2	19	1	0.25	0.05	0	0
3	21	1	0.25	0.05	0	0
4	23	1	0.25	0.05	0	0
5	25	1	0.25	0.05	0	0
6	17	2	0.25	0.05	85	200
7	19	2	0.25	0.05	83	200
8	21	2	0.25	0.05	81	200
9	23	2	0.25	0.05	79	200
10	25	2	0.25	0.05	78	200
11	17	3	0.25	0.05	36	30
12	19	3	0.25	0.05	34	29
13	21	3	0.25	0.05	33	30
14	23	3	0.25	0.05	31	29
15	25	3	0.25	0.05	29	28
16	17	4	0.25	0.05	17	23
17	19	4	0.25	0.05	17	24
18	21	4	0.25	0.05	16	23
19	23	4	0.25	0.05	15	22
20	25	4	0.25	0.05	14	21
21	17	5	0.25	0.05	10	18
22	19	5	0.25	0.05	10	19
23	21	5	0.25	0.05	9	17
24	23	5	0.25	0.05	9	17
25	25	5	0.25	0.05	9	18
26	17	6	0.25	0.05	7	16
27	19	6	0.25	0.05	7	16
28	21	6	0.25	0.05	7	16
29	23	6	0.25	0.05	7	16
30	25	6	0.25	0.05	7	17
31	17	7	0.25	0.05	6	16
32	19	7	0.25	0.05	6	16
33	21	7	0.25	0.05	6	16

34	23	7	0.25	0.05	6	16
35	25	7	0.25	0.05	6	17
36	17	8	0.25	0.05	6	20
37	19	8	0.25	0.05	6	20
38	21	8	0.25	0.05	6	19
39	23	8	0.25	0.05	6	20
40	25	8	0.25	0.05	6	20
41	17	9	0.25	0.05	5	18
42	19	9	0.25	0.05	5	18
43	21	9	0.25	0.05	5	18
44	23	9	0.25	0.05	5	18
45	25	9	0.25	0.05	5	18
46	17	10	0.25	0.05	5	21
47	19	10	0.25	0.05	5	21
48	21	10	0.25	0.05	5	20
49	23	10	0.25	0.05	5	20
50	25	10	0.25	0.05	5	21
51	17	1	0.3	0.05	0	0
52	19	1	0.3	0.05	0	0
53	21	1	0.3	0.05	0	0
54	23	1	0.3	0.05	0	0
55	25	1	0.3	0.05	200	8
56	17	2	0.3	0.05	72	200
57	19	2	0.3	0.05	70	200
58	21	2	0.3	0.05	62	83
59	23	2	0.3	0.05	49	36
60	25	2	0.3	0.05	46	37
61	17	3	0.3	0.05	29	36
62	19	3	0.3	0.05	28	36
63	21	3	0.3	0.05	26	34
64	23	3	0.3	0.05	24	33
65	25	3	0.3	0.05	22	32
66	17	4	0.3	0.05	14	25
67	19	4	0.3	0.05	13	24
68	21	4	0.3	0.05	13	25
69	23	4	0.3	0.05	12	24
70	25	4	0.3	0.05	10	21
71	17	5	0.3	0.05	9	21
72	19	5	0.3	0.05	9	21
73	21	5	0.3	0.05	8	19
74	23	5	0.3	0.05	8	20
75	25	5	0.3	0.05	7	18

76	17	6	0.3	0.05	7	20
77	19	6	0.3	0.05	7	20
78	21	6	0.3	0.05	7	20
79	23	6	0.3	0.05	6	17
80	25	6	0.3	0.05	6	19
81	17	7	0.3	0.05	6	20
82	19	7	0.3	0.05	6	19
83	21	7	0.3	0.05	6	20
84	23	7	0.3	0.05	6	21
85	25	7	0.3	0.05	5	17
86	17	8	0.3	0.05	5	18
87	19	8	0.3	0.05	5	18
88	21	8	0.3	0.05	5	18
89	23	8	0.3	0.05	5	19
90	25	8	0.3	0.05	5	20
91	17	9	0.3	0.05	5	21
92	19	9	0.3	0.05	5	21
93	21	9	0.3	0.05	5	21
94	23	9	0.3	0.05	5	22
95	25	9	0.3	0.05	5	23
96	17	10	0.3	0.05	5	24
97	19	10	0.3	0.05	5	24
98	21	10	0.3	0.05	5	24
99	23	10	0.3	0.05	5	24
100	25	10	0.3	0.05	5	26
101	17	1	0.35	0.05	0	0
102	19	1	0.35	0.05	0	0
103	21	1	0.35	0.05	200	67
104	23	1	0.35	0.05	200	95
105	25	1	0.35	0.05	200	121
106	17	2	0.35	0.05	46	48
107	19	2	0.35	0.05	44	48
108	21	2	0.35	0.05	42	47
109	23	2	0.35	0.05	39	47
110	25	2	0.35	0.05	35	48
111	17	3	0.35	0.05	23	40
112	19	3	0.35	0.05	22	39
113	21	3	0.35	0.05	20	37
114	23	3	0.35	0.05	16	32
115	25	3	0.35	0.05	8	21
116	17	4	0.35	0.05	12	28
117	19	4	0.35	0.05	11	26

118	21	4	0.35	0.05	10	25
119	23	4	0.35	0.05	8	22
120	25	4	0.35	0.05	5	19
121	17	5	0.35	0.05	8	23
122	19	5	0.35	0.05	7	20
123	21	5	0.35	0.05	7	21
124	23	5	0.35	0.05	6	20
125	25	5	0.35	0.05	5	24
126	17	6	0.35	0.05	6	20
127	19	6	0.35	0.05	6	20
128	21	6	0.35	0.05	6	21
129	23	6	0.35	0.05	5	19
130	25	6	0.35	0.05	5	30
131	17	7	0.35	0.05	6	23
132	19	7	0.35	0.05	5	19
133	21	7	0.35	0.05	5	20
134	23	7	0.35	0.05	5	22
135	25	7	0.35	0.05	5	35
136	17	8	0.35	0.05	5	21
137	19	8	0.35	0.05	5	22
138	21	8	0.35	0.05	5	23
139	23	8	0.35	0.05	5	26
140	25	8	0.35	0.05	5	41
141	17	9	0.35	0.05	5	24
142	19	9	0.35	0.05	5	25
143	21	9	0.35	0.05	5	26
144	23	9	0.35	0.05	5	29
145	25	9	0.35	0.05	4	46
146	17	10	0.35	0.05	5	27
147	19	10	0.35	0.05	5	28
148	21	10	0.35	0.05	5	28
149	23	10	0.35	0.05	4	33
150	25	10	0.35	0.05	4	52
151	17	1	0.4	0.05	200	165
152	19	1	0.4	0.05	96	77
153	21	1	0.4	0.05	73	62
154	23	1	0.4	0.05	61	58
155	25	1	0.4	0.05	4	49
156	17	2	0.4	0.05	38	59
157	19	2	0.4	0.05	36	58
158	21	2	0.4	0.05	33	57
159	23	2	0.4	0.05	24	52

160	25	2	0.4	0.05	4	101
161	17	3	0.4	0.05	18	42
162	19	3	0.4	0.05	16	39
163	21	3	0.4	0.05	12	32
164	23	3	0.4	0.05	5	22
165	25	3	0.4	0.05	4	153
166	17	4	0.4	0.05	10	30
167	19	4	0.4	0.05	8	25
168	21	4	0.4	0.05	6	21
169	23	4	0.4	0.05	5	30
170	25	4	0.4	0.05	1	204
171	17	5	0.4	0.05	7	25
172	19	5	0.4	0.05	6	22
173	21	5	0.4	0.05	5	20
174	23	5	0.4	0.05	4	39
175	25	5	0.4	0.05	1	256
176	17	6	0.4	0.05	6	25
177	19	6	0.4	0.05	5	21
178	21	6	0.4	0.05	5	24
179	23	6	0.4	0.05	4	47
180	25	6	0.4	0.05	1	308
181	17	7	0.4	0.05	5	23
182	19	7	0.4	0.05	5	24
183	21	7	0.4	0.05	4	29
184	23	7	0.4	0.05	4	55
185	25	7	0.4	0.05	1	360
186	17	8	0.4	0.05	5	26
187	19	8	0.4	0.05	5	27
188	21	8	0.4	0.05	4	33
189	23	8	0.4	0.05	4	63
190	25	8	0.4	0.05	1	411
191	17	9	0.4	0.05	5	29
192	19	9	0.4	0.05	4	25
193	21	9	0.4	0.05	4	38
194	23	9	0.4	0.05	4	72
195	25	9	0.4	0.05	1	463
196	17	10	0.4	0.05	4	25
197	19	10	0.4	0.05	4	28
198	21	10	0.4	0.05	4	42
199	23	10	0.4	0.05	4	80
200	25	10	0.4	0.05	1	515
201	17	1	0.25	0.1	0	0

202	19	1	0.25	0.1	0	0
203	21	1	0.25	0.1	0	0
204	23	1	0.25	0.1	0	0
205	25	1	0.25	0.1	0	0
206	17	2	0.25	0.1	200	66
207	19	2	0.25	0.1	97	200
208	21	2	0.25	0.1	86	200
209	23	2	0.25	0.1	79	200
210	25	2	0.25	0.1	75	200
211	17	3	0.25	0.1	37	40
212	19	3	0.25	0.1	35	39
213	21	3	0.25	0.1	34	40
214	23	3	0.25	0.1	32	38
215	25	3	0.25	0.1	30	37
216	17	4	0.25	0.1	18	31
217	19	4	0.25	0.1	17	29
218	21	4	0.25	0.1	17	30
219	23	4	0.25	0.1	16	29
220	25	4	0.25	0.1	15	27
221	17	5	0.25	0.1	10	23
222	19	5	0.25	0.1	10	23
223	21	5	0.25	0.1	10	23
224	23	5	0.25	0.1	10	23
225	25	5	0.25	0.1	9	21
226	17	6	0.25	0.1	8	23
227	19	6	0.25	0.1	8	23
228	21	6	0.25	0.1	8	23
229	23	6	0.25	0.1	8	23
230	25	6	0.25	0.1	8	23
231	17	7	0.25	0.1	6	20
232	19	7	0.25	0.1	6	19
233	21	7	0.25	0.1	7	24
234	23	7	0.25	0.1	7	24
235	25	7	0.25	0.1	7	24
236	17	8	0.25	0.1	6	24
237	19	8	0.25	0.1	6	24
238	21	8	0.25	0.1	6	23
239	23	8	0.25	0.1	6	23
240	25	8	0.25	0.1	6	23
241	17	9	0.25	0.1	5	22
242	19	9	0.25	0.1	5	21
243	21	9	0.25	0.1	6	27

244	23	9	0.25	0.1	6	27
245	25	9	0.25	0.1	6	27
246	17	10	0.25	0.1	5	25
247	19	10	0.25	0.1	5	25
248	21	10	0.25	0.1	5	24
249	23	10	0.25	0.1	5	24
250	25	10	0.25	0.1	5	24
251	17	1	0.3	0.1	0	0
252	19	1	0.3	0.1	0	0
253	21	1	0.3	0.1	0	0
254	23	1	0.3	0.1	0	0
255	25	1	0.3	0.1	200	20
256	17	2	0.3	0.1	69	200
257	19	2	0.3	0.1	67	200
258	21	2	0.3	0.1	63	148
259	23	2	0.3	0.1	50	49
260	25	2	0.3	0.1	47	48
261	17	3	0.3	0.1	30	48
262	19	3	0.3	0.1	28	45
263	21	3	0.3	0.1	27	45
264	23	3	0.3	0.1	25	43
265	25	3	0.3	0.1	23	41
266	17	4	0.3	0.1	15	34
267	19	4	0.3	0.1	14	32
268	21	4	0.3	0.1	13	30
269	23	4	0.3	0.1	13	31
270	25	4	0.3	0.1	11	27
271	17	5	0.3	0.1	9	26
272	19	5	0.3	0.1	9	26
273	21	5	0.3	0.1	9	26
274	23	5	0.3	0.1	8	23
275	25	5	0.3	0.1	8	25
276	17	6	0.3	0.1	7	24
277	19	6	0.3	0.1	7	24
278	21	6	0.3	0.1	7	24
279	23	6	0.3	0.1	7	25
280	25	6	0.3	0.1	6	21
281	17	7	0.3	0.1	6	24
282	19	7	0.3	0.1	6	24
283	21	7	0.3	0.1	6	23
284	23	7	0.3	0.1	6	24
285	25	7	0.3	0.1	6	25

286	17	8	0.3	0.1	6	28
287	19	8	0.3	0.1	6	28
288	21	8	0.3	0.1	6	27
289	23	8	0.3	0.1	6	28
290	25	8	0.3	0.1	5	23
291	17	9	0.3	0.1	5	25
292	19	9	0.3	0.1	5	25
293	21	9	0.3	0.1	5	25
294	23	9	0.3	0.1	5	25
295	25	9	0.3	0.1	5	26
296	17	10	0.3	0.1	5	29
297	19	10	0.3	0.1	5	28
298	21	10	0.3	0.1	5	28
299	23	10	0.3	0.1	5	28
300	25	10	0.3	0.1	5	29
301	17	1	0.35	0.1	0	0
302	19	1	0.35	0.1	0	0
303	21	1	0.35	0.1	200	126
304	23	1	0.35	0.1	200	150
305	25	1	0.35	0.1	200	165
306	17	2	0.35	0.1	47	65
307	19	2	0.35	0.1	44	62
308	21	2	0.35	0.1	42	61
309	23	2	0.35	0.1	40	61
310	25	2	0.35	0.1	36	60
311	17	3	0.35	0.1	24	53
312	19	3	0.35	0.1	22	49
313	21	3	0.35	0.1	21	48
314	23	3	0.35	0.1	18	43
315	25	3	0.35	0.1	13	36
316	17	4	0.35	0.1	12	35
317	19	4	0.35	0.1	11	32
318	21	4	0.35	0.1	11	33
319	23	4	0.35	0.1	9	29
320	25	4	0.35	0.1	6	23
321	17	5	0.35	0.1	8	28
322	19	5	0.35	0.1	8	28
323	21	5	0.35	0.1	7	25
324	23	5	0.35	0.1	7	27
325	25	5	0.35	0.1	5	24
326	17	6	0.35	0.1	7	29
327	19	6	0.35	0.1	6	24

328	21	6	0.35	0.1	6	25
329	23	6	0.35	0.1	6	27
330	25	6	0.35	0.1	5	30
331	17	7	0.35	0.1	6	28
332	19	7	0.35	0.1	6	28
333	21	7	0.35	0.1	6	29
334	23	7	0.35	0.1	5	25
335	25	7	0.35	0.1	5	35
336	17	8	0.35	0.1	5	26
337	19	8	0.35	0.1	5	26
338	21	8	0.35	0.1	5	27
339	23	8	0.35	0.1	5	28
340	25	8	0.35	0.1	5	41
341	17	9	0.35	0.1	5	30
342	19	9	0.35	0.1	5	29
343	21	9	0.35	0.1	5	30
344	23	9	0.35	0.1	5	32
345	25	9	0.35	0.1	5	46
346	17	10	0.35	0.1	5	33
347	19	10	0.35	0.1	5	33
348	21	10	0.35	0.1	5	33
349	23	10	0.35	0.1	5	35
350	25	10	0.35	0.1	4	52
351	17	1	0.4	0.1	177	200
352	19	1	0.4	0.1	98	105
353	21	1	0.4	0.1	75	84
354	23	1	0.4	0.1	63	77
355	25	1	0.4	0.1	5	49
356	17	2	0.4	0.1	39	78
357	19	2	0.4	0.1	37	75
358	21	2	0.4	0.1	34	73
359	23	2	0.4	0.1	28	70
360	25	2	0.4	0.1	4	101
361	17	3	0.4	0.1	18	53
362	19	3	0.4	0.1	17	51
363	21	3	0.4	0.1	14	45
364	23	3	0.4	0.1	6	26
365	25	3	0.4	0.1	4	153
366	17	4	0.4	0.1	10	37
367	19	4	0.4	0.1	9	34
368	21	4	0.4	0.1	8	33
369	23	4	0.4	0.1	5	30

370	25	4	0.4	0.1	1	204
371	17	5	0.4	0.1	7	30
372	19	5	0.4	0.1	7	31
373	21	5	0.4	0.1	6	29
374	23	5	0.4	0.1	4	39
375	25	5	0.4	0.1	1	256
376	17	6	0.4	0.1	6	30
377	19	6	0.4	0.1	6	31
378	21	6	0.4	0.1	5	28
379	23	6	0.4	0.1	4	47
380	25	6	0.4	0.1	1	308
381	17	7	0.4	0.1	5	27
382	19	7	0.4	0.1	5	28
383	21	7	0.4	0.1	5	31
384	23	7	0.4	0.1	4	55
385	25	7	0.4	0.1	1	360
386	17	8	0.4	0.1	5	31
387	19	8	0.4	0.1	5	32
388	21	8	0.4	0.1	4	33
389	23	8	0.4	0.1	4	63
390	25	8	0.4	0.1	1	411
391	17	9	0.4	0.1	5	35
392	19	9	0.4	0.1	5	36
393	21	9	0.4	0.1	4	38
394	23	9	0.4	0.1	4	72
395	25	9	0.4	0.1	1	463
396	17	10	0.4	0.1	5	38
397	19	10	0.4	0.1	4	31
398	21	10	0.4	0.1	4	42
399	23	10	0.4	0.1	4	80
400	25	10	0.4	0.1	1	515
401	17	1	0.25	0.15	0	0
402	19	1	0.25	0.15	0	0
403	21	1	0.25	0.15	0	0
404	23	1	0.25	0.15	0	0
405	25	1	0.25	0.15	0	0
406	17	2	0.25	0.15	200	33
407	19	2	0.25	0.15	200	70
408	21	2	0.25	0.15	91	200
409	23	2	0.25	0.15	79	200
410	25	2	0.25	0.15	73	200
411	17	3	0.25	0.15	38	55

412	19	3	0.25	0.15	36	53
413	21	3	0.25	0.15	34	50
414	23	3	0.25	0.15	33	50
415	25	3	0.25	0.15	31	48
416	17	4	0.25	0.15	19	42
417	19	4	0.25	0.15	18	40
418	21	4	0.25	0.15	17	37
419	23	4	0.25	0.15	16	35
420	25	4	0.25	0.15	16	36
421	17	5	0.25	0.15	10	28
422	19	5	0.25	0.15	10	28
423	21	5	0.25	0.15	10	28
424	23	5	0.25	0.15	10	28
425	25	5	0.25	0.15	10	29
426	17	6	0.25	0.15	8	29
427	19	6	0.25	0.15	8	28
428	21	6	0.25	0.15	8	28
429	23	6	0.25	0.15	8	28
430	25	6	0.25	0.15	8	28
431	17	7	0.25	0.15	6	24
432	19	7	0.25	0.15	7	30
433	21	7	0.25	0.15	7	29
434	23	7	0.25	0.15	7	29
435	25	7	0.25	0.15	7	28
436	17	8	0.25	0.15	6	30
437	19	8	0.25	0.15	6	29
438	21	8	0.25	0.15	6	28
439	23	8	0.25	0.15	6	28
440	25	8	0.25	0.15	6	27
441	17	9	0.25	0.15	5	27
442	19	9	0.25	0.15	6	34
443	21	9	0.25	0.15	6	33
444	23	9	0.25	0.15	6	32
445	25	9	0.25	0.15	6	32
446	17	10	0.25	0.15	5	31
447	19	10	0.25	0.15	5	30
448	21	10	0.25	0.15	5	29
449	23	10	0.25	0.15	5	29
450	25	10	0.25	0.15	6	36
451	17	1	0.3	0.15	0	0
452	19	1	0.3	0.15	0	0
453	21	1	0.3	0.15	0	0

454	23	1	0.3	0.15	0	0
455	25	1	0.3	0.15	200	49
456	17	2	0.3	0.15	66	200
457	19	2	0.3	0.15	64	200
458	21	2	0.3	0.15	63	200
459	23	2	0.3	0.15	50	64
460	25	2	0.3	0.15	48	64
461	17	3	0.3	0.15	30	62
462	19	3	0.3	0.15	29	60
463	21	3	0.3	0.15	27	56
464	23	3	0.3	0.15	26	55
465	25	3	0.3	0.15	24	52
466	17	4	0.3	0.15	15	43
467	19	4	0.3	0.15	14	40
468	21	4	0.3	0.15	14	40
469	23	4	0.3	0.15	13	37
470	25	4	0.3	0.15	12	35
471	17	5	0.3	0.15	9	32
472	19	5	0.3	0.15	9	32
473	21	5	0.3	0.15	9	32
474	23	5	0.3	0.15	9	32
475	25	5	0.3	0.15	8	29
476	17	6	0.3	0.15	7	30
477	19	6	0.3	0.15	7	29
478	21	6	0.3	0.15	7	29
479	23	6	0.3	0.15	7	29
480	25	6	0.3	0.15	7	30
481	17	7	0.3	0.15	6	29
482	19	7	0.3	0.15	6	28
483	21	7	0.3	0.15	6	28
484	23	7	0.3	0.15	6	28
485	25	7	0.3	0.15	6	29
486	17	8	0.3	0.15	6	35
487	19	8	0.3	0.15	6	34
488	21	8	0.3	0.15	6	33
489	23	8	0.3	0.15	6	33
490	25	8	0.3	0.15	6	34
491	17	9	0.3	0.15	5	31
492	19	9	0.3	0.15	5	30
493	21	9	0.3	0.15	5	30
494	23	9	0.3	0.15	5	30
495	25	9	0.3	0.15	5	31

496	17	10	0.3	0.15	5	36
497	19	10	0.3	0.15	5	34
498	21	10	0.3	0.15	5	34
499	23	10	0.3	0.15	5	33
500	25	10	0.3	0.15	5	34
501	17	1	0.35	0.15	0	0
502	19	1	0.35	0.15	0	0
503	21	1	0.35	0.15	198	200
504	23	1	0.35	0.15	185	200
505	25	1	0.35	0.15	180	200
506	17	2	0.35	0.15	47	85
507	19	2	0.35	0.15	45	82
508	21	2	0.35	0.15	43	80
509	23	2	0.35	0.15	41	78
510	25	2	0.35	0.15	38	78
511	17	3	0.35	0.15	24	67
512	19	3	0.35	0.15	23	65
513	21	3	0.35	0.15	21	60
514	23	3	0.35	0.15	19	56
515	25	3	0.35	0.15	16	52
516	17	4	0.35	0.15	12	44
517	19	4	0.35	0.15	12	44
518	21	4	0.35	0.15	11	40
519	23	4	0.35	0.15	10	38
520	25	4	0.35	0.15	8	35
521	17	5	0.35	0.15	8	35
522	19	5	0.35	0.15	8	35
523	21	5	0.35	0.15	8	35
524	23	5	0.35	0.15	7	32
525	25	5	0.35	0.15	6	31
526	17	6	0.35	0.15	7	36
527	19	6	0.35	0.15	7	36
528	21	6	0.35	0.15	7	36
529	23	6	0.35	0.15	6	31
530	25	6	0.35	0.15	5	30
531	17	7	0.35	0.15	6	35
532	19	7	0.35	0.15	6	35
533	21	7	0.35	0.15	6	35
534	23	7	0.35	0.15	6	36
535	25	7	0.35	0.15	5	35
536	17	8	0.35	0.15	5	32
537	19	8	0.35	0.15	5	31

538	21	8	0.35	0.15	5	32
539	23	8	0.35	0.15	5	33
540	25	8	0.35	0.15	5	41
541	17	9	0.35	0.15	5	36
542	19	9	0.35	0.15	5	36
543	21	9	0.35	0.15	5	36
544	23	9	0.35	0.15	5	37
545	25	9	0.35	0.15	5	46
546	17	10	0.35	0.15	5	41
547	19	10	0.35	0.15	5	40
548	21	10	0.35	0.15	5	40
549	23	10	0.35	0.15	5	41
550	25	10	0.35	0.15	5	52
551	17	1	0.4	0.15	135	200
552	19	1	0.4	0.15	99	140
553	21	1	0.4	0.15	76	111
554	23	1	0.4	0.15	65	102
555	25	1	0.4	0.15	5	49
556	17	2	0.4	0.15	39	100
557	19	2	0.4	0.15	37	96
558	21	2	0.4	0.15	35	93
559	23	2	0.4	0.15	30	90
560	25	2	0.4	0.15	4	101
561	17	3	0.4	0.15	19	71
562	19	3	0.4	0.15	18	67
563	21	3	0.4	0.15	16	62
564	23	3	0.4	0.15	9	43
565	25	3	0.4	0.15	4	153
566	17	4	0.4	0.15	10	46
567	19	4	0.4	0.15	10	46
568	21	4	0.4	0.15	9	44
569	23	4	0.4	0.15	5	30
570	25	4	0.4	0.15	1	204
571	17	5	0.4	0.15	7	37
572	19	5	0.4	0.15	7	38
573	21	5	0.4	0.15	6	34
574	23	5	0.4	0.15	5	39
575	25	5	0.4	0.15	1	256
576	17	6	0.4	0.15	6	36
577	19	6	0.4	0.15	6	37
578	21	6	0.4	0.15	5	32
579	23	6	0.4	0.15	4	47

580	25	6	0.4	0.15	1	308
581	17	7	0.4	0.15	6	42
582	19	7	0.4	0.15	5	34
583	21	7	0.4	0.15	5	37
584	23	7	0.4	0.15	4	55
585	25	7	0.4	0.15	1	360
586	17	8	0.4	0.15	5	38
587	19	8	0.4	0.15	5	38
588	21	8	0.4	0.15	5	41
589	23	8	0.4	0.15	4	63
590	25	8	0.4	0.15	1	411
591	17	9	0.4	0.15	5	43
592	19	9	0.4	0.15	5	43
593	21	9	0.4	0.15	5	45
594	23	9	0.4	0.15	4	72
595	25	9	0.4	0.15	1	463
596	17	10	0.4	0.15	5	47
597	19	10	0.4	0.15	5	47
598	21	10	0.4	0.15	4	42
599	23	10	0.4	0.15	4	80
600	25	10	0.4	0.15	1	515
601	17	1	0.25	0.2	0	0
602	19	1	0.25	0.2	0	0
603	21	1	0.25	0.2	0	0
604	23	1	0.25	0.2	0	0
605	25	1	0.25	0.2	0	0
606	17	2	0.25	0.2	200	47
607	19	2	0.25	0.2	200	88
608	21	2	0.25	0.2	95	200
609	23	2	0.25	0.2	78	200
610	25	2	0.25	0.2	71	200
611	17	3	0.25	0.2	38	70
612	19	3	0.25	0.2	36	67
613	21	3	0.25	0.2	35	67
614	23	3	0.25	0.2	33	63
615	25	3	0.25	0.2	32	62
616	17	4	0.25	0.2	19	53
617	19	4	0.25	0.2	18	50
618	21	4	0.25	0.2	17	46
619	23	4	0.25	0.2	17	47
620	25	4	0.25	0.2	16	44
621	17	5	0.25	0.2	11	40

622	19	5	0.25	0.2	10	35
623	21	5	0.25	0.2	10	35
624	23	5	0.25	0.2	10	35
625	25	5	0.25	0.2	10	35
626	17	6	0.25	0.2	8	36
627	19	6	0.25	0.2	8	35
628	21	6	0.25	0.2	8	34
629	23	6	0.25	0.2	8	34
630	25	6	0.25	0.2	8	33
631	17	7	0.25	0.2	6	30
632	19	7	0.25	0.2	7	37
633	21	7	0.25	0.2	7	35
634	23	7	0.25	0.2	7	35
635	25	7	0.25	0.2	7	34
636	17	8	0.25	0.2	6	37
637	19	8	0.25	0.2	6	35
638	21	8	0.25	0.2	6	34
639	23	8	0.25	0.2	6	33
640	25	8	0.25	0.2	6	33
641	17	9	0.25	0.2	5	33
642	19	9	0.25	0.2	6	42
643	21	9	0.25	0.2	6	40
644	23	9	0.25	0.2	6	39
645	25	9	0.25	0.2	6	38
646	17	10	0.25	0.2	5	38
647	19	10	0.25	0.2	5	37
648	21	10	0.25	0.2	5	35
649	23	10	0.25	0.2	6	44
650	25	10	0.25	0.2	6	43
651	17	1	0.3	0.2	0	0
652	19	1	0.3	0.2	0	0
653	21	1	0.3	0.2	0	0
654	23	1	0.3	0.2	0	0
655	25	1	0.3	0.2	200	116
656	17	2	0.3	0.2	64	200
657	19	2	0.3	0.2	62	200
658	21	2	0.3	0.2	60	200
659	23	2	0.3	0.2	51	86
660	25	2	0.3	0.2	48	81
661	17	3	0.3	0.2	30	79
662	19	3	0.3	0.2	29	77
663	21	3	0.3	0.2	28	74

664	23	3	0.3	0.2	26	69
665	25	3	0.3	0.2	25	67
666	17	4	0.3	0.2	15	54
667	19	4	0.3	0.2	14	50
668	21	4	0.3	0.2	14	50
669	23	4	0.3	0.2	14	50
670	25	4	0.3	0.2	13	47
671	17	5	0.3	0.2	9	40
672	19	5	0.3	0.2	9	39
673	21	5	0.3	0.2	9	39
674	23	5	0.3	0.2	9	39
675	25	5	0.3	0.2	9	40
676	17	6	0.3	0.2	7	37
677	19	6	0.3	0.2	7	36
678	21	6	0.3	0.2	7	35
679	23	6	0.3	0.2	7	35
680	25	6	0.3	0.2	7	36
681	17	7	0.3	0.2	6	36
682	19	7	0.3	0.2	6	35
683	21	7	0.3	0.2	6	34
684	23	7	0.3	0.2	6	34
685	25	7	0.3	0.2	6	35
686	17	8	0.3	0.2	6	43
687	19	8	0.3	0.2	6	41
688	21	8	0.3	0.2	6	40
689	23	8	0.3	0.2	6	40
690	25	8	0.3	0.2	6	40
691	17	9	0.3	0.2	5	39
692	19	9	0.3	0.2	5	37
693	21	9	0.3	0.2	6	46
694	23	9	0.3	0.2	6	45
695	25	9	0.3	0.2	6	45
696	17	10	0.3	0.2	5	44
697	19	10	0.3	0.2	5	42
698	21	10	0.3	0.2	5	41
699	23	10	0.3	0.2	5	40
700	25	10	0.3	0.2	5	40
701	17	1	0.35	0.2	0	0
702	19	1	0.35	0.2	0	0
703	21	1	0.35	0.2	144	200
704	23	1	0.35	0.2	141	200
705	25	1	0.35	0.2	141	200

706	17	2	0.35	0.2	47	111
707	19	2	0.35	0.2	45	106
708	21	2	0.35	0.2	43	102
709	23	2	0.35	0.2	41	99
710	25	2	0.35	0.2	39	99
711	17	3	0.35	0.2	24	86
712	19	3	0.35	0.2	23	82
713	21	3	0.35	0.2	22	78
714	23	3	0.35	0.2	20	72
715	25	3	0.35	0.2	18	69
716	17	4	0.35	0.2	12	56
717	19	4	0.35	0.2	12	55
718	21	4	0.35	0.2	12	55
719	23	4	0.35	0.2	11	51
720	25	4	0.35	0.2	9	45
721	17	5	0.35	0.2	8	44
722	19	5	0.35	0.2	8	43
723	21	5	0.35	0.2	8	43
724	23	5	0.35	0.2	8	44
725	25	5	0.35	0.2	7	43
726	17	6	0.35	0.2	7	45
727	19	6	0.35	0.2	7	44
728	21	6	0.35	0.2	7	44
729	23	6	0.35	0.2	7	45
730	25	6	0.35	0.2	6	42
731	17	7	0.35	0.2	6	44
732	19	7	0.35	0.2	6	42
733	21	7	0.35	0.2	6	42
734	23	7	0.35	0.2	6	43
735	25	7	0.35	0.2	5	39
736	17	8	0.35	0.2	5	40
737	19	8	0.35	0.2	6	49
738	21	8	0.35	0.2	6	48
739	23	8	0.35	0.2	5	39
740	25	8	0.35	0.2	5	43
741	17	9	0.35	0.2	5	45
742	19	9	0.35	0.2	5	43
743	21	9	0.35	0.2	5	43
744	23	9	0.35	0.2	5	44
745	25	9	0.35	0.2	5	48
746	17	10	0.35	0.2	5	51
747	19	10	0.35	0.2	5	48

748	21	10	0.35	0.2	5	48
749	23	10	0.35	0.2	5	49
750	25	10	0.35	0.2	5	53
751	17	1	0.4	0.2	102	200
752	19	1	0.4	0.2	99	184
753	21	1	0.4	0.2	76	146
754	23	1	0.4	0.2	66	133
755	25	1	0.4	0.2	5	49
756	17	2	0.4	0.2	39	130
757	19	2	0.4	0.2	37	123
758	21	2	0.4	0.2	35	118
759	23	2	0.4	0.2	32	116
760	25	2	0.4	0.2	4	101
761	17	3	0.4	0.2	19	91
762	19	3	0.4	0.2	18	85
763	21	3	0.4	0.2	16	77
764	23	3	0.4	0.2	12	66
765	25	3	0.4	0.2	4	153
766	17	4	0.4	0.2	10	59
767	19	4	0.4	0.2	10	58
768	21	4	0.4	0.2	9	53
769	23	4	0.4	0.2	6	42
770	25	4	0.4	0.2	1	204
771	17	5	0.4	0.2	8	55
772	19	5	0.4	0.2	7	46
773	21	5	0.4	0.2	7	48
774	23	5	0.4	0.2	5	40
775	25	5	0.4	0.2	1	256
776	17	6	0.4	0.2	6	46
777	19	6	0.4	0.2	6	45
778	21	6	0.4	0.2	6	47
779	23	6	0.4	0.2	5	47
780	25	6	0.4	0.2	1	308
781	17	7	0.4	0.2	6	53
782	19	7	0.4	0.2	6	52
783	21	7	0.4	0.2	5	44
784	23	7	0.4	0.2	4	55
785	25	7	0.4	0.2	1	360
786	17	8	0.4	0.2	5	47
787	19	8	0.4	0.2	5	47
788	21	8	0.4	0.2	5	49
789	23	8	0.4	0.2	4	63

790	25	8	0.4	0.2	1	411
791	17	9	0.4	0.2	5	53
792	19	9	0.4	0.2	5	52
793	21	9	0.4	0.2	5	54
794	23	9	0.4	0.2	4	72
795	25	9	0.4	0.2	1	463
796	17	10	0.4	0.2	5	58
797	19	10	0.4	0.2	5	57
798	21	10	0.4	0.2	5	59
799	23	10	0.4	0.2	4	80
800	25	10	0.4	0.2	1	515
801	17	1	0.25	0.25	0	0
802	19	1	0.25	0.25	0	0
803	21	1	0.25	0.25	0	0
804	23	1	0.25	0.25	0	0
805	25	1	0.25	0.25	0	0
806	17	2	0.25	0.25	200	77
807	19	2	0.25	0.25	200	127
808	21	2	0.25	0.25	97	200
809	23	2	0.25	0.25	77	200
810	25	2	0.25	0.25	70	200
811	17	3	0.25	0.25	38	91
812	19	3	0.25	0.25	37	90
813	21	3	0.25	0.25	35	85
814	23	3	0.25	0.25	34	83
815	25	3	0.25	0.25	32	78
816	17	4	0.25	0.25	19	67
817	19	4	0.25	0.25	18	62
818	21	4	0.25	0.25	18	63
819	23	4	0.25	0.25	17	58
820	25	4	0.25	0.25	17	58
821	17	5	0.25	0.25	11	50
822	19	5	0.25	0.25	11	50
823	21	5	0.25	0.25	11	49
824	23	5	0.25	0.25	11	48
825	25	5	0.25	0.25	11	48
826	17	6	0.25	0.25	8	45
827	19	6	0.25	0.25	8	43
828	21	6	0.25	0.25	8	42
829	23	6	0.25	0.25	8	41
830	25	6	0.25	0.25	8	40
831	17	7	0.25	0.25	6	37

832	19	7	0.25	0.25	7	45
833	21	7	0.25	0.25	7	44
834	23	7	0.25	0.25	7	42
835	25	7	0.25	0.25	7	41
836	17	8	0.25	0.25	6	45
837	19	8	0.25	0.25	6	44
838	21	8	0.25	0.25	6	42
839	23	8	0.25	0.25	6	40
840	25	8	0.25	0.25	6	39
841	17	9	0.25	0.25	5	41
842	19	9	0.25	0.25	6	51
843	21	9	0.25	0.25	6	49
844	23	9	0.25	0.25	6	47
845	25	9	0.25	0.25	6	45
846	17	10	0.25	0.25	5	47
847	19	10	0.25	0.25	5	45
848	21	10	0.25	0.25	5	43
849	23	10	0.25	0.25	6	54
850	25	10	0.25	0.25	6	52
851	17	1	0.3	0.25	0	0
852	19	1	0.3	0.25	0	0
853	21	1	0.3	0.25	0	0
854	23	1	0.3	0.25	0	0
855	25	1	0.3	0.25	190	200
856	17	2	0.3	0.25	62	200
857	19	2	0.3	0.25	60	200
858	21	2	0.3	0.25	58	200
859	23	2	0.3	0.25	51	111
860	25	2	0.3	0.25	49	107
861	17	3	0.3	0.25	30	101
862	19	3	0.3	0.25	29	98
863	21	3	0.3	0.25	28	94
864	23	3	0.3	0.25	27	90
865	25	3	0.3	0.25	25	84
866	17	4	0.3	0.25	15	69
867	19	4	0.3	0.25	15	68
868	21	4	0.3	0.25	14	62
869	23	4	0.3	0.25	14	62
870	25	4	0.3	0.25	13	57
871	17	5	0.3	0.25	9	51
872	19	5	0.3	0.25	9	49
873	21	5	0.3	0.25	9	48

874	23	5	0.3	0.25	9	48
875	25	5	0.3	0.25	9	48
876	17	6	0.3	0.25	7	46
877	19	6	0.3	0.25	7	45
878	21	6	0.3	0.25	7	44
879	23	6	0.3	0.25	8	51
880	25	6	0.3	0.25	8	50
881	17	7	0.3	0.25	6	46
882	19	7	0.3	0.25	6	44
883	21	7	0.3	0.25	6	42
884	23	7	0.3	0.25	7	51
885	25	7	0.3	0.25	7	50
886	17	8	0.3	0.25	6	54
887	19	8	0.3	0.25	6	51
888	21	8	0.3	0.25	6	50
889	23	8	0.3	0.25	6	48
890	25	8	0.3	0.25	6	47
891	17	9	0.3	0.25	5	48
892	19	9	0.3	0.25	5	46
893	21	9	0.3	0.25	6	57
894	23	9	0.3	0.25	6	55
895	25	9	0.3	0.25	6	54
896	17	10	0.3	0.25	5	55
897	19	10	0.3	0.25	5	52
898	21	10	0.3	0.25	5	50
899	23	10	0.3	0.25	5	48
900	25	10	0.3	0.25	5	48
901	17	1	0.35	0.25	0	0
902	19	1	0.35	0.25	0	0
903	21	1	0.35	0.25	109	200
904	23	1	0.35	0.25	109	200
905	25	1	0.35	0.25	110	200
906	17	2	0.35	0.25	47	145
907	19	2	0.35	0.25	45	138
908	21	2	0.35	0.25	43	131
909	23	2	0.35	0.25	41	126
910	25	2	0.35	0.25	39	123
911	17	3	0.35	0.25	24	111
912	19	3	0.35	0.25	23	104
913	21	3	0.35	0.25	22	99
914	23	3	0.35	0.25	21	94
915	25	3	0.35	0.25	19	89

916	17	4	0.35	0.25	12	71
917	19	4	0.35	0.25	12	70
918	21	4	0.35	0.25	12	68
919	23	4	0.35	0.25	11	62
920	25	4	0.35	0.25	10	60
921	17	5	0.35	0.25	8	56
922	19	5	0.35	0.25	8	54
923	21	5	0.35	0.25	8	53
924	23	5	0.35	0.25	8	53
925	25	5	0.35	0.25	7	49
926	17	6	0.35	0.25	7	57
927	19	6	0.35	0.25	7	55
928	21	6	0.35	0.25	7	54
929	23	6	0.35	0.25	7	54
930	25	6	0.35	0.25	6	48
931	17	7	0.35	0.25	6	55
932	19	7	0.35	0.25	6	53
933	21	7	0.35	0.25	6	51
934	23	7	0.35	0.25	6	51
935	25	7	0.35	0.25	6	56
936	17	8	0.35	0.25	5	50
937	19	8	0.35	0.25	6	61
938	21	8	0.35	0.25	6	59
939	23	8	0.35	0.25	6	58
940	25	8	0.35	0.25	5	51
941	17	9	0.35	0.25	5	57
942	19	9	0.35	0.25	5	54
943	21	9	0.35	0.25	5	52
944	23	9	0.35	0.25	5	52
945	25	9	0.35	0.25	5	56
946	17	10	0.35	0.25	5	63
947	19	10	0.35	0.25	5	61
948	21	10	0.35	0.25	5	58
949	23	10	0.35	0.25	5	58
950	25	10	0.35	0.25	5	62
951	17	1	0.4	0.25	74	200
952	19	1	0.4	0.25	77	200
953	21	1	0.4	0.25	76	190
954	23	1	0.4	0.25	67	173
955	25	1	0.4	0.25	5	49
956	17	2	0.4	0.25	39	170
957	19	2	0.4	0.25	37	159

958	21	2	0.4	0.25	36	153
959	23	2	0.4	0.25	33	148
960	25	2	0.4	0.25	4	101
961	17	3	0.4	0.25	19	117
962	19	3	0.4	0.25	18	109
963	21	3	0.4	0.25	17	102
964	23	3	0.4	0.25	14	91
965	25	3	0.4	0.25	4	153
966	17	4	0.4	0.25	10	75
967	19	4	0.4	0.25	10	73
968	21	4	0.4	0.25	10	74
969	23	4	0.4	0.25	8	65
970	25	4	0.4	0.25	1	204
971	17	5	0.4	0.25	8	71
972	19	5	0.4	0.25	8	68
973	21	5	0.4	0.25	7	59
974	23	5	0.4	0.25	6	58
975	25	5	0.4	0.25	1	256
976	17	6	0.4	0.25	6	59
977	19	6	0.4	0.25	6	56
978	21	6	0.4	0.25	6	57
979	23	6	0.4	0.25	5	54
980	25	6	0.4	0.25	1	308
981	17	7	0.4	0.25	6	67
982	19	7	0.4	0.25	6	64
983	21	7	0.4	0.25	6	65
984	23	7	0.4	0.25	5	61
985	25	7	0.4	0.25	1	360
986	17	8	0.4	0.25	5	60
987	19	8	0.4	0.25	5	58
988	21	8	0.4	0.25	5	58
989	23	8	0.4	0.25	5	68
990	25	8	0.4	0.25	1	411
991	17	9	0.4	0.25	5	67
992	19	9	0.4	0.25	5	65
993	21	9	0.4	0.25	5	65
994	23	9	0.4	0.25	4	72
995	25	9	0.4	0.25	1	463
996	17	10	0.4	0.25	5	75
997	19	10	0.4	0.25	5	71
998	21	10	0.4	0.25	5	72
999	23	10	0.4	0.25	4	80

1000	25	10	0.4	0.25	1	515
1001	17	1	0.25	0.3	0	0
1002	19	1	0.25	0.3	0	0
1003	21	1	0.25	0.3	0	0
1004	23	1	0.25	0.3	0	0
1005	25	1	0.25	0.3	0	0
1006	17	2	0.25	0.3	200	123
1007	19	2	0.25	0.3	200	186
1008	21	2	0.25	0.3	96	200
1009	23	2	0.25	0.3	75	200
1010	25	2	0.25	0.3	68	200
1011	17	3	0.25	0.3	39	122
1012	19	3	0.25	0.3	37	115
1013	21	3	0.25	0.3	35	108
1014	23	3	0.25	0.3	34	105
1015	25	3	0.25	0.3	32	98
1016	17	4	0.25	0.3	19	85
1017	19	4	0.25	0.3	18	79
1018	21	4	0.25	0.3	18	78
1019	23	4	0.25	0.3	17	73
1020	25	4	0.25	0.3	17	72
1021	17	5	0.25	0.3	11	64
1022	19	5	0.25	0.3	11	62
1023	21	5	0.25	0.3	11	61
1024	23	5	0.25	0.3	11	60
1025	25	5	0.25	0.3	11	59
1026	17	6	0.25	0.3	8	56
1027	19	6	0.25	0.3	8	54
1028	21	6	0.25	0.3	8	52
1029	23	6	0.25	0.3	8	51
1030	25	6	0.25	0.3	8	49
1031	17	7	0.25	0.3	6	47
1032	19	7	0.25	0.3	7	56
1033	21	7	0.25	0.3	7	54
1034	23	7	0.25	0.3	7	52
1035	25	7	0.25	0.3	7	50
1036	17	8	0.25	0.3	6	57
1037	19	8	0.25	0.3	6	54
1038	21	8	0.25	0.3	6	52
1039	23	8	0.25	0.3	6	50
1040	25	8	0.25	0.3	7	60
1041	17	9	0.25	0.3	5	51

1042	19	9	0.25	0.3	6	64
1043	21	9	0.25	0.3	6	61
1044	23	9	0.25	0.3	6	58
1045	25	9	0.25	0.3	6	55
1046	17	10	0.25	0.3	5	59
1047	19	10	0.25	0.3	5	56
1048	21	10	0.25	0.3	5	53
1049	23	10	0.25	0.3	6	66
1050	25	10	0.25	0.3	6	63
1051	17	1	0.3	0.3	0	0
1052	19	1	0.3	0.3	0	0
1053	21	1	0.3	0.3	0	0
1054	23	1	0.3	0.3	0	0
1055	25	1	0.3	0.3	132	200
1056	17	2	0.3	0.3	60	200
1057	19	2	0.3	0.3	58	200
1058	21	2	0.3	0.3	56	200
1059	23	2	0.3	0.3	51	143
1060	25	2	0.3	0.3	49	136
1061	17	3	0.3	0.3	30	130
1062	19	3	0.3	0.3	29	125
1063	21	3	0.3	0.3	28	119
1064	23	3	0.3	0.3	27	114
1065	25	3	0.3	0.3	26	109
1066	17	4	0.3	0.3	15	88
1067	19	4	0.3	0.3	15	87
1068	21	4	0.3	0.3	14	78
1069	23	4	0.3	0.3	14	77
1070	25	4	0.3	0.3	14	77
1071	17	5	0.3	0.3	9	64
1072	19	5	0.3	0.3	9	62
1073	21	5	0.3	0.3	9	61
1074	23	5	0.3	0.3	9	59
1075	25	5	0.3	0.3	9	58
1076	17	6	0.3	0.3	7	59
1077	19	6	0.3	0.3	7	56
1078	21	6	0.3	0.3	7	54
1079	23	6	0.3	0.3	8	63
1080	25	6	0.3	0.3	8	61
1081	17	7	0.3	0.3	6	58
1082	19	7	0.3	0.3	6	55
1083	21	7	0.3	0.3	7	65

1084	23	7	0.3	0.3	7	63
1085	25	7	0.3	0.3	7	61
1086	17	8	0.3	0.3	6	68
1087	19	8	0.3	0.3	6	65
1088	21	8	0.3	0.3	6	62
1089	23	8	0.3	0.3	6	59
1090	25	8	0.3	0.3	6	58
1091	17	9	0.3	0.3	5	61
1092	19	9	0.3	0.3	5	57
1093	21	9	0.3	0.3	6	71
1094	23	9	0.3	0.3	6	67
1095	25	9	0.3	0.3	6	66
1096	17	10	0.3	0.3	5	69
1097	19	10	0.3	0.3	5	65
1098	21	10	0.3	0.3	5	62
1099	23	10	0.3	0.3	5	59
1100	25	10	0.3	0.3	6	74
1101	17	1	0.35	0.3	0	0
1102	19	1	0.35	0.3	0	0
1103	21	1	0.35	0.3	83	200
1104	23	1	0.35	0.3	83	200
1105	25	1	0.35	0.3	84	200
1106	17	2	0.35	0.3	47	190
1107	19	2	0.35	0.3	45	179
1108	21	2	0.35	0.3	43	169
1109	23	2	0.35	0.3	41	161
1110	25	2	0.35	0.3	40	158
1111	17	3	0.35	0.3	24	143
1112	19	3	0.35	0.3	23	134
1113	21	3	0.35	0.3	22	126
1114	23	3	0.35	0.3	21	118
1115	25	3	0.35	0.3	20	115
1116	17	4	0.35	0.3	12	92
1117	19	4	0.35	0.3	12	89
1118	21	4	0.35	0.3	12	87
1119	23	4	0.35	0.3	12	85
1120	25	4	0.35	0.3	11	80
1121	17	5	0.35	0.3	8	72
1122	19	5	0.35	0.3	8	69
1123	21	5	0.35	0.3	9	77
1124	23	5	0.35	0.3	8	66
1125	25	5	0.35	0.3	8	68

1126	17	6	0.35	0.3	7	74
1127	19	6	0.35	0.3	7	70
1128	21	6	0.35	0.3	7	68
1129	23	6	0.35	0.3	7	66
1130	25	6	0.35	0.3	7	69
1131	17	7	0.35	0.3	6	71
1132	19	7	0.35	0.3	6	67
1133	21	7	0.35	0.3	6	64
1134	23	7	0.35	0.3	6	63
1135	25	7	0.35	0.3	6	66
1136	17	8	0.35	0.3	5	64
1137	19	8	0.35	0.3	6	77
1138	21	8	0.35	0.3	6	74
1139	23	8	0.35	0.3	6	72
1140	25	8	0.35	0.3	5	60
1141	17	9	0.35	0.3	5	72
1142	19	9	0.35	0.3	5	68
1143	21	9	0.35	0.3	5	65
1144	23	9	0.35	0.3	5	64
1145	25	9	0.35	0.3	5	67
1146	17	10	0.35	0.3	5	81
1147	19	10	0.35	0.3	5	77
1148	21	10	0.35	0.3	5	73
1149	23	10	0.35	0.3	5	71
1150	25	10	0.35	0.3	5	74
1151	17	1	0.4	0.3	51	200
1152	19	1	0.4	0.3	52	200
1153	21	1	0.4	0.3	54	200
1154	23	1	0.4	0.3	56	200
1155	25	1	0.4	0.3	35	200
1156	17	2	0.4	0.3	34	200
1157	19	2	0.4	0.3	35	200
1158	21	2	0.4	0.3	36	199
1159	23	2	0.4	0.3	33	187
1160	25	2	0.4	0.3	5	101
1161	17	3	0.4	0.3	19	154
1162	19	3	0.4	0.3	18	141
1163	21	3	0.4	0.3	17	130
1164	23	3	0.4	0.3	15	120
1165	25	3	0.4	0.3	4	153
1166	17	4	0.4	0.3	11	110
1167	19	4	0.4	0.3	10	95

1168	21	4	0.4	0.3	10	93
1169	23	4	0.4	0.3	9	89
1170	25	4	0.4	0.3	1	204
1171	17	5	0.4	0.3	8	92
1172	19	5	0.4	0.3	8	88
1173	21	5	0.4	0.3	8	86
1174	23	5	0.4	0.3	7	81
1175	25	5	0.4	0.3	1	256
1176	17	6	0.4	0.3	6	76
1177	19	6	0.4	0.3	7	88
1178	21	6	0.4	0.3	6	71
1179	23	6	0.4	0.3	6	79
1180	25	6	0.4	0.3	1	308
1181	17	7	0.4	0.3	6	87
1182	19	7	0.4	0.3	6	83
1183	21	7	0.4	0.3	6	81
1184	23	7	0.4	0.3	5	72
1185	25	7	0.4	0.3	1	360
1186	17	8	0.4	0.3	5	78
1187	19	8	0.4	0.3	5	74
1188	21	8	0.4	0.3	5	73
1189	23	8	0.4	0.3	5	80
1190	25	8	0.4	0.3	1	411
1191	17	9	0.4	0.3	5	88
1192	19	9	0.4	0.3	5	83
1193	21	9	0.4	0.3	5	81
1194	23	9	0.4	0.3	5	89
1195	25	9	0.4	0.3	1	463
1196	17	10	0.4	0.3	5	97
1197	19	10	0.4	0.3	5	91
1198	21	10	0.4	0.3	5	89
1199	23	10	0.4	0.3	5	97
1200	25	10	0.4	0.3	1	515
1201	17	1	0.25	0.35	0	0
1202	19	1	0.25	0.35	0	0
1203	21	1	0.25	0.35	0	0
1204	23	1	0.25	0.35	0	0
1205	25	1	0.25	0.35	0	0
1206	17	2	0.25	0.35	200	191
1207	19	2	0.25	0.35	101	200
1208	21	2	0.25	0.35	87	200
1209	23	2	0.25	0.35	73	200

1210	25	2	0.25	0.35	66	200
1211	17	3	0.25	0.35	39	158
1212	19	3	0.25	0.35	37	147
1213	21	3	0.25	0.35	35	137
1214	23	3	0.25	0.35	34	133
1215	25	3	0.25	0.35	32	123
1216	17	4	0.25	0.35	19	108
1217	19	4	0.25	0.35	18	100
1218	21	4	0.25	0.35	18	99
1219	23	4	0.25	0.35	17	91
1220	25	4	0.25	0.35	17	90
1221	17	5	0.25	0.35	11	80
1222	19	5	0.25	0.35	11	78
1223	21	5	0.25	0.35	11	76
1224	23	5	0.25	0.35	11	74
1225	25	5	0.25	0.35	11	73
1226	17	6	0.25	0.35	8	71
1227	19	6	0.25	0.35	8	68
1228	21	6	0.25	0.35	8	65
1229	23	6	0.25	0.35	8	63
1230	25	6	0.25	0.35	8	61
1231	17	7	0.25	0.35	6	59
1232	19	7	0.25	0.35	7	71
1233	21	7	0.25	0.35	7	67
1234	23	7	0.25	0.35	7	64
1235	25	7	0.25	0.35	7	62
1236	17	8	0.25	0.35	6	71
1237	19	8	0.25	0.35	6	68
1238	21	8	0.25	0.35	6	64
1239	23	8	0.25	0.35	6	61
1240	25	8	0.25	0.35	7	74
1241	17	9	0.25	0.35	5	64
1242	19	9	0.25	0.35	6	80
1243	21	9	0.25	0.35	6	75
1244	23	9	0.25	0.35	6	71
1245	25	9	0.25	0.35	6	68
1246	17	10	0.25	0.35	5	73
1247	19	10	0.25	0.35	5	69
1248	21	10	0.25	0.35	5	66
1249	23	10	0.25	0.35	6	82
1250	25	10	0.25	0.35	6	78
1251	17	1	0.3	0.35	0	0

1252	19	1	0.3	0.35	0	0
1253	21	1	0.3	0.35	0	0
1254	23	1	0.3	0.35	0	0
1255	25	1	0.3	0.35	99	200
1256	17	2	0.3	0.35	57	200
1257	19	2	0.3	0.35	55	200
1258	21	2	0.3	0.35	54	200
1259	23	2	0.3	0.35	51	184
1260	25	2	0.3	0.35	49	174
1261	17	3	0.3	0.35	30	168
1262	19	3	0.3	0.35	29	160
1263	21	3	0.3	0.35	28	152
1264	23	3	0.3	0.35	27	144
1265	25	3	0.3	0.35	26	136
1266	17	4	0.3	0.35	15	113
1267	19	4	0.3	0.35	15	111
1268	21	4	0.3	0.35	14	99
1269	23	4	0.3	0.35	14	97
1270	25	4	0.3	0.35	14	95
1271	17	5	0.3	0.35	9	83
1272	19	5	0.3	0.35	9	80
1273	21	5	0.3	0.35	9	77
1274	23	5	0.3	0.35	10	84
1275	25	5	0.3	0.35	10	82
1276	17	6	0.3	0.35	7	75
1277	19	6	0.3	0.35	7	72
1278	21	6	0.3	0.35	8	82
1279	23	6	0.3	0.35	8	78
1280	25	6	0.3	0.35	8	76
1281	17	7	0.3	0.35	6	74
1282	19	7	0.3	0.35	6	70
1283	21	7	0.3	0.35	7	82
1284	23	7	0.3	0.35	7	78
1285	25	7	0.3	0.35	7	75
1286	17	8	0.3	0.35	6	87
1287	19	8	0.3	0.35	6	82
1288	21	8	0.3	0.35	6	77
1289	23	8	0.3	0.35	6	74
1290	25	8	0.3	0.35	6	70
1291	17	9	0.3	0.35	5	77
1292	19	9	0.3	0.35	5	73
1293	21	9	0.3	0.35	6	89

1294	23	9	0.3	0.35	6	84
1295	25	9	0.3	0.35	6	80
1296	17	10	0.3	0.35	5	88
1297	19	10	0.3	0.35	5	82
1298	21	10	0.3	0.35	5	77
1299	23	10	0.3	0.35	5	73
1300	25	10	0.3	0.35	6	90
1301	17	1	0.35	0.35	0	0
1302	19	1	0.35	0.35	0	0
1303	21	1	0.35	0.35	61	200
1304	23	1	0.35	0.35	62	200
1305	25	1	0.35	0.35	62	200
1306	17	2	0.35	0.35	37	200
1307	19	2	0.35	0.35	38	200
1308	21	2	0.35	0.35	39	200
1309	23	2	0.35	0.35	40	200
1310	25	2	0.35	0.35	40	199
1311	17	3	0.35	0.35	24	188
1312	19	3	0.35	0.35	23	175
1313	21	3	0.35	0.35	22	162
1314	23	3	0.35	0.35	21	151
1315	25	3	0.35	0.35	20	143
1316	17	4	0.35	0.35	12	120
1317	19	4	0.35	0.35	12	115
1318	21	4	0.35	0.35	12	111
1319	23	4	0.35	0.35	12	108
1320	25	4	0.35	0.35	11	98
1321	17	5	0.35	0.35	8	94
1322	19	5	0.35	0.35	8	89
1323	21	5	0.35	0.35	9	98
1324	23	5	0.35	0.35	9	95
1325	25	5	0.35	0.35	8	83
1326	17	6	0.35	0.35	7	96
1327	19	6	0.35	0.35	7	91
1328	21	6	0.35	0.35	7	86
1329	23	6	0.35	0.35	7	82
1330	25	6	0.35	0.35	7	83
1331	17	7	0.35	0.35	6	92
1332	19	7	0.35	0.35	6	87
1333	21	7	0.35	0.35	6	82
1334	23	7	0.35	0.35	6	78
1335	25	7	0.35	0.35	6	79

1336	17	8	0.35	0.35	5	83
1337	19	8	0.35	0.35	6	99
1338	21	8	0.35	0.35	6	94
1339	23	8	0.35	0.35	6	89
1340	25	8	0.35	0.35	6	90
1341	17	9	0.35	0.35	5	94
1342	19	9	0.35	0.35	5	88
1343	21	9	0.35	0.35	5	83
1344	23	9	0.35	0.35	6	100
1345	25	9	0.35	0.35	5	80
1346	17	10	0.35	0.35	5	106
1347	19	10	0.35	0.35	5	98
1348	21	10	0.35	0.35	5	92
1349	23	10	0.35	0.35	5	88
1350	25	10	0.35	0.35	5	89
1351	17	1	0.4	0.35	35	200
1352	19	1	0.4	0.35	36	200
1353	21	1	0.4	0.35	37	200
1354	23	1	0.4	0.35	37	200
1355	25	1	0.4	0.35	27	200
1356	17	2	0.4	0.35	25	200
1357	19	2	0.4	0.35	26	200
1358	21	2	0.4	0.35	27	200
1359	23	2	0.4	0.35	27	200
1360	25	2	0.4	0.35	5	101
1361	17	3	0.4	0.35	19	200
1362	19	3	0.4	0.35	18	187
1363	21	3	0.4	0.35	17	170
1364	23	3	0.4	0.35	16	161
1365	25	3	0.4	0.35	4	153
1366	17	4	0.4	0.35	11	147
1367	19	4	0.4	0.35	10	125
1368	21	4	0.4	0.35	10	120
1369	23	4	0.4	0.35	10	122
1370	25	4	0.4	0.35	1	204
1371	17	5	0.4	0.35	8	124
1372	19	5	0.4	0.35	8	116
1373	21	5	0.4	0.35	8	111
1374	23	5	0.4	0.35	7	98
1375	25	5	0.4	0.35	1	256
1376	17	6	0.4	0.35	6	102
1377	19	6	0.4	0.35	7	115

1378	21	6	0.4	0.35	7	109
1379	23	6	0.4	0.35	6	96
1380	25	6	0.4	0.35	1	308
1381	17	7	0.4	0.35	6	117
1382	19	7	0.4	0.35	6	109
1383	21	7	0.4	0.35	6	103
1384	23	7	0.4	0.35	5	88
1385	25	7	0.4	0.35	1	360
1386	17	8	0.4	0.35	5	105
1387	19	8	0.4	0.35	5	97
1388	21	8	0.4	0.35	6	116
1389	23	8	0.4	0.35	5	98
1390	25	8	0.4	0.35	1	411
1391	17	9	0.4	0.35	5	117
1392	19	9	0.4	0.35	5	109
1393	21	9	0.4	0.35	5	102
1394	23	9	0.4	0.35	5	108
1395	25	9	0.4	0.35	1	463
1396	17	10	0.4	0.35	5	130
1397	19	10	0.4	0.35	5	120
1398	21	10	0.4	0.35	5	113
1399	23	10	0.4	0.35	5	119
1400	25	10	0.4	0.35	1	515

4. RESULT OF SIMULATION FOR NORMAL SPREADING LOAD

No of simulation	Angle of friction	Cohesion	Coefficient of earth pressure at rest	coefficient of residual friction	Number of elements	Final Load
	ϕ'	c'	K_0	K_r	No.	P
	°	kPa				%
1	17	1	0.25	0.05	0	0
2	19	1	0.25	0.05	0	0
3	21	1	0.25	0.05	0	0
4	23	1	0.25	0.05	0	0
5	25	1	0.25	0.05	0	0
6	17	2	0.25	0.05	200	2
7	19	2	0.25	0.05	200	2
8	21	2	0.25	0.05	200	3
9	23	2	0.25	0.05	200	4
10	25	2	0.25	0.05	200	7
11	17	3	0.25	0.05	200	101
12	19	3	0.25	0.05	168	200
13	21	3	0.25	0.05	143	200
14	23	3	0.25	0.05	132	200
15	25	3	0.25	0.05	126	200
16	17	4	0.25	0.05	99	200
17	19	4	0.25	0.05	98	200
18	21	4	0.25	0.05	98	200
19	23	4	0.25	0.05	97	200
20	25	4	0.25	0.05	93	200
21	17	5	0.25	0.05	83	200
22	19	5	0.25	0.05	82	200
23	21	5	0.25	0.05	81	200
24	23	5	0.25	0.05	81	200
25	25	5	0.25	0.05	80	200
26	17	6	0.25	0.05	76	200
27	19	6	0.25	0.05	74	200
28	21	6	0.25	0.05	71	200
29	23	6	0.25	0.05	69	200
30	25	6	0.25	0.05	67	200
31	17	7	0.25	0.05	64	200
32	19	7	0.25	0.05	63	200

33	21	7	0.25	0.05	62	200
34	23	7	0.25	0.05	60	200
35	25	7	0.25	0.05	60	200
36	17	8	0.25	0.05	59	200
37	19	8	0.25	0.05	58	200
38	21	8	0.25	0.05	56	200
39	23	8	0.25	0.05	55	200
40	25	8	0.25	0.05	54	200
41	17	9	0.25	0.05	54	200
42	19	9	0.25	0.05	52	200
43	21	9	0.25	0.05	52	200
44	23	9	0.25	0.05	51	200
45	25	9	0.25	0.05	50	200
46	17	10	0.25	0.05	50	200
47	19	10	0.25	0.05	49	200
48	21	10	0.25	0.05	48	200
49	23	10	0.25	0.05	48	200
50	25	10	0.25	0.05	47	200
51	17	1	0.3	0.05	0	0
52	19	1	0.3	0.05	0	0
53	21	1	0.3	0.05	0	0
54	23	1	0.3	0.05	0	0
55	25	1	0.3	0.05	200	3
56	17	2	0.3	0.05	200	8
57	19	2	0.3	0.05	200	19
58	21	2	0.3	0.05	200	38
59	23	2	0.3	0.05	200	70
60	25	2	0.3	0.05	200	123
61	17	3	0.3	0.05	117	200
62	19	3	0.3	0.05	109	200
63	21	3	0.3	0.05	102	200
64	23	3	0.3	0.05	97	200
65	25	3	0.3	0.05	92	200
66	17	4	0.3	0.05	83	200
67	19	4	0.3	0.05	81	200
68	21	4	0.3	0.05	79	200
69	23	4	0.3	0.05	73	200
70	25	4	0.3	0.05	69	200
71	17	5	0.3	0.05	67	200
72	19	5	0.3	0.05	64	200
73	21	5	0.3	0.05	62	200
74	23	5	0.3	0.05	60	200
75	25	5	0.3	0.05	58	200

76	17	6	0.3	0.05	58	200
77	19	6	0.3	0.05	56	200
78	21	6	0.3	0.05	54	200
79	23	6	0.3	0.05	52	200
80	25	6	0.3	0.05	50	200
81	17	7	0.3	0.05	52	200
82	19	7	0.3	0.05	50	200
83	21	7	0.3	0.05	49	200
84	23	7	0.3	0.05	48	200
85	25	7	0.3	0.05	46	200
86	17	8	0.3	0.05	48	200
87	19	8	0.3	0.05	47	200
88	21	8	0.3	0.05	46	200
89	23	8	0.3	0.05	45	200
90	25	8	0.3	0.05	43	200
91	17	9	0.3	0.05	45	200
92	19	9	0.3	0.05	44	200
93	21	9	0.3	0.05	43	200
94	23	9	0.3	0.05	42	200
95	25	9	0.3	0.05	41	200
96	17	10	0.3	0.05	43	200
97	19	10	0.3	0.05	42	200
98	21	10	0.3	0.05	41	200
99	23	10	0.3	0.05	41	200
100	25	10	0.3	0.05	37	200
101	17	1	0.35	0.05	0	0
102	19	1	0.35	0.05	0	0
103	21	1	0.35	0.05	200	68
104	23	1	0.35	0.05	200	196
105	25	1	0.35	0.05	111	200
106	17	2	0.35	0.05	98	200
107	19	2	0.35	0.05	87	200
108	21	2	0.35	0.05	76	200
109	23	2	0.35	0.05	64	200
110	25	2	0.35	0.05	54	200
111	17	3	0.35	0.05	64	200
112	19	3	0.35	0.05	58	200
113	21	3	0.35	0.05	53	200
114	23	3	0.35	0.05	47	200
115	25	3	0.35	0.05	40	200
116	17	4	0.35	0.05	51	200
117	19	4	0.35	0.05	48	200
118	21	4	0.35	0.05	44	200

119	23	4	0.35	0.05	40	200
120	25	4	0.35	0.05	35	200
121	17	5	0.35	0.05	46	200
122	19	5	0.35	0.05	42	200
123	21	5	0.35	0.05	37	200
124	23	5	0.35	0.05	35	200
125	25	5	0.35	0.05	32	200
126	17	6	0.35	0.05	41	200
127	19	6	0.35	0.05	37	200
128	21	6	0.35	0.05	35	200
129	23	6	0.35	0.05	32	200
130	25	6	0.35	0.05	26	200
131	17	7	0.35	0.05	37	200
132	19	7	0.35	0.05	35	200
133	21	7	0.35	0.05	33	200
134	23	7	0.35	0.05	30	200
135	25	7	0.35	0.05	26	200
136	17	8	0.35	0.05	35	200
137	19	8	0.35	0.05	33	200
138	21	8	0.35	0.05	32	200
139	23	8	0.35	0.05	26	200
140	25	8	0.35	0.05	21	200
141	17	9	0.35	0.05	33	200
142	19	9	0.35	0.05	32	200
143	21	9	0.35	0.05	30	200
144	23	9	0.35	0.05	26	200
145	25	9	0.35	0.05	21	200
146	17	10	0.35	0.05	32	200
147	19	10	0.35	0.05	30	200
148	21	10	0.35	0.05	26	200
149	23	10	0.35	0.05	25	200
150	25	10	0.35	0.05	8	200
151	17	1	0.4	0.05	5	200
152	19	1	0.4	0.05	5	200
153	21	1	0.4	0.05	4	200
154	23	1	0.4	0.05	1	200
155	25	1	0.4	0.05	1	200
156	17	2	0.4	0.05	5	200
157	19	2	0.4	0.05	4	200
158	21	2	0.4	0.05	4	200
159	23	2	0.4	0.05	1	200
160	25	2	0.4	0.05	1	205
161	17	3	0.4	0.05	5	200

162	19	3	0.4	0.05	4	200
163	21	3	0.4	0.05	4	200
164	23	3	0.4	0.05	1	200
165	25	3	0.4	0.05	1	310
166	17	4	0.4	0.05	5	200
167	19	4	0.4	0.05	4	200
168	21	4	0.4	0.05	4	200
169	23	4	0.4	0.05	1	200
170	25	4	0.4	0.05	1	415
171	17	5	0.4	0.05	5	200
172	19	5	0.4	0.05	4	200
173	21	5	0.4	0.05	4	200
174	23	5	0.4	0.05	1	200
175	25	5	0.4	0.05	1	520
176	17	6	0.4	0.05	5	200
177	19	6	0.4	0.05	4	200
178	21	6	0.4	0.05	4	200
179	23	6	0.4	0.05	1	200
180	25	6	0.4	0.05	1	625
181	17	7	0.4	0.05	4	200
182	19	7	0.4	0.05	4	200
183	21	7	0.4	0.05	4	200
184	23	7	0.4	0.05	1	200
185	25	7	0.4	0.05	1	730
186	17	8	0.4	0.05	4	200
187	19	8	0.4	0.05	4	200
188	21	8	0.4	0.05	4	200
189	23	8	0.4	0.05	1	200
190	25	8	0.4	0.05	1	835
191	17	9	0.4	0.05	4	200
192	19	9	0.4	0.05	4	200
193	21	9	0.4	0.05	4	200
194	23	9	0.4	0.05	1	200
195	25	9	0.4	0.05	1	940
196	17	10	0.4	0.05	4	200
197	19	10	0.4	0.05	4	200
198	21	10	0.4	0.05	4	200
199	23	10	0.4	0.05	1	200
200	25	10	0.4	0.05	1	1045
201	17	1	0.25	0.1	0	0
202	19	1	0.25	0.1	0	0
203	21	1	0.25	0.1	0	0
204	23	1	0.25	0.1	0	0

205	25	1	0.25	0.1	0	0
206	17	2	0.25	0.1	200	2
207	19	2	0.25	0.1	200	2
208	21	2	0.25	0.1	200	3
209	23	2	0.25	0.1	200	4
210	25	2	0.25	0.1	200	6
211	17	3	0.25	0.1	200	44
212	19	3	0.25	0.1	200	72
213	21	3	0.25	0.1	200	117
214	23	3	0.25	0.1	200	198
215	25	3	0.25	0.1	146	200
216	17	4	0.25	0.1	101	200
217	19	4	0.25	0.1	98	200
218	21	4	0.25	0.1	95	200
219	23	4	0.25	0.1	93	200
220	25	4	0.25	0.1	91	200
221	17	5	0.25	0.1	83	200
222	19	5	0.25	0.1	82	200
223	21	5	0.25	0.1	81	200
224	23	5	0.25	0.1	79	200
225	25	5	0.25	0.1	77	200
226	17	6	0.25	0.1	73	200
227	19	6	0.25	0.1	69	200
228	21	6	0.25	0.1	67	200
229	23	6	0.25	0.1	64	200
230	25	6	0.25	0.1	63	200
231	17	7	0.25	0.1	62	200
232	19	7	0.25	0.1	60	200
233	21	7	0.25	0.1	59	200
234	23	7	0.25	0.1	58	200
235	25	7	0.25	0.1	56	200
236	17	8	0.25	0.1	57	200
237	19	8	0.25	0.1	55	200
238	21	8	0.25	0.1	54	200
239	23	8	0.25	0.1	52	200
240	25	8	0.25	0.1	51	200
241	17	9	0.25	0.1	52	200
242	19	9	0.25	0.1	51	200
243	21	9	0.25	0.1	50	200
244	23	9	0.25	0.1	49	200
245	25	9	0.25	0.1	48	200
246	17	10	0.25	0.1	49	200
247	19	10	0.25	0.1	48	200

248	21	10	0.25	0.1	47	200
249	23	10	0.25	0.1	46	200
250	25	10	0.25	0.1	46	200
251	17	1	0.3	0.1	0	0
252	19	1	0.3	0.1	0	0
253	21	1	0.3	0.1	0	0
254	23	1	0.3	0.1	0	0
255	25	1	0.3	0.1	200	3
256	17	2	0.3	0.1	200	15
257	19	2	0.3	0.1	200	38
258	21	2	0.3	0.1	200	82
259	23	2	0.3	0.1	200	153
260	25	2	0.3	0.1	141	200
261	17	3	0.3	0.1	100	200
262	19	3	0.3	0.1	94	200
263	21	3	0.3	0.1	89	200
264	23	3	0.3	0.1	84	200
265	25	3	0.3	0.1	80	200
266	17	4	0.3	0.1	79	200
267	19	4	0.3	0.1	71	200
268	21	4	0.3	0.1	66	200
269	23	4	0.3	0.1	62	200
270	25	4	0.3	0.1	59	200
271	17	5	0.3	0.1	61	200
272	19	5	0.3	0.1	58	200
273	21	5	0.3	0.1	55	200
274	23	5	0.3	0.1	53	200
275	25	5	0.3	0.1	50	200
276	17	6	0.3	0.1	53	200
277	19	6	0.3	0.1	51	200
278	21	6	0.3	0.1	49	200
279	23	6	0.3	0.1	47	200
280	25	6	0.3	0.1	44	200
281	17	7	0.3	0.1	49	200
282	19	7	0.3	0.1	47	200
283	21	7	0.3	0.1	45	200
284	23	7	0.3	0.1	43	200
285	25	7	0.3	0.1	42	200
286	17	8	0.3	0.1	46	200
287	19	8	0.3	0.1	43	200
288	21	8	0.3	0.1	42	200
289	23	8	0.3	0.1	40	200
290	25	8	0.3	0.1	37	200

291	17	9	0.3	0.1	42	200
292	19	9	0.3	0.1	41	200
293	21	9	0.3	0.1	40	200
294	23	9	0.3	0.1	37	200
295	25	9	0.3	0.1	35	200
296	17	10	0.3	0.1	40	200
297	19	10	0.3	0.1	39	200
298	21	10	0.3	0.1	36	200
299	23	10	0.3	0.1	35	200
300	25	10	0.3	0.1	33	200
301	17	1	0.35	0.1	0	0
302	19	1	0.35	0.1	0	0
303	21	1	0.35	0.1	84	200
304	23	1	0.35	0.1	47	200
305	25	1	0.35	0.1	6	200
306	17	2	0.35	0.1	67	200
307	19	2	0.35	0.1	56	200
308	21	2	0.35	0.1	45	200
309	23	2	0.35	0.1	26	200
310	25	2	0.35	0.1	6	200
311	17	3	0.35	0.1	49	200
312	19	3	0.35	0.1	43	200
313	21	3	0.35	0.1	34	200
314	23	3	0.35	0.1	8	200
315	25	3	0.35	0.1	5	200
316	17	4	0.35	0.1	41	200
317	19	4	0.35	0.1	36	200
318	21	4	0.35	0.1	31	200
319	23	4	0.35	0.1	8	200
320	25	4	0.35	0.1	5	200
321	17	5	0.35	0.1	36	200
322	19	5	0.35	0.1	31	200
323	21	5	0.35	0.1	26	200
324	23	5	0.35	0.1	6	200
325	25	5	0.35	0.1	5	200
326	17	6	0.35	0.1	33	200
327	19	6	0.35	0.1	30	200
328	21	6	0.35	0.1	25	200
329	23	6	0.35	0.1	6	200
330	25	6	0.35	0.1	5	200
331	17	7	0.35	0.1	31	200
332	19	7	0.35	0.1	26	200
333	21	7	0.35	0.1	19	200

334	23	7	0.35	0.1	6	200
335	25	7	0.35	0.1	1	200
336	17	8	0.35	0.1	30	200
337	19	8	0.35	0.1	25	200
338	21	8	0.35	0.1	19	200
339	23	8	0.35	0.1	5	200
340	25	8	0.35	0.1	1	200
341	17	9	0.35	0.1	26	200
342	19	9	0.35	0.1	23	200
343	21	9	0.35	0.1	13	200
344	23	9	0.35	0.1	5	200
345	25	9	0.35	0.1	1	200
346	17	10	0.35	0.1	25	200
347	19	10	0.35	0.1	21	200
348	21	10	0.35	0.1	8	200
349	23	10	0.35	0.1	5	200
350	25	10	0.35	0.1	1	200
351	17	1	0.4	0.1	4	200
352	19	1	0.4	0.1	3	200
353	21	1	0.4	0.1	3	200
354	23	1	0.4	0.1	1	200
355	25	1	0.4	0.1	1	200
356	17	2	0.4	0.1	4	200
357	19	2	0.4	0.1	3	200
358	21	2	0.4	0.1	3	200
359	23	2	0.4	0.1	1	200
360	25	2	0.4	0.1	1	205
361	17	3	0.4	0.1	4	200
362	19	3	0.4	0.1	3	200
363	21	3	0.4	0.1	3	200
364	23	3	0.4	0.1	1	200
365	25	3	0.4	0.1	1	310
366	17	4	0.4	0.1	3	200
367	19	4	0.4	0.1	3	200
368	21	4	0.4	0.1	3	200
369	23	4	0.4	0.1	1	200
370	25	4	0.4	0.1	1	415
371	17	5	0.4	0.1	3	200
372	19	5	0.4	0.1	3	200
373	21	5	0.4	0.1	3	200
374	23	5	0.4	0.1	1	200
375	25	5	0.4	0.1	1	520
376	17	6	0.4	0.1	3	200

377	19	6	0.4	0.1	3	200
378	21	6	0.4	0.1	3	200
379	23	6	0.4	0.1	1	200
380	25	6	0.4	0.1	1	625
381	17	7	0.4	0.1	3	200
382	19	7	0.4	0.1	3	200
383	21	7	0.4	0.1	3	200
384	23	7	0.4	0.1	1	200
385	25	7	0.4	0.1	1	730
386	17	8	0.4	0.1	3	200
387	19	8	0.4	0.1	3	200
388	21	8	0.4	0.1	1	200
389	23	8	0.4	0.1	1	200
390	25	8	0.4	0.1	1	835
391	17	9	0.4	0.1	3	200
392	19	9	0.4	0.1	3	200
393	21	9	0.4	0.1	1	200
394	23	9	0.4	0.1	1	200
395	25	9	0.4	0.1	1	940
396	17	10	0.4	0.1	3	200
397	19	10	0.4	0.1	3	200
398	21	10	0.4	0.1	1	200
399	23	10	0.4	0.1	1	200
400	25	10	0.4	0.1	1	1045
401	17	1	0.25	0.15	0	0
402	19	1	0.25	0.15	0	0
403	21	1	0.25	0.15	0	0
404	23	1	0.25	0.15	0	0
405	25	1	0.25	0.15	0	0
406	17	2	0.25	0.15	200	2
407	19	2	0.25	0.15	200	2
408	21	2	0.25	0.15	200	3
409	23	2	0.25	0.15	200	4
410	25	2	0.25	0.15	200	7
411	17	3	0.25	0.15	200	39
412	19	3	0.25	0.15	200	69
413	21	3	0.25	0.15	200	114
414	23	3	0.25	0.15	200	180
415	25	3	0.25	0.15	135	200
416	17	4	0.25	0.15	98	200
417	19	4	0.25	0.15	94	200
418	21	4	0.25	0.15	91	200
419	23	4	0.25	0.15	89	200

420	25	4	0.25	0.15	86	200
421	17	5	0.25	0.15	82	200
422	19	5	0.25	0.15	80	200
423	21	5	0.25	0.15	79	200
424	23	5	0.25	0.15	73	200
425	25	5	0.25	0.15	69	200
426	17	6	0.25	0.15	68	200
427	19	6	0.25	0.15	65	200
428	21	6	0.25	0.15	63	200
429	23	6	0.25	0.15	61	200
430	25	6	0.25	0.15	59	200
431	17	7	0.25	0.15	60	200
432	19	7	0.25	0.15	58	200
433	21	7	0.25	0.15	56	200
434	23	7	0.25	0.15	54	200
435	25	7	0.25	0.15	53	200
436	17	8	0.25	0.15	54	200
437	19	8	0.25	0.15	53	200
438	21	8	0.25	0.15	51	200
439	23	8	0.25	0.15	50	200
440	25	8	0.25	0.15	49	200
441	17	9	0.25	0.15	50	200
442	19	9	0.25	0.15	49	200
443	21	9	0.25	0.15	48	200
444	23	9	0.25	0.15	47	200
445	25	9	0.25	0.15	46	200
446	17	10	0.25	0.15	47	200
447	19	10	0.25	0.15	46	200
448	21	10	0.25	0.15	46	200
449	23	10	0.25	0.15	44	200
450	25	10	0.25	0.15	43	200
451	17	1	0.3	0.15	0	0
452	19	1	0.3	0.15	0	0
453	21	1	0.3	0.15	0	0
454	23	1	0.3	0.15	0	0
455	25	1	0.3	0.15	200	22
456	17	2	0.3	0.15	200	58
457	19	2	0.3	0.15	200	134
458	21	2	0.3	0.15	127	200
459	23	2	0.3	0.15	102	200
460	25	2	0.3	0.15	89	200
461	17	3	0.3	0.15	87	200
462	19	3	0.3	0.15	82	200

463	21	3	0.3	0.15	72	200
464	23	3	0.3	0.15	65	200
465	25	3	0.3	0.15	58	200
466	17	4	0.3	0.15	64	200
467	19	4	0.3	0.15	61	200
468	21	4	0.3	0.15	56	200
469	23	4	0.3	0.15	52	200
470	25	4	0.3	0.15	48	200
471	17	5	0.3	0.15	54	200
472	19	5	0.3	0.15	51	200
473	21	5	0.3	0.15	48	200
474	23	5	0.3	0.15	45	200
475	25	5	0.3	0.15	41	200
476	17	6	0.3	0.15	48	200
477	19	6	0.3	0.15	47	200
478	21	6	0.3	0.15	44	200
479	23	6	0.3	0.15	41	200
480	25	6	0.3	0.15	37	200
481	17	7	0.3	0.15	44	200
482	19	7	0.3	0.15	43	200
483	21	7	0.3	0.15	40	200
484	23	7	0.3	0.15	37	200
485	25	7	0.3	0.15	34	200
486	17	8	0.3	0.15	42	200
487	19	8	0.3	0.15	40	200
488	21	8	0.3	0.15	37	200
489	23	8	0.3	0.15	34	200
490	25	8	0.3	0.15	33	200
491	17	9	0.3	0.15	40	200
492	19	9	0.3	0.15	37	200
493	21	9	0.3	0.15	34	200
494	23	9	0.3	0.15	33	200
495	25	9	0.3	0.15	31	200
496	17	10	0.3	0.15	37	200
497	19	10	0.3	0.15	34	200
498	21	10	0.3	0.15	33	200
499	23	10	0.3	0.15	31	200
500	25	10	0.3	0.15	30	200
501	17	1	0.35	0.15	0	0
502	19	1	0.35	0.15	0	0
503	21	1	0.35	0.15	5	200
504	23	1	0.35	0.15	4	200
505	25	1	0.35	0.15	1	200

506	17	2	0.35	0.15	39	200
507	19	2	0.35	0.15	13	200
508	21	2	0.35	0.15	5	200
509	23	2	0.35	0.15	4	200
510	25	2	0.35	0.15	1	200
511	17	3	0.35	0.15	32	200
512	19	3	0.35	0.15	7	200
513	21	3	0.35	0.15	5	200
514	23	3	0.35	0.15	4	200
515	25	3	0.35	0.15	1	200
516	17	4	0.35	0.15	27	200
517	19	4	0.35	0.15	6	200
518	21	4	0.35	0.15	5	200
519	23	4	0.35	0.15	4	200
520	25	4	0.35	0.15	1	200
521	17	5	0.35	0.15	26	200
522	19	5	0.35	0.15	5	200
523	21	5	0.35	0.15	4	200
524	23	5	0.35	0.15	4	200
525	25	5	0.35	0.15	1	200
526	17	6	0.35	0.15	22	200
527	19	6	0.35	0.15	5	200
528	21	6	0.35	0.15	4	200
529	23	6	0.35	0.15	4	200
530	25	6	0.35	0.15	1	200
531	17	7	0.35	0.15	17	200
532	19	7	0.35	0.15	5	200
533	21	7	0.35	0.15	4	200
534	23	7	0.35	0.15	4	200
535	25	7	0.35	0.15	1	200
536	17	8	0.35	0.15	16	200
537	19	8	0.35	0.15	5	200
538	21	8	0.35	0.15	4	200
539	23	8	0.35	0.15	4	200
540	25	8	0.35	0.15	1	200
541	17	9	0.35	0.15	12	200
542	19	9	0.35	0.15	5	200
543	21	9	0.35	0.15	4	200
544	23	9	0.35	0.15	4	200
545	25	9	0.35	0.15	1	200
546	17	10	0.35	0.15	7	200
547	19	10	0.35	0.15	5	200
548	21	10	0.35	0.15	4	200

549	23	10	0.35	0.15	3	200
550	25	10	0.35	0.15	1	200
551	17	1	0.4	0.15	3	200
552	19	1	0.4	0.15	3	200
553	21	1	0.4	0.15	1	200
554	23	1	0.4	0.15	1	200
555	25	1	0.4	0.15	1	200
556	17	2	0.4	0.15	3	200
557	19	2	0.4	0.15	2	200
558	21	2	0.4	0.15	1	200
559	23	2	0.4	0.15	1	200
560	25	2	0.4	0.15	1	205
561	17	3	0.4	0.15	3	200
562	19	3	0.4	0.15	2	200
563	21	3	0.4	0.15	1	200
564	23	3	0.4	0.15	1	200
565	25	3	0.4	0.15	1	310
566	17	4	0.4	0.15	3	200
567	19	4	0.4	0.15	2	200
568	21	4	0.4	0.15	1	200
569	23	4	0.4	0.15	1	200
570	25	4	0.4	0.15	1	415
571	17	5	0.4	0.15	3	200
572	19	5	0.4	0.15	2	200
573	21	5	0.4	0.15	1	200
574	23	5	0.4	0.15	1	200
575	25	5	0.4	0.15	1	520
576	17	6	0.4	0.15	3	200
577	19	6	0.4	0.15	2	200
578	21	6	0.4	0.15	1	200
579	23	6	0.4	0.15	1	200
580	25	6	0.4	0.15	1	625
581	17	7	0.4	0.15	3	200
582	19	7	0.4	0.15	2	200
583	21	7	0.4	0.15	1	200
584	23	7	0.4	0.15	1	200
585	25	7	0.4	0.15	1	730
586	17	8	0.4	0.15	3	200
587	19	8	0.4	0.15	2	200
588	21	8	0.4	0.15	1	200
589	23	8	0.4	0.15	1	200
590	25	8	0.4	0.15	1	835
591	17	9	0.4	0.15	3	200

592	19	9	0.4	0.15	2	200
593	21	9	0.4	0.15	1	200
594	23	9	0.4	0.15	1	200
595	25	9	0.4	0.15	1	940
596	17	10	0.4	0.15	2	200
597	19	10	0.4	0.15	2	200
598	21	10	0.4	0.15	1	200
599	23	10	0.4	0.15	1	200
600	25	10	0.4	0.15	1	1045
601	17	1	0.25	0.2	0	0
602	19	1	0.25	0.2	0	0
603	21	1	0.25	0.2	0	0
604	23	1	0.25	0.2	0	0
605	25	1	0.25	0.2	0	0
606	17	2	0.25	0.2	200	2
607	19	2	0.25	0.2	200	2
608	21	2	0.25	0.2	200	3
609	23	2	0.25	0.2	200	4
610	25	2	0.25	0.2	200	14
611	17	3	0.25	0.2	200	54
612	19	3	0.25	0.2	200	102
613	21	3	0.25	0.2	200	172
614	23	3	0.25	0.2	124	200
615	25	3	0.25	0.2	109	200
616	17	4	0.25	0.2	93	200
617	19	4	0.25	0.2	89	200
618	21	4	0.25	0.2	86	200
619	23	4	0.25	0.2	84	200
620	25	4	0.25	0.2	81	200
621	17	5	0.25	0.2	81	200
622	19	5	0.25	0.2	73	200
623	21	5	0.25	0.2	68	200
624	23	5	0.25	0.2	65	200
625	25	5	0.25	0.2	62	200
626	17	6	0.25	0.2	63	200
627	19	6	0.25	0.2	62	200
628	21	6	0.25	0.2	59	200
629	23	6	0.25	0.2	56	200
630	25	6	0.25	0.2	54	200
631	17	7	0.25	0.2	56	200
632	19	7	0.25	0.2	54	200
633	21	7	0.25	0.2	52	200
634	23	7	0.25	0.2	51	200

635	25	7	0.25	0.2	49	200
636	17	8	0.25	0.2	51	200
637	19	8	0.25	0.2	50	200
638	21	8	0.25	0.2	48	200
639	23	8	0.25	0.2	47	200
640	25	8	0.25	0.2	45	200
641	17	9	0.25	0.2	48	200
642	19	9	0.25	0.2	47	200
643	21	9	0.25	0.2	45	200
644	23	9	0.25	0.2	44	200
645	25	9	0.25	0.2	43	200
646	17	10	0.25	0.2	46	200
647	19	10	0.25	0.2	44	200
648	21	10	0.25	0.2	43	200
649	23	10	0.25	0.2	42	200
650	25	10	0.25	0.2	41	200
651	17	1	0.3	0.2	0	0
652	19	1	0.3	0.2	0	0
653	21	1	0.3	0.2	0	0
654	23	1	0.3	0.2	0	0
655	25	1	0.3	0.2	124	200
656	17	2	0.3	0.2	116	200
657	19	2	0.3	0.2	95	200
658	21	2	0.3	0.2	84	200
659	23	2	0.3	0.2	67	200
660	25	2	0.3	0.2	55	200
661	17	3	0.3	0.2	69	200
662	19	3	0.3	0.2	62	200
663	21	3	0.3	0.2	55	200
664	23	3	0.3	0.2	49	200
665	25	3	0.3	0.2	42	200
666	17	4	0.3	0.2	54	200
667	19	4	0.3	0.2	50	200
668	21	4	0.3	0.2	46	200
669	23	4	0.3	0.2	41	200
670	25	4	0.3	0.2	35	200
671	17	5	0.3	0.2	48	200
672	19	5	0.3	0.2	44	200
673	21	5	0.3	0.2	41	200
674	23	5	0.3	0.2	35	200
675	25	5	0.3	0.2	32	200
676	17	6	0.3	0.2	43	200
677	19	6	0.3	0.2	41	200

678	21	6	0.3	0.2	37	200
679	23	6	0.3	0.2	32	200
680	25	6	0.3	0.2	27	200
681	17	7	0.3	0.2	41	200
682	19	7	0.3	0.2	37	200
683	21	7	0.3	0.2	34	200
684	23	7	0.3	0.2	31	200
685	25	7	0.3	0.2	27	200
686	17	8	0.3	0.2	37	200
687	19	8	0.3	0.2	34	200
688	21	8	0.3	0.2	32	200
689	23	8	0.3	0.2	29	200
690	25	8	0.3	0.2	22	200
691	17	9	0.3	0.2	34	200
692	19	9	0.3	0.2	32	200
693	21	9	0.3	0.2	31	200
694	23	9	0.3	0.2	27	200
695	25	9	0.3	0.2	22	200
696	17	10	0.3	0.2	33	200
697	19	10	0.3	0.2	31	200
698	21	10	0.3	0.2	29	200
699	23	10	0.3	0.2	26	200
700	25	10	0.3	0.2	21	200
701	17	1	0.35	0.2	0	0
702	19	1	0.35	0.2	0	0
703	21	1	0.35	0.2	3	200
704	23	1	0.35	0.2	3	200
705	25	1	0.35	0.2	1	200
706	17	2	0.35	0.2	4	200
707	19	2	0.35	0.2	4	200
708	21	2	0.35	0.2	3	200
709	23	2	0.35	0.2	3	200
710	25	2	0.35	0.2	1	200
711	17	3	0.35	0.2	4	200
712	19	3	0.35	0.2	4	200
713	21	3	0.35	0.2	3	200
714	23	3	0.35	0.2	3	200
715	25	3	0.35	0.2	1	200
716	17	4	0.35	0.2	4	200
717	19	4	0.35	0.2	4	200
718	21	4	0.35	0.2	3	200
719	23	4	0.35	0.2	3	200
720	25	4	0.35	0.2	1	200

721	17	5	0.35	0.2	4	200
722	19	5	0.35	0.2	4	200
723	21	5	0.35	0.2	3	200
724	23	5	0.35	0.2	3	200
725	25	5	0.35	0.2	1	200
726	17	6	0.35	0.2	4	200
727	19	6	0.35	0.2	3	200
728	21	6	0.35	0.2	3	200
729	23	6	0.35	0.2	3	200
730	25	6	0.35	0.2	1	200
731	17	7	0.35	0.2	4	200
732	19	7	0.35	0.2	3	200
733	21	7	0.35	0.2	3	200
734	23	7	0.35	0.2	2	200
735	25	7	0.35	0.2	1	200
736	17	8	0.35	0.2	4	200
737	19	8	0.35	0.2	3	200
738	21	8	0.35	0.2	3	200
739	23	8	0.35	0.2	2	200
740	25	8	0.35	0.2	1	200
741	17	9	0.35	0.2	4	200
742	19	9	0.35	0.2	3	200
743	21	9	0.35	0.2	3	200
744	23	9	0.35	0.2	1	200
745	25	9	0.35	0.2	1	200
746	17	10	0.35	0.2	4	200
747	19	10	0.35	0.2	3	200
748	21	10	0.35	0.2	3	200
749	23	10	0.35	0.2	1	200
750	25	10	0.35	0.2	1	200
751	17	1	0.4	0.2	2	200
752	19	1	0.4	0.2	2	200
753	21	1	0.4	0.2	1	200
754	23	1	0.4	0.2	1	200
755	25	1	0.4	0.2	1	200
756	17	2	0.4	0.2	2	200
757	19	2	0.4	0.2	2	200
758	21	2	0.4	0.2	1	200
759	23	2	0.4	0.2	1	200
760	25	2	0.4	0.2	1	205
761	17	3	0.4	0.2	2	200
762	19	3	0.4	0.2	2	200
763	21	3	0.4	0.2	1	200

764	23	3	0.4	0.2	1	200
765	25	3	0.4	0.2	1	310
766	17	4	0.4	0.2	2	200
767	19	4	0.4	0.2	2	200
768	21	4	0.4	0.2	1	200
769	23	4	0.4	0.2	1	200
770	25	4	0.4	0.2	1	415
771	17	5	0.4	0.2	2	200
772	19	5	0.4	0.2	2	200
773	21	5	0.4	0.2	1	200
774	23	5	0.4	0.2	1	200
775	25	5	0.4	0.2	1	520
776	17	6	0.4	0.2	2	200
777	19	6	0.4	0.2	2	200
778	21	6	0.4	0.2	1	200
779	23	6	0.4	0.2	1	200
780	25	6	0.4	0.2	1	625
781	17	7	0.4	0.2	2	200
782	19	7	0.4	0.2	2	200
783	21	7	0.4	0.2	1	200
784	23	7	0.4	0.2	1	200
785	25	7	0.4	0.2	1	730
786	17	8	0.4	0.2	2	200
787	19	8	0.4	0.2	1	200
788	21	8	0.4	0.2	1	200
789	23	8	0.4	0.2	1	200
790	25	8	0.4	0.2	1	835
791	17	9	0.4	0.2	2	200
792	19	9	0.4	0.2	1	200
793	21	9	0.4	0.2	1	200
794	23	9	0.4	0.2	1	200
795	25	9	0.4	0.2	1	940
796	17	10	0.4	0.2	2	200
797	19	10	0.4	0.2	1	200
798	21	10	0.4	0.2	1	200
799	23	10	0.4	0.2	1	200
800	25	10	0.4	0.2	1	1045
801	17	1	0.25	0.25	0	0
802	19	1	0.25	0.25	0	0
803	21	1	0.25	0.25	0	0
804	23	1	0.25	0.25	0	0
805	25	1	0.25	0.25	0	0
806	17	2	0.25	0.25	200	2

807	19	2	0.25	0.25	200	3
808	21	2	0.25	0.25	200	3
809	23	2	0.25	0.25	200	18
810	25	2	0.25	0.25	200	56
811	17	3	0.25	0.25	200	113
812	19	3	0.25	0.25	140	200
813	21	3	0.25	0.25	108	200
814	23	3	0.25	0.25	97	200
815	25	3	0.25	0.25	90	200
816	17	4	0.25	0.25	87	200
817	19	4	0.25	0.25	85	200
818	21	4	0.25	0.25	79	200
819	23	4	0.25	0.25	71	200
820	25	4	0.25	0.25	66	200
821	17	5	0.25	0.25	69	200
822	19	5	0.25	0.25	65	200
823	21	5	0.25	0.25	62	200
824	23	5	0.25	0.25	58	200
825	25	5	0.25	0.25	55	200
826	17	6	0.25	0.25	59	200
827	19	6	0.25	0.25	56	200
828	21	6	0.25	0.25	53	200
829	23	6	0.25	0.25	51	200
830	25	6	0.25	0.25	49	200
831	17	7	0.25	0.25	52	200
832	19	7	0.25	0.25	51	200
833	21	7	0.25	0.25	49	200
834	23	7	0.25	0.25	47	200
835	25	7	0.25	0.25	45	200
836	17	8	0.25	0.25	49	200
837	19	8	0.25	0.25	47	200
838	21	8	0.25	0.25	45	200
839	23	8	0.25	0.25	44	200
840	25	8	0.25	0.25	42	200
841	17	9	0.25	0.25	46	200
842	19	9	0.25	0.25	44	200
843	21	9	0.25	0.25	43	200
844	23	9	0.25	0.25	41	200
845	25	9	0.25	0.25	39	200
846	17	10	0.25	0.25	44	200
847	19	10	0.25	0.25	42	200
848	21	10	0.25	0.25	41	200
849	23	10	0.25	0.25	38	200

850	25	10	0.25	0.25	37	200
851	17	1	0.3	0.25	0	0
852	19	1	0.3	0.25	0	0
853	21	1	0.3	0.25	0	0
854	23	1	0.3	0.25	0	0
855	25	1	0.3	0.25	7	200
856	17	2	0.3	0.25	78	200
857	19	2	0.3	0.25	62	200
858	21	2	0.3	0.25	51	200
859	23	2	0.3	0.25	39	200
860	25	2	0.3	0.25	6	200
861	17	3	0.3	0.25	53	200
862	19	3	0.3	0.25	47	200
863	21	3	0.3	0.25	39	200
864	23	3	0.3	0.25	32	200
865	25	3	0.3	0.25	5	200
866	17	4	0.3	0.25	45	200
867	19	4	0.3	0.25	40	200
868	21	4	0.3	0.25	35	200
869	23	4	0.3	0.25	25	200
870	25	4	0.3	0.25	5	200
871	17	5	0.3	0.25	40	200
872	19	5	0.3	0.25	35	200
873	21	5	0.3	0.25	32	200
874	23	5	0.3	0.25	20	200
875	25	5	0.3	0.25	5	200
876	17	6	0.3	0.25	36	200
877	19	6	0.3	0.25	32	200
878	21	6	0.3	0.25	27	200
879	23	6	0.3	0.25	19	200
880	25	6	0.3	0.25	5	200
881	17	7	0.3	0.25	33	200
882	19	7	0.3	0.25	30	200
883	21	7	0.3	0.25	25	200
884	23	7	0.3	0.25	7	200
885	25	7	0.3	0.25	5	200
886	17	8	0.3	0.25	32	200
887	19	8	0.3	0.25	28	200
888	21	8	0.3	0.25	22	200
889	23	8	0.3	0.25	6	200
890	25	8	0.3	0.25	4	200
891	17	9	0.3	0.25	30	200
892	19	9	0.3	0.25	25	200

893	21	9	0.3	0.25	21	200
894	23	9	0.3	0.25	5	200
895	25	9	0.3	0.25	4	200
896	17	10	0.3	0.25	28	200
897	19	10	0.3	0.25	24	200
898	21	10	0.3	0.25	19	200
899	23	10	0.3	0.25	5	200
900	25	10	0.3	0.25	4	200
901	17	1	0.35	0.25	0	0
902	19	1	0.35	0.25	0	0
903	21	1	0.35	0.25	2	200
904	23	1	0.35	0.25	2	200
905	25	1	0.35	0.25	1	200
906	17	2	0.35	0.25	3	200
907	19	2	0.35	0.25	3	200
908	21	2	0.35	0.25	2	200
909	23	2	0.35	0.25	1	200
910	25	2	0.35	0.25	1	200
911	17	3	0.35	0.25	3	200
912	19	3	0.35	0.25	3	200
913	21	3	0.35	0.25	2	200
914	23	3	0.35	0.25	1	200
915	25	3	0.35	0.25	1	200
916	17	4	0.35	0.25	3	200
917	19	4	0.35	0.25	3	200
918	21	4	0.35	0.25	2	200
919	23	4	0.35	0.25	1	200
920	25	4	0.35	0.25	1	200
921	17	5	0.35	0.25	3	200
922	19	5	0.35	0.25	3	200
923	21	5	0.35	0.25	2	200
924	23	5	0.35	0.25	1	200
925	25	5	0.35	0.25	1	200
926	17	6	0.35	0.25	3	200
927	19	6	0.35	0.25	3	200
928	21	6	0.35	0.25	2	200
929	23	6	0.35	0.25	1	200
930	25	6	0.35	0.25	1	200
931	17	7	0.35	0.25	3	200
932	19	7	0.35	0.25	3	200
933	21	7	0.35	0.25	2	200
934	23	7	0.35	0.25	1	200
935	25	7	0.35	0.25	1	200

936	17	8	0.35	0.25	3	200
937	19	8	0.35	0.25	3	200
938	21	8	0.35	0.25	2	200
939	23	8	0.35	0.25	1	200
940	25	8	0.35	0.25	1	200
941	17	9	0.35	0.25	3	200
942	19	9	0.35	0.25	2	200
943	21	9	0.35	0.25	2	200
944	23	9	0.35	0.25	1	200
945	25	9	0.35	0.25	1	200
946	17	10	0.35	0.25	3	200
947	19	10	0.35	0.25	2	200
948	21	10	0.35	0.25	2	200
949	23	10	0.35	0.25	1	200
950	25	10	0.35	0.25	1	200
951	17	1	0.4	0.25	2	200
952	19	1	0.4	0.25	1	200
953	21	1	0.4	0.25	1	200
954	23	1	0.4	0.25	1	200
955	25	1	0.4	0.25	1	200
956	17	2	0.4	0.25	2	200
957	19	2	0.4	0.25	1	200
958	21	2	0.4	0.25	1	200
959	23	2	0.4	0.25	1	200
960	25	2	0.4	0.25	1	205
961	17	3	0.4	0.25	2	200
962	19	3	0.4	0.25	1	200
963	21	3	0.4	0.25	1	200
964	23	3	0.4	0.25	1	200
965	25	3	0.4	0.25	1	310
966	17	4	0.4	0.25	2	200
967	19	4	0.4	0.25	1	200
968	21	4	0.4	0.25	1	200
969	23	4	0.4	0.25	1	200
970	25	4	0.4	0.25	1	415
971	17	5	0.4	0.25	2	200
972	19	5	0.4	0.25	1	200
973	21	5	0.4	0.25	1	200
974	23	5	0.4	0.25	1	200
975	25	5	0.4	0.25	1	520
976	17	6	0.4	0.25	2	200
977	19	6	0.4	0.25	1	200
978	21	6	0.4	0.25	1	200

979	23	6	0.4	0.25	1	200
980	25	6	0.4	0.25	1	625
981	17	7	0.4	0.25	2	200
982	19	7	0.4	0.25	1	200
983	21	7	0.4	0.25	1	200
984	23	7	0.4	0.25	1	200
985	25	7	0.4	0.25	1	730
986	17	8	0.4	0.25	2	200
987	19	8	0.4	0.25	1	200
988	21	8	0.4	0.25	1	200
989	23	8	0.4	0.25	1	200
990	25	8	0.4	0.25	1	835
991	17	9	0.4	0.25	2	200
992	19	9	0.4	0.25	1	200
993	21	9	0.4	0.25	1	200
994	23	9	0.4	0.25	1	200
995	25	9	0.4	0.25	1	940
996	17	10	0.4	0.25	2	200
997	19	10	0.4	0.25	1	200
998	21	10	0.4	0.25	1	200
999	23	10	0.4	0.25	1	200
1000	25	10	0.4	0.25	1	1045
1001	17	1	0.25	0.3	0	0
1002	19	1	0.25	0.3	0	0
1003	21	1	0.25	0.3	0	0
1004	23	1	0.25	0.3	0	0
1005	25	1	0.25	0.3	0	0
1006	17	2	0.25	0.3	200	3
1007	19	2	0.25	0.3	200	4
1008	21	2	0.25	0.3	200	33
1009	23	2	0.25	0.3	200	101
1010	25	2	0.25	0.3	131	200
1011	17	3	0.25	0.3	109	200
1012	19	3	0.25	0.3	97	200
1013	21	3	0.25	0.3	90	200
1014	23	3	0.25	0.3	85	200
1015	25	3	0.25	0.3	70	200
1016	17	4	0.25	0.3	84	200
1017	19	4	0.25	0.3	71	200
1018	21	4	0.25	0.3	65	200
1019	23	4	0.25	0.3	59	200
1020	25	4	0.25	0.3	55	200
1021	17	5	0.25	0.3	63	200

1022	19	5	0.25	0.3	57	200
1023	21	5	0.25	0.3	54	200
1024	23	5	0.25	0.3	51	200
1025	25	5	0.25	0.3	49	200
1026	17	6	0.25	0.3	53	200
1027	19	6	0.25	0.3	51	200
1028	21	6	0.25	0.3	49	200
1029	23	6	0.25	0.3	46	200
1030	25	6	0.25	0.3	43	200
1031	17	7	0.25	0.3	49	200
1032	19	7	0.25	0.3	47	200
1033	21	7	0.25	0.3	45	200
1034	23	7	0.25	0.3	43	200
1035	25	7	0.25	0.3	39	200
1036	17	8	0.25	0.3	46	200
1037	19	8	0.25	0.3	44	200
1038	21	8	0.25	0.3	42	200
1039	23	8	0.25	0.3	39	200
1040	25	8	0.25	0.3	37	200
1041	17	9	0.25	0.3	43	200
1042	19	9	0.25	0.3	42	200
1043	21	9	0.25	0.3	39	200
1044	23	9	0.25	0.3	37	200
1045	25	9	0.25	0.3	35	200
1046	17	10	0.25	0.3	41	200
1047	19	10	0.25	0.3	39	200
1048	21	10	0.25	0.3	37	200
1049	23	10	0.25	0.3	35	200
1050	25	10	0.25	0.3	33	200
1051	17	1	0.3	0.3	0	0
1052	19	1	0.3	0.3	0	0
1053	21	1	0.3	0.3	0	0
1054	23	1	0.3	0.3	0	0
1055	25	1	0.3	0.3	3	200
1056	17	2	0.3	0.3	49	200
1057	19	2	0.3	0.3	37	200
1058	21	2	0.3	0.3	6	200
1059	23	2	0.3	0.3	4	200
1060	25	2	0.3	0.3	3	200
1061	17	3	0.3	0.3	39	200
1062	19	3	0.3	0.3	30	200
1063	21	3	0.3	0.3	5	200
1064	23	3	0.3	0.3	4	200

1065	25	3	0.3	0.3	3	200
1066	17	4	0.3	0.3	33	200
1067	19	4	0.3	0.3	27	200
1068	21	4	0.3	0.3	5	200
1069	23	4	0.3	0.3	4	200
1070	25	4	0.3	0.3	3	200
1071	17	5	0.3	0.3	30	200
1072	19	5	0.3	0.3	22	200
1073	21	5	0.3	0.3	5	200
1074	23	5	0.3	0.3	4	200
1075	25	5	0.3	0.3	3	200
1076	17	6	0.3	0.3	27	200
1077	19	6	0.3	0.3	18	200
1078	21	6	0.3	0.3	4	200
1079	23	6	0.3	0.3	4	200
1080	25	6	0.3	0.3	3	200
1081	17	7	0.3	0.3	25	200
1082	19	7	0.3	0.3	15	200
1083	21	7	0.3	0.3	4	200
1084	23	7	0.3	0.3	3	200
1085	25	7	0.3	0.3	3	200
1086	17	8	0.3	0.3	23	200
1087	19	8	0.3	0.3	7	200
1088	21	8	0.3	0.3	4	200
1089	23	8	0.3	0.3	3	200
1090	25	8	0.3	0.3	3	200
1091	17	9	0.3	0.3	22	200
1092	19	9	0.3	0.3	6	200
1093	21	9	0.3	0.3	4	200
1094	23	9	0.3	0.3	3	200
1095	25	9	0.3	0.3	3	200
1096	17	10	0.3	0.3	20	200
1097	19	10	0.3	0.3	5	200
1098	21	10	0.3	0.3	4	200
1099	23	10	0.3	0.3	3	200
1100	25	10	0.3	0.3	3	200
1101	17	1	0.35	0.3	0	0
1102	19	1	0.35	0.3	0	0
1103	21	1	0.35	0.3	2	200
1104	23	1	0.35	0.3	1	200
1105	25	1	0.35	0.3	1	200
1106	17	2	0.35	0.3	3	200
1107	19	2	0.35	0.3	2	200

1108	21	2	0.35	0.3	2	200
1109	23	2	0.35	0.3	1	200
1110	25	2	0.35	0.3	1	200
1111	17	3	0.35	0.3	2	200
1112	19	3	0.35	0.3	2	200
1113	21	3	0.35	0.3	2	200
1114	23	3	0.35	0.3	1	200
1115	25	3	0.35	0.3	1	200
1116	17	4	0.35	0.3	2	200
1117	19	4	0.35	0.3	2	200
1118	21	4	0.35	0.3	2	200
1119	23	4	0.35	0.3	1	200
1120	25	4	0.35	0.3	1	200
1121	17	5	0.35	0.3	2	200
1122	19	5	0.35	0.3	2	200
1123	21	5	0.35	0.3	2	200
1124	23	5	0.35	0.3	1	200
1125	25	5	0.35	0.3	1	200
1126	17	6	0.35	0.3	2	200
1127	19	6	0.35	0.3	2	200
1128	21	6	0.35	0.3	2	200
1129	23	6	0.35	0.3	1	200
1130	25	6	0.35	0.3	1	200
1131	17	7	0.35	0.3	2	200
1132	19	7	0.35	0.3	2	200
1133	21	7	0.35	0.3	2	200
1134	23	7	0.35	0.3	1	200
1135	25	7	0.35	0.3	1	200
1136	17	8	0.35	0.3	2	200
1137	19	8	0.35	0.3	2	200
1138	21	8	0.35	0.3	2	200
1139	23	8	0.35	0.3	1	200
1140	25	8	0.35	0.3	1	200
1141	17	9	0.35	0.3	2	200
1142	19	9	0.35	0.3	2	200
1143	21	9	0.35	0.3	1	200
1144	23	9	0.35	0.3	1	200
1145	25	9	0.35	0.3	1	200
1146	17	10	0.35	0.3	2	200
1147	19	10	0.35	0.3	2	200
1148	21	10	0.35	0.3	1	200
1149	23	10	0.35	0.3	1	200
1150	25	10	0.35	0.3	1	200

1151	17	1	0.4	0.3	2	200
1152	19	1	0.4	0.3	1	200
1153	21	1	0.4	0.3	1	200
1154	23	1	0.4	0.3	1	200
1155	25	1	0.4	0.3	1	200
1156	17	2	0.4	0.3	2	200
1157	19	2	0.4	0.3	1	200
1158	21	2	0.4	0.3	1	200
1159	23	2	0.4	0.3	1	200
1160	25	2	0.4	0.3	1	205
1161	17	3	0.4	0.3	2	200
1162	19	3	0.4	0.3	1	200
1163	21	3	0.4	0.3	1	200
1164	23	3	0.4	0.3	1	200
1165	25	3	0.4	0.3	1	310
1166	17	4	0.4	0.3	2	200
1167	19	4	0.4	0.3	1	200
1168	21	4	0.4	0.3	1	200
1169	23	4	0.4	0.3	1	200
1170	25	4	0.4	0.3	1	415
1171	17	5	0.4	0.3	2	200
1172	19	5	0.4	0.3	1	200
1173	21	5	0.4	0.3	1	200
1174	23	5	0.4	0.3	1	200
1175	25	5	0.4	0.3	1	520
1176	17	6	0.4	0.3	1	200
1177	19	6	0.4	0.3	1	200
1178	21	6	0.4	0.3	1	200
1179	23	6	0.4	0.3	1	200
1180	25	6	0.4	0.3	1	625
1181	17	7	0.4	0.3	1	200
1182	19	7	0.4	0.3	1	200
1183	21	7	0.4	0.3	1	200
1184	23	7	0.4	0.3	1	200
1185	25	7	0.4	0.3	1	730
1186	17	8	0.4	0.3	1	200
1187	19	8	0.4	0.3	1	200
1188	21	8	0.4	0.3	1	200
1189	23	8	0.4	0.3	1	200
1190	25	8	0.4	0.3	1	835
1191	17	9	0.4	0.3	1	200
1192	19	9	0.4	0.3	1	200
1193	21	9	0.4	0.3	1	200

1194	23	9	0.4	0.3	1	200
1195	25	9	0.4	0.3	1	940
1196	17	10	0.4	0.3	1	200
1197	19	10	0.4	0.3	1	200
1198	21	10	0.4	0.3	1	200
1199	23	10	0.4	0.3	1	200
1200	25	10	0.4	0.3	1	1045
1201	17	1	0.25	0.35	0	0
1202	19	1	0.25	0.35	0	0
1203	21	1	0.25	0.35	0	0
1204	23	1	0.25	0.35	0	0
1205	25	1	0.25	0.35	0	0
1206	17	2	0.25	0.35	200	5
1207	19	2	0.25	0.35	200	67
1208	21	2	0.25	0.35	138	200
1209	23	2	0.25	0.35	98	200
1210	25	2	0.25	0.35	80	200
1211	17	3	0.25	0.35	92	200
1212	19	3	0.25	0.35	87	200
1213	21	3	0.25	0.35	70	200
1214	23	3	0.25	0.35	61	200
1215	25	3	0.25	0.35	54	200
1216	17	4	0.25	0.35	66	200
1217	19	4	0.25	0.35	59	200
1218	21	4	0.25	0.35	54	200
1219	23	4	0.25	0.35	50	200
1220	25	4	0.25	0.35	46	200
1221	17	5	0.25	0.35	54	200
1222	19	5	0.25	0.35	51	200
1223	21	5	0.25	0.35	48	200
1224	23	5	0.25	0.35	44	200
1225	25	5	0.25	0.35	40	200
1226	17	6	0.25	0.35	49	200
1227	19	6	0.25	0.35	46	200
1228	21	6	0.25	0.35	44	200
1229	23	6	0.25	0.35	40	200
1230	25	6	0.25	0.35	36	200
1231	17	7	0.25	0.35	45	200
1232	19	7	0.25	0.35	43	200
1233	21	7	0.25	0.35	40	200
1234	23	7	0.25	0.35	37	200
1235	25	7	0.25	0.35	33	200
1236	17	8	0.25	0.35	43	200

1237	19	8	0.25	0.35	40	200
1238	21	8	0.25	0.35	37	200
1239	23	8	0.25	0.35	34	200
1240	25	8	0.25	0.35	31	200
1241	17	9	0.25	0.35	40	200
1242	19	9	0.25	0.35	37	200
1243	21	9	0.25	0.35	35	200
1244	23	9	0.25	0.35	33	200
1245	25	9	0.25	0.35	30	200
1246	17	10	0.25	0.35	38	200
1247	19	10	0.25	0.35	36	200
1248	21	10	0.25	0.35	33	200
1249	23	10	0.25	0.35	30	200
1250	25	10	0.25	0.35	28	200
1251	17	1	0.3	0.35	0	0
1252	19	1	0.3	0.35	0	0
1253	21	1	0.3	0.35	0	0
1254	23	1	0.3	0.35	0	0
1255	25	1	0.3	0.35	2	200
1256	17	2	0.3	0.35	20	200
1257	19	2	0.3	0.35	4	200
1258	21	2	0.3	0.35	3	200
1259	23	2	0.3	0.35	3	200
1260	25	2	0.3	0.35	2	200
1261	17	3	0.3	0.35	8	200
1262	19	3	0.3	0.35	4	200
1263	21	3	0.3	0.35	3	200
1264	23	3	0.3	0.35	3	200
1265	25	3	0.3	0.35	2	200
1266	17	4	0.3	0.35	6	200
1267	19	4	0.3	0.35	4	200
1268	21	4	0.3	0.35	3	200
1269	23	4	0.3	0.35	3	200
1270	25	4	0.3	0.35	2	200
1271	17	5	0.3	0.35	5	200
1272	19	5	0.3	0.35	4	200
1273	21	5	0.3	0.35	3	200
1274	23	5	0.3	0.35	3	200
1275	25	5	0.3	0.35	2	200
1276	17	6	0.3	0.35	5	200
1277	19	6	0.3	0.35	4	200
1278	21	6	0.3	0.35	3	200
1279	23	6	0.3	0.35	3	200

1280	25	6	0.3	0.35	2	200
1281	17	7	0.3	0.35	4	200
1282	19	7	0.3	0.35	3	200
1283	21	7	0.3	0.35	3	200
1284	23	7	0.3	0.35	2	200
1285	25	7	0.3	0.35	2	200
1286	17	8	0.3	0.35	4	200
1287	19	8	0.3	0.35	3	200
1288	21	8	0.3	0.35	3	200
1289	23	8	0.3	0.35	2	200
1290	25	8	0.3	0.35	1	200
1291	17	9	0.3	0.35	4	200
1292	19	9	0.3	0.35	3	200
1293	21	9	0.3	0.35	3	200
1294	23	9	0.3	0.35	2	200
1295	25	9	0.3	0.35	1	200
1296	17	10	0.3	0.35	4	200
1297	19	10	0.3	0.35	3	200
1298	21	10	0.3	0.35	3	200
1299	23	10	0.3	0.35	2	200
1300	25	10	0.3	0.35	1	200
1301	17	1	0.35	0.35	0	0
1302	19	1	0.35	0.35	0	0
1303	21	1	0.35	0.35	2	200
1304	23	1	0.35	0.35	1	200
1305	25	1	0.35	0.35	1	200
1306	17	2	0.35	0.35	2	200
1307	19	2	0.35	0.35	2	200
1308	21	2	0.35	0.35	1	200
1309	23	2	0.35	0.35	1	200
1310	25	2	0.35	0.35	1	200
1311	17	3	0.35	0.35	2	200
1312	19	3	0.35	0.35	2	200
1313	21	3	0.35	0.35	1	200
1314	23	3	0.35	0.35	1	200
1315	25	3	0.35	0.35	1	200
1316	17	4	0.35	0.35	2	200
1317	19	4	0.35	0.35	2	200
1318	21	4	0.35	0.35	1	200
1319	23	4	0.35	0.35	1	200
1320	25	4	0.35	0.35	1	200
1321	17	5	0.35	0.35	2	200
1322	19	5	0.35	0.35	2	200

1323	21	5	0.35	0.35	1	200
1324	23	5	0.35	0.35	1	200
1325	25	5	0.35	0.35	1	200
1326	17	6	0.35	0.35	2	200
1327	19	6	0.35	0.35	2	200
1328	21	6	0.35	0.35	1	200
1329	23	6	0.35	0.35	1	200
1330	25	6	0.35	0.35	1	200
1331	17	7	0.35	0.35	2	200
1332	19	7	0.35	0.35	2	200
1333	21	7	0.35	0.35	1	200
1334	23	7	0.35	0.35	1	200
1335	25	7	0.35	0.35	1	200
1336	17	8	0.35	0.35	2	200
1337	19	8	0.35	0.35	2	200
1338	21	8	0.35	0.35	1	200
1339	23	8	0.35	0.35	1	200
1340	25	8	0.35	0.35	1	200
1341	17	9	0.35	0.35	2	200
1342	19	9	0.35	0.35	2	200
1343	21	9	0.35	0.35	1	200
1344	23	9	0.35	0.35	1	200
1345	25	9	0.35	0.35	1	200
1346	17	10	0.35	0.35	2	200
1347	19	10	0.35	0.35	2	200
1348	21	10	0.35	0.35	1	200
1349	23	10	0.35	0.35	1	200
1350	25	10	0.35	0.35	1	200
1351	17	1	0.4	0.35	1	200
1352	19	1	0.4	0.35	1	200
1353	21	1	0.4	0.35	1	200
1354	23	1	0.4	0.35	1	200
1355	25	1	0.4	0.35	1	200
1356	17	2	0.4	0.35	1	200
1357	19	2	0.4	0.35	1	200
1358	21	2	0.4	0.35	1	200
1359	23	2	0.4	0.35	1	200
1360	25	2	0.4	0.35	1	205
1361	17	3	0.4	0.35	1	200
1362	19	3	0.4	0.35	1	200
1363	21	3	0.4	0.35	1	200
1364	23	3	0.4	0.35	1	200
1365	25	3	0.4	0.35	1	310

1366	17	4	0.4	0.35	1	200
1367	19	4	0.4	0.35	1	200
1368	21	4	0.4	0.35	1	200
1369	23	4	0.4	0.35	1	200
1370	25	4	0.4	0.35	1	415
1371	17	5	0.4	0.35	1	200
1372	19	5	0.4	0.35	1	200
1373	21	5	0.4	0.35	1	200
1374	23	5	0.4	0.35	1	200
1375	25	5	0.4	0.35	1	520
1376	17	6	0.4	0.35	1	200
1377	19	6	0.4	0.35	1	200
1378	21	6	0.4	0.35	1	200
1379	23	6	0.4	0.35	1	200
1380	25	6	0.4	0.35	1	625
1381	17	7	0.4	0.35	1	200
1382	19	7	0.4	0.35	1	200
1383	21	7	0.4	0.35	1	200
1384	23	7	0.4	0.35	1	200
1385	25	7	0.4	0.35	1	730
1386	17	8	0.4	0.35	1	200
1387	19	8	0.4	0.35	1	200
1388	21	8	0.4	0.35	1	200
1389	23	8	0.4	0.35	1	200
1390	25	8	0.4	0.35	1	835
1391	17	9	0.4	0.35	1	200
1392	19	9	0.4	0.35	1	200
1393	21	9	0.4	0.35	1	200
1394	23	9	0.4	0.35	1	200
1395	25	9	0.4	0.35	1	940
1396	17	10	0.4	0.35	1	200
1397	19	10	0.4	0.35	1	200
1398	21	10	0.4	0.35	1	200
1399	23	10	0.4	0.35	1	200
1400	25	10	0.4	0.35	1	1045